

REACTION MECHANISMS
AT CATHODES IN
LITHIUM/OXYGEN BATTERIES

Reaktionsmechanismen an Kathoden in Lithium/Sauerstoff-Batterien

Adrian Schürmann
December 2021

*Dem Fachbereich Biologie und Chemie
der Justus-Liebig-Universität Gießen
vorgelegte Dissertation zur Erlangung
des akademischen Grades
Doktor der Naturwissenschaften*

Adrian Schürmann.

Reaction Mechanisms at Cathodes in Lithium/Oxygen Batteries.

Dem Fachbereich Biologie und Chemie der Justus-Liebig-Universität
Gießen vorgelegte Dissertation zur Erlangung des akademischen
Grades Doktor der Naturwissenschaften.

EINGEREICHT AM 23.12.2021

DEKAN

Prof. Dr. Thomas Wilke

1. GUTACHTER

Prof. Dr. Jürgen Janek

2. GUTACHTER

Prof. Dr.-Ing. Daniel Schröder

Die vorliegende Arbeit wurde im Zeitraum vom 01.06.2016 bis 23.12.2021 am Physikalisch-Chemischen Institut der Justus-Liebig-Universität Gießen unter Betreuung von Prof. Dr. Jürgen Janek angefertigt.

Ich erkläre: Ich habe die vorgelegte Dissertation selbstständig und ohne unerlaubte fremde Hilfe und nur mit den Hilfen angefertigt, die ich in der Dissertation angegeben habe. Alle Textstellen, die wörtlich oder sinngemäß aus veröffentlichten Schriften entnommen sind, und alle Angaben, die auf mündlichen Auskünften beruhen, sind als solche kenntlich gemacht. Ich stimme einer evtl. Überprüfung meiner Dissertation durch eine Antiplagiat-Software zu. Bei den von mir durchgeführten und in der Dissertation erwähnten Untersuchungen habe ich die Grundsätze guter wissenschaftlicher Praxis, wie sie in der „Satzung der Justus-Liebig-Universität Gießen zur Sicherung guter wissenschaftlicher Praxis“ niedergelegt sind, eingehalten.

Gießen, 23.12.2021

Adrian Schürmann

When life gives you lemons, build batteries.

Dedicated to Hanna.

Abstract

Aprotic lithium/oxygen (Li/O₂) batteries are still seen as a highly promising technology for mobile energy storage, as they, in theory, exceed the theoretical energy density of state-of-the-art lithium-ion batteries (LIBs) by roughly an order of magnitude. However, Li/O₂ batteries are plagued by a low lifetime and high charging overvoltages rooting in the poor electronic conductivity of the discharge product lithium peroxide (Li₂O₂) and manifold degradation reactions. This thesis examines two key aspects of Li/O₂ batteries in detail: first, the solubility and diffusivity of oxygen within the electrolyte and second, the possible formation of singlet oxygen (¹O₂) from reactions involving superoxides and peroxides during cell cycling.

In detail, this thesis contains a systematic study to determine a consistent set of Henry's law constants and diffusion coefficients of oxygen in different glymes and perfluorinated solvents. The study uses an experimental approach (time dependent pressure measurements) as well as simulations (molecular dynamic simulation) to determine the diffusion coefficients of oxygen. The difference between simulated and measured diffusion coefficients is sufficiently small, showing that both approaches can be used to determine these values. The established methods and protocols can be adapted to study emerging electrolytes for metal/O₂ batteries with different polarity and varying magnitudes of Henry's law constants and diffusion coefficients.

In recent years, ¹O₂ was identified as possible root cause of the manifold degradation reactions observed in Li/O₂ batteries. While experimental indications were found, a complete picture including electron transfer theory was missing and thus the role of ¹O₂ is still controversially discussed. Therefore, literature on singlet oxygen with a focus on Li/O₂ batteries is reviewed in this thesis, starting from the first detection of ¹O₂ in the 1960s. Experimental techniques for detecting and quantifying ¹O₂ such as trapping, quenching and luminescence as well as their potential pitfalls are evaluated and discussed. Moreover, for the first time Marcus(-Hush-Chidsey) theory as a model to describe and understand ¹O₂ in electrochemistry and especially Li/O₂ batteries is introduced and critically discussed. Overall, the review reveals that the evidence to date is insufficient to assume ¹O₂ formation. The reaction mechanisms proposed for ¹O₂ formation in the literature must also be considered with caution.

The findings of this work provide a profound understanding of the transport and reaction mechanisms of oxygen and its reduced counterparts superoxide and peroxide in Li/O₂ batteries. The concepts introduced in this thesis can be transferred to neighboring areas like fuel cells, water electrolysis and metal corrosion processes, thus advancing the understanding of oxygen reactivity in electrochemical systems.

Zusammenfassung

Aprotische Lithium-Sauerstoff-Batterien (Li/O₂-Batterien) gelten nach wie vor als vielversprechende Technologie für die mobile Energiespeicherung, da sie theoretisch moderne Lithium-Ionen-Batterien (LIBs) in Bezug auf ihre theoretische Energiedichte übertreffen. Li/O₂-Batterien leiden jedoch unter kurzen Lebensdauern und hohen Ladeüberspannungen, die wiederum hauptsächlich auf eine geringe elektronische Leitfähigkeit des Entladungsprodukts Lithiumperoxid (Li₂O₂) und zahlreiche Degradationsreaktionen zurückzuführen sind. In dieser Thesis werden zwei wichtige Aspekte von Li/O₂-Batterien näher beleuchtet: erstens die Löslichkeit und Diffusionsfähigkeit von Sauerstoff im Elektrolyten und zweitens die Möglichkeit der Entstehung von Singulett-Sauerstoff (¹O₂) durch Reaktionen mit Superoxiden und Peroxiden während des Zellbetriebs.

Diese Dissertation enthält eine systematische Studie zur Bestimmung einer kohärenten Reihe von Henry-Konstanten und Diffusionskoeffizienten für Sauerstoff in verschiedenen Glycolthern und perfluorierten Lösungsmitteln. Die Studie verwendet sowohl einen experimentellen Ansatz (zeitabhängige Druckmessungen) als auch Simulationen (Molekulardynamik-Simulation) zur Bestimmung der Diffusionskoeffizienten von Sauerstoff. Der Unterschied zwischen simulierten und gemessenen Diffusionskoeffizienten ist hinreichend gering, was zeigt, dass beide Ansätze zur Bestimmung dieser Größen verwendet werden können. Die etablierten Methoden und Protokolle können für die Untersuchung neuer Elektrolyte für Metall/O₂-Batterien mit unterschiedlicher Polarität und unterschiedlichen Größenordnungen von Henry-Konstanten und Diffusionskoeffizient adaptiert werden.

In den letzten Jahren wurde Singulett-Sauerstoff als mögliche Ursache für die zahlreich beobachteten Degradationsreaktionen in Li/O₂-Batterien identifiziert. Zwar konnten experimentelle Hinweise gefunden werden, jedoch fehlte bislang ein vollständiges Bild einschließlich Elektronentransfertheorien, sodass die Rolle von Singulett-Sauerstoff nach wie vor kontrovers diskutiert wird. Daher wird in dieser Thesis die Literatur zu Singulett-Sauerstoff in Li/O₂-Batterien analysiert, beginnend mit dem ersten Nachweis von ¹O₂ in den 1960er Jahren. In diesem Zusammenhang werden experimentelle Techniken zum Nachweis und zur Quantifizierung von Singulett-Sauerstoff wie Trapping, Quenching und Lumineszenz sowie deren

potenzielle Probleme evaluiert. Außerdem wird zum ersten Mal die Marcus(-Hush-Chidsey)-Theorie als Modell zur Beschreibung und zum Verständnis von Singulett-Sauerstoff in der Elektrochemie und insbesondere in Li/O₂-Batterien vorgestellt und kritisch diskutiert. Diese Thesis zeigt, dass die bisherigen Erkenntnisse nicht ausreichen, um die Entstehung von Singulett-Sauerstoff anzunehmen. Auch die in der Literatur angenommenen Reaktionsmechanismen müssen mit Vorsicht betrachtet werden.

Die wissenschaftlichen Erkenntnisse dieser Dissertation ermöglichen ein vertieftes Verständnis der Transport- und Reaktionsmechanismen von Sauerstoff und seinen reduzierten Pendanten Superoxid und Peroxid in Li/O₂-Batterien. Die entwickelten Konzepte können auf benachbarte Gebiete wie Brennstoffzellen, Wasserelektrolyse und Korrosion von Metallen übertragen werden und so das Verständnis der Reaktivität von Sauerstoff in elektrochemischen Systemen fördern.

Danksagungen

Hier möchte ich mich bei allen bedanken, die mich auf meinem Weg zu dieser Dissertation begleitet und unterstützt haben. Ohne euch wäre diese Arbeit nicht diese Arbeit. Und ohne euch hätte ich nicht so viel auf meinem Weg gelernt.

Ein besonderes Dankeschön möchte ich Prof. Dr. Jürgen Janek aussprechen, der mich in meiner Bachelorzeit in seiner Arbeitsgruppe willkommen hieß und mich seitdem unterstützend und fördernd begleitet hat. Seine fortlaufende Unterstützung und sein Interesse an meiner fundamentalen Arbeit – auch abseits direkter Anwendungen – haben mich motiviert, auch die letzten Aspekte der Elektrochemie erkunden zu wollen. Das von ihm entgegengebrachte Vertrauen trug maßgeblich zum Gelingen meiner Arbeit bei und half mir, meinen Zielen stetig näher zu kommen.

Prof. Dr.-Ing. Daniel Schröder möchte ich herzlichst für die Betreuung und Unterstützung im Rahmen meiner Dissertation und des Projektes „BenchBatt“ danken. Seine Hilfe und Hinweise haben dazu beigetragen, meine Ziele nicht aus den Augen zu verlieren und diese Arbeit zu einem Abschluss zu bringen. Auch für seinen Blick auf Themen aus der Sichtweise eines Ingenieurs bin ich dankbar.

Prof. Dr. Doreen Mollenhauer danke ich für die zahlreichen Diskussionen, Literaturhinweise und Ergänzungen im Rahmen meiner zweiten Veröffentlichung.

Dr. Bjoern Luerßen möchte ich für seine Unterstützung rund um meine Promotion danken. Egal, ob Laborverantwortlichkeit, Grafiken oder Texte: Deine Ratschläge und Rückendeckung waren immer hilfreich und willkommen. Vielen Dank dafür, deine Hilfe kann nicht in Rumkugeln aufgewogen werden.

Auch meine Freunde, Bürokollegen und Labormitstreiter möchte ich an dieser Stelle erwähnen. Euch verdanke ich viele kurzweilige Momente, viel Koffein, Kohlenhydrate und gelegentlich auch Ethanol. Im Besonderen sind hier zu nennen: Dr. Felix Walther und Christine Kern, mit denen ich ein Büro in der Diaspora teilen durfte und die mit mir ihr Wissen über ToF-SIMS, XPS und Katzen teilten. Dr. Daniel Stock, der mich jeden Tag pünktlich zum Mittagessen einsammelte und mir zeigte, dass die Zinkbatterie noch lange nicht abgeschlossen ist. Dr. Peter Schmitz, der mit mir zusammen die Sauerstoffchemie kennenlernen durfte und mir zeigte, welche Hamster es auf YouTube zu sehen gibt. Raika Oppermann und Michele Bastianello für zahlreiche

Kaffeepausen mit mal mehr und mal weniger wissenschaftlichem Bezug und mal mehr oder weniger schwarzem Humor. Elisa Monte danke ich für die viele Arbeit, die sie in die Journal Cover für Chemical Reviews gesteckt hat.

Ebenso danke ich Harald Weigand, Harry Heidt und der gesamten feinmechanischen Werkstatt für die Umsetzung meiner Ideen in die Realität und die zahlreichen Reparaturen, die *natürlich* nicht durch mich verschuldeten waren.

Dr. Joachim Sann möchte ich für die vielen technischen Ratschläge und Informationen rund um Batterien danken. Dr. Boris Mogwitz gilt mein Dank für seine anpackende Art und die viele Hilfe bei sämtlichen Laborreparaturen. Zudem bedanke ich mich bei der gesamten Arbeitsgruppenleitung für die Organisation und dafür, dass sie den Laden am Laufen hält.

Mein Dank gilt an dieser Stelle auch meiner Familie, die während des Studiums und der Promotion immer an mich geglaubt und mich stets tatkräftig unterstützt haben.

Meinen besonderen Dank möchte ich auch meiner Lebensgefährtin Hanna aussprechen, die mich all die Jahre immer unterstützend und motivierend durch mein Studium und meine Promotion begleitet hat. Du hast die Tiefen weniger tief und die Höhen noch höher gemacht.

Contents

Introduction

1	Motivation and Outline	3
2	The Aprotic Lithium/Oxygen Battery	7
2.1	Architectures of Lithium/Oxygen Batteries	7
2.2	Limitations of Aprotic Lithium/Oxygen Batteries	12
2.3	Fundamental Reactions in Li/O ₂ Batteries	15
3	Diffusion and Solubility of Gases in Liquids	21
3.1	Solubility of Gases in Liquids	21
3.2	Diffusion of Gases in Liquids	23
4	Theory of Electron Transfer	27
4.1	Bulter–Volmer Kinetics	27
4.2	Marcus–Theory	30
4.3	Gerischer Model	32
4.4	Description of Electron Transfer in Batteries	34

Results and Discussion

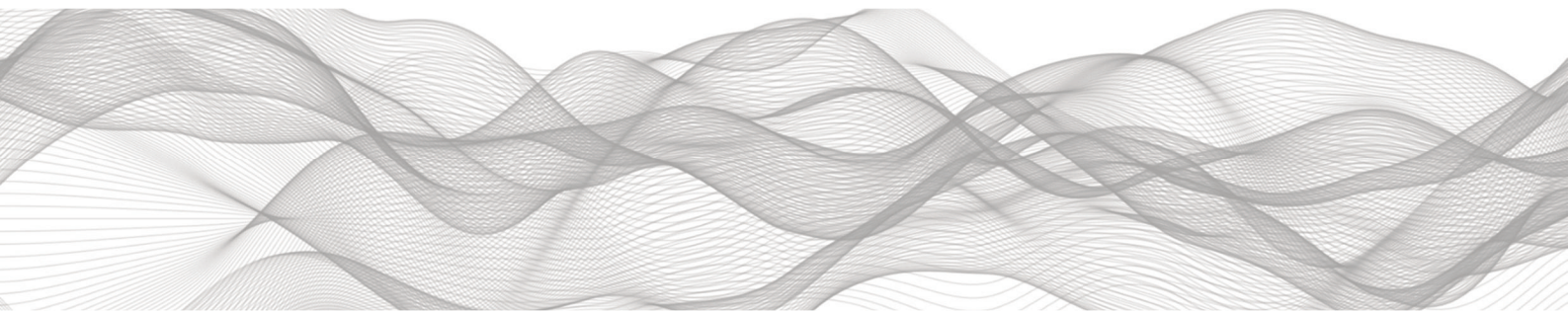
5	Diffusivity and Solubility of Oxygen in Solvents for Metal/Oxygen Batteries: A Combined Theoretical and Experimental Study	39
5.1	Introduction	40
5.2	Experimental	41
5.2.1	Chemicals	41
5.2.2	Determination of Gas Volumes	41
5.2.3	Oxygen Uptake Experiments for Henry’s Law Constants	41
5.2.4	Oxygen Uptake Experiments for Diffusion Coefficients	41
5.2.5	Molecular Dynamic Simulations	41

5.3	Results and Discussion	41
5.3.1	Diffusion Coefficients and Henry's Law Constants of Oxygen	41
5.3.2	Self-diffusion and Viscosity of Solvents	42
5.4	Conclusions	43
5.5	References	43
6	Singlet Oxygen in Electrochemical Cells: A Critical Review of Literature and Theory	45
6.1	Introduction	46
6.2	Background and Literature Review	47
6.3	Theoretical Considerations	50
6.3.1	Molecular Orbital Description	50
6.3.2	Deactivation of Singlet Oxygen	51
6.3.3	Spin Conservation and Wigner's Rules	52
6.3.4	Marcus Theory	53
6.4	Reaction Mechanisms Leading to Singlet Oxygen	57
6.4.1	Discharging Me/O ₂ Cells: Singlet Oxygen from Chemical Reactions	57
6.4.2	Charging Me/O ₂ Cells: Singlet Oxygen from Electrochemical Reactions	58
6.4.3	Singlet Oxygen from Side Reactions	59
6.4.4	Specificity of Singlet Oxygen Traps	59
6.5	Conclusions	60
6.6	References	62
	Too long; didn't read	
7	Conclusions and Outlook	69
	Bibliography	75
	Appendices	
A	Appendix to the Introduction	95
A.1	Sum of Mechanisms in a given Scheme of Squares	95
A.2	Numerical Values and Fit Parameters of Figure 3.1	97

B	Supporting Information for Publication I	99
B.1	Determination of Gas Volumes	99
B.2	Oxygen Uptake Experiments for Henry's Law Constants	99
B.3	Oxygen Uptake Experiments for Diffusion Coefficients	102
B.4	Densities of n-glymes and PFCs	104
B.5	Self-diffusion Coefficients	105
B.6	Impact of Conducting Salt on Henry's Law Constant	106
B.7	References	106
C	Symbols	109
D	Acronyms	111
E	Contributions	113
E.1	Publications	113
E.2	Oral Presentations	113
E.3	Poster Presentations	114

PART I

INTRODUCTION



Motivation and Outline

Human life has never changed as rapidly as it has in the last century.¹ While in many cases this change has been positive, the rapid industrialization and digitalization of every part of our daily lives has taken its toll: The composition of Earth's atmosphere changed for the worse. Years of greenhouse gas emissions have led to an increase in the concentration of gases such as CO₂ in our atmosphere and, as a result, a rise in global temperatures.^{2,3} Recently, awareness of this climate change has grown and policies have begun to be put in place to stop it. Germany enacted the Renewable Energy Sources Act (Erneuerbare-Energien-Gesetz, EEG), targeting a reduction of its CO₂ emissions from 810 Mt of carbon dioxide equivalent per year in 2019 to less than 100 Mt in 2050.⁴ The share of renewable energy sources in all electricity produced in Germany is planned to be increased from currently 46% in 2020 to 100% in the same period.^{4,5} These plans will inevitably result in an electrification of all industry sectors and our daily lives. Since renewable energy sources such as wind and photovoltaics are unable to deliver energy continuously, resilient energy storage systems are necessary. In addition to the need for improved batteries for comprehensive electrification of the transport sector, there is a high demand for batteries for medium- and small-scale energy storage, an important prerequisite for reducing greenhouse gas emissions and the transition to renewable energies. While the electrochemical battery has been around for over 200 years, using them in vehicles and storage applications in a manner, that could be considered competitive with petroleum-based fuels and natural gas, has been an incredible challenge. It is only within the last twenty years of innovation that the concept has finally become feasible. Today's high-capacity lithium-ion battery cell technologies can be seen as the first hopeful steps in transitioning society towards a new standard in practical and economical transportation by electric vehicles and energy storage solutions.

Since their commercialization in 1991 by Sony and Asahi Kahei, lithium-ion batteries were continuously improved, reaching nowadays a theoretical specific energy w_{th} of the total cell (electrodes, current collectors and separator) of 421 Wh kg^{-1} , using $\text{LiNi}_x\text{Co}_y\text{Mn}_{1-x-y}\text{O}$ (NCM) as a cathode active material in combination with a graphite anode.^{6,7} However, specific energy and energy density are approaching their physicochemical limits and alternative battery chemistries are under investigation to meet the even higher requirements of the

1

future.⁸⁻¹⁰ One of these concepts is the transition to all-solid-state batteries (SSBs), where the normally liquid organic electrolyte is replaced by a solid, probably polymer-based or inorganic, ion conductor. These systems could potentially allow the use of lithium metal anodes while boosting energy density (and also possibly improving cells safety in case of an internal short circuit).^{8,11}

Alternatively, new cell concepts could be employed. One of these promising concepts are conversion-type batteries such as lithium/oxygen cells (Li/O₂). As oxygen is available from our surrounding atmosphere and additionally provides a high oxidizing potential, battery concepts based on oxygen emerged as the *holy grail of electrochemistry*.¹² In 1996, Abraham and Jiang first described the Li/O₂ battery by combining a lithium metal anode with an oxygen cathode.¹³ Since lithium is a lightweight element and oxygen theoretically does not need to be stored in the battery but can be obtained directly from the atmosphere, Li/O₂ batteries exhibit an exceptionally high energy density and specific energy.

Theoretically, a specific energy of 3485 W h kg⁻¹ could be reached with such cells (at active material basis and a fully discharged state, essentially the capacity of Li₂O₂).¹⁴ The promising high theoretical energy densities and demand for new battery chemistries sparked substantial efforts over the last 15 years to investigate and develop Li/O₂ batteries, which manifested in numerous scientific publications and patents. Nevertheless, the euphoric interest of the early years quickly eased as serious chemical and electrochemical challenges surfaced, involving the core working principles of this battery system. Li/O₂ batteries typically exhibit high overvoltages during discharging and charging, and thus low round trip efficiency factors.¹⁵ One of the causes is that the discharge product, lithium peroxide (Li₂O₂), is insoluble in the organic electrolytes and has, at best, modest electronic conductivity.¹⁶ On the other hand, the exact discharge and charge reaction mechanism has not yet been fully elucidated. However, it can be assumed that it contains purely chemical steps which cause additional energy contributions.¹⁷ In addition, all liquid electrolytes applied, such as the carbonates used initially, and ethers, sulfoxides and ionic liquids used later, have been shown to decompose under the unfavourable combination of high cell voltages and reactive oxygen species.¹⁸⁻²² But not only the electrolytes used decompose, also the porous carbon cathodes and lithium metal anodes are prone to corrosion in contact with reactive oxygen species, leading to surface passivation and CO₂ formation.^{21,23} Recent experimental work has

identified singlet oxygen ($^1\text{O}_2$) as a possible reactive oxygen species and root cause of the aforementioned problems.²⁴ To date, these hurdles have not been overcome despite intensive research over the past two decades, and thus the electrochemical performance of Li/O₂ batteries in terms of energy efficiency and cycle life remains poor.

This doctoral thesis focuses on the role of oxygen in Li/O₂ batteries, to gain a deeper understanding of the fundamentals of these systems and thus to pave the way for new research areas. As a starting point, the electrochemical and chemical fundamentals of aprotic Li/O₂ batteries are presented and the different cell architectures are explained in more detail in Chapter 2. The major challenges of Li/O₂ batteries are identified and strategies to overcome these challenges are presented. Subsequently, Chapter 3 briefly summarizes concepts describing the solubility and diffusion of gases inside solvents, electrolytes and Li/O₂ batteries. In Chapter 4, different electron transfer models and their relevance in (electro)chemistry, especially batteries, are presented.

The main results of this doctoral thesis are summarized in two scientific publications. Chapter 5 (Publication I) covers the diffusion coefficients and Henry's law constants of oxygen in different solvents. The publication "*Diffusivity and Solubility of Oxygen in Solvents for Metal/Oxygen Batteries: A Combined Theoretical and Experimental Study*" determines experimental and theoretical values for both parameters, which are often unknown or scatter widely in literature.²⁵ Evaluating these parameters in typical solvents and electrolytes is essential towards better quantitative understanding and finally improvement of metal/oxygen batteries. Using oxygen uptake experiments and molecular dynamics simulations (performed by cooperation partners at Tel Aviv University), theoretical and experimental approaches to determine oxygen diffusion coefficients in several commonly used solvents are compared. Diffusion coefficients and Henry's law constants of oxygen for a series of glymes with different chain length and perfluorinated solvents are reported. The benefits of using both experiment and simulation to determine these parameters are also discussed. The difference between simulated and measured diffusion coefficients is small in comparison to the magnitude of the coefficients in all nine investigated solvents, opening up the possibilities of using simulations instead of experiments.

Chapter 6 (Publication II) covers the current understanding of singlet oxygen in metal/O₂ batteries, with a focus on the Li/O₂ system. The review article "*Singlet Oxygen in Electrochemical Cells: A Critical Review of Literature and Theory*" provides an extensive literature

overview and discussion of the historic development of the understanding of $^1\text{O}_2$ in (electro)chemistry.²⁶ Validation, evaluation and understanding of the formation of $^1\text{O}_2$ is essential for improving metal/ O_2 batteries, therefore Marcus(-Hush-Chidsey) theory is used for the first time to discuss the possibility of $^1\text{O}_2$ formation in metal/ O_2 batteries as a product from (electro)chemical reactions. It can be concluded that experimental evidence is yet not fully conclusive and side reactions can play a major role in verifying the existence of $^1\text{O}_2$. Following the in-depth analysis, the conclusion that $^1\text{O}_2$ can only originate from a chemical step is drawn. A direct electrochemical generation of $^1\text{O}_2$, as proposed by others, can be excluded based on theoretical arguments.

Lastly, in the concluding Chapter 7, the findings presented in the publications of this doctoral thesis are summarised and evaluated in the context of the scientific background. Open questions in the areas of diffusion and solubility of oxygen, as well as the electrochemistry of oxygen, are identified, and approaches to solve them are proposed. The thesis closes with an outlook on future research in the field of the electrochemistry of oxygen, which builds on the work and findings presented here.

The Aprotic Lithium/Oxygen Battery

The Li/O₂ electrochemical couple in a secondary battery was first experimentally introduced by Semkow and Sammells in 1987.²⁷ Their setup contained a Li-alloy anode in a molten salt electrolyte, separated from an oxygen cathode by an oxygen-conducting solid electrolyte. When discharged, lithium oxide (Li₂O) is formed as a product, which dissolves in the molten salt electrolyte. The use of a solid electrolyte and a molten salt electrolyte required temperatures between 600-800 °C for operation. The Li/O₂ electrochemical couple was later rediscovered by Abraham and Jiang in 1996.¹³ The discovery was made coincidentally during *in situ* investigations on the electrochemical intercalation of Li⁺ into graphite in a Li/C cell with a polymer electrolyte.²⁸ They extracted the gases formed during intercalation with a syringe and accidentally injected oxygen into the cell. When the experiment resumed, a higher voltage of about 3 V versus Li⁺/Li and an increased capacity were observed. Later, they introduced oxygen into a Li/C cell to demonstrate the feasibility of a Li/O₂ battery with an organic, Li⁺-conducting electrolyte. They also identified the main discharge product as lithium peroxide (Li₂O₂).¹³ Their publication can be understood as the birth of the modern Li/O₂ battery, since today's batteries, although progress has been made, do not differ significantly in their architecture from Abraham and Jiang's original design.

2

2.1 ARCHITECTURES OF LITHIUM/OXYGEN BATTERIES

Aprotic Li/O₂ batteries are based on the formation and decomposition of Li₂O₂ at the cathode, according to the following (simplified) reaction:



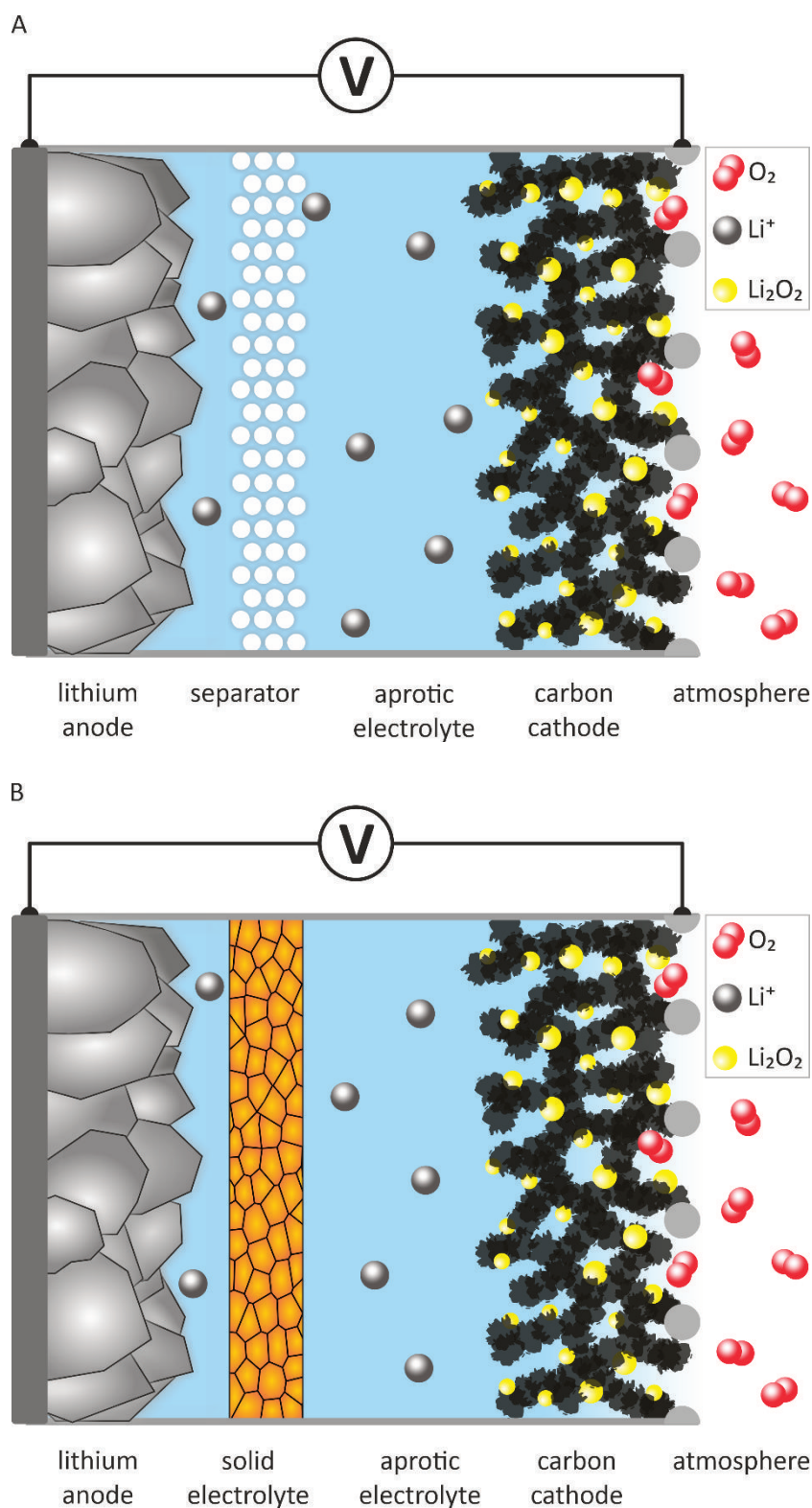
The Li₂O₂ formed is practically insoluble in aprotic electrolytes and therefore deposits on the cathode surface in the form of thin films or toroidal clusters, depending on the exact electrolyte used. In the literature, several values are used for the theoretical energy densities of such a Li/O₂ battery. Theoretically, gravimetric energy densities of up to 11400 Wh kg⁻¹ and volumetric energy densities of up to 6080 Wh L⁻¹ are possible in the fully charged state, assuming that no oxygen is stored in the battery.¹⁴ These values correspond, in principle, to the capacity of the lithium metal anode, ignoring the mass and volume of the oxygen needed for operation. However, during the discharge process, oxygen is

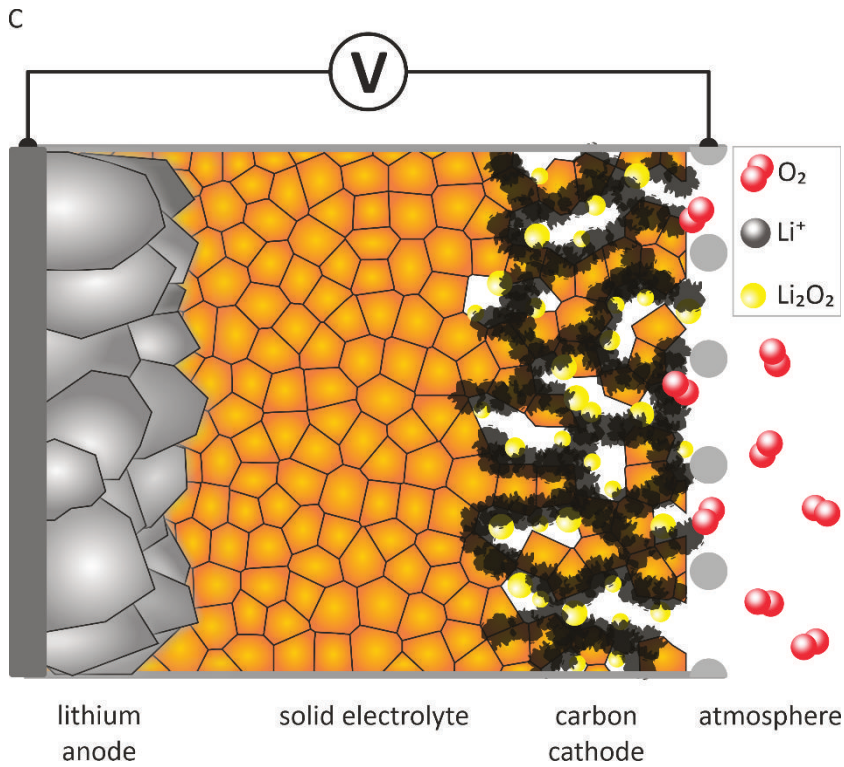
Figure 2.1. Cell architectures of Li/O₂ batteries.

A) Aprotic, single-compartment architecture.

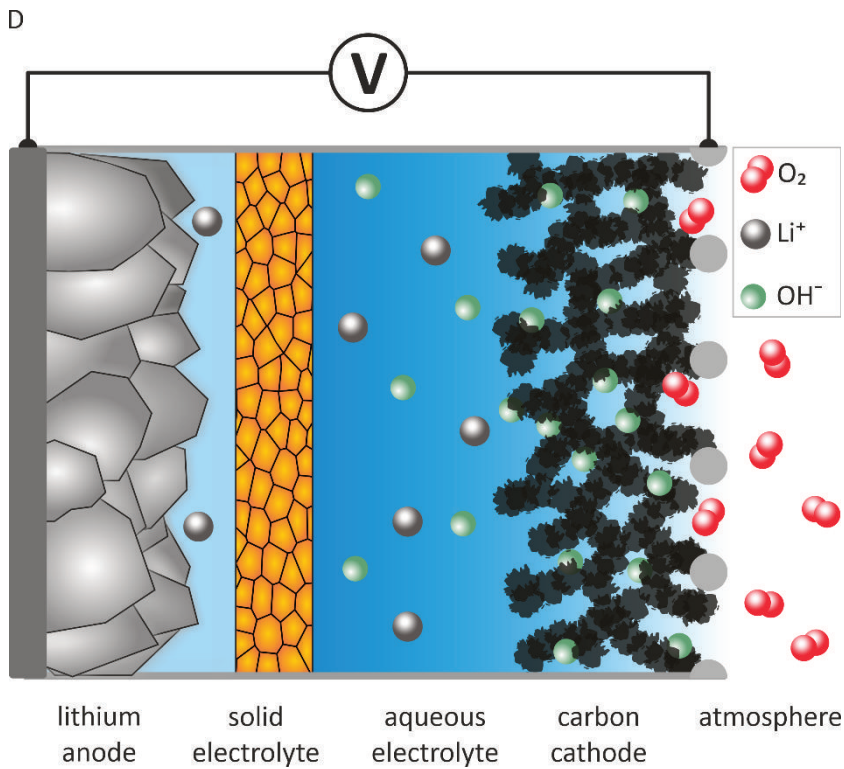
This design is the most prevalent in literature due to its relatively simple setup. The electrolyte used is commonly based on DMSO or diglyme as solvent, LiTFSI is often used as conducting salt. Glass fiber papers or polymer films are used as separators.

B) Aprotic, two-compartment architecture. The electrolyte is separated into two compartments by a lithium-ion conducting solid electrolyte. The separation prevents the diffusion of dissolved gases, intermediates, and side products at the cathode side to the anode as well as a crosstalk between electrodes. Both compartments use the same electrolyte, which are in general DMSO and glycol ether-based electrolytes.





C) All-solid-state architecture. The liquid electrolyte is replaced by lithium-ion conducting solid electrolyte. Solid electrolytes commonly used in the literature are, for example, LISICON, LAGP, LATP and LLZO. The cathode consists of a porous mixture of solid electrolyte and carbon. D) Aqueous, two-compartment architecture. Again, the electrolyte is separated into two compartments, one containing an aprotic electrolyte and the lithium metal anode, the other containing an aqueous electrolyte and the cathode. Discharging a Li/O₂ cell in an aqueous electrolyte results in LiOH dissolved in the electrolyte, in contrast to Li₂O₂, which is deposited onto the electrode.



incorporated into the battery in the form of lithium peroxide. If the discharge product lithium peroxide is chosen as the basis for calculation, values of 3458 Wh kg^{-1} and 3445 Wh L^{-1} are obtained for the fully discharged state, respectively.¹⁴ These values are even further decreased by taking other components of the battery into account, such as the current collectors, the electrolyte or the porous carbon cathode. When considering the inactive components of the battery in the calculations, it should be noted that several cell architectures can be distinguished. For practical applications, pure oxygen must be provided to the battery to suppress side reactions with H_2O , CO_2 , and N_2 , and two possible approaches can be distinguished. On the one hand, closed systems, providing oxygen by means of an internal tank. On the other hand, open systems, which obtain oxygen from the atmosphere. In this case, additional filters are required to remove CO_2 , H_2O and N_2 from the gas flow into the cell and to prevent evaporation of the electrolyte. If the aforementioned cell components are taken into account, practical energy densities in a range of $\sim 450\text{--}600 \text{ Wh kg}^{-1}$ and $450\text{--}700 \text{ Wh L}^{-1}$ can be assumed.^{14,29,30} These values are considerably lower than their theoretical counterparts, but still higher than theoretical and practical values of materials used today in lithium-ion battery, which are around 250 Wh kg^{-1} .³¹ An accurate determination of practical energy densities of Li/O_2 batteries seems not possible these days, since this technology is still at an early stage of research and no well-working prototypes exist.

Today, different cell architectures are used, which are shown in Figure 2.1. Their structure and setup-related problems/drawbacks are briefly described in the following.

A conventional single-compartment setup consists of a lithium metal anode, a liquid aprotic Li^+ -conducting electrolyte, and a porous carbon-based cathode permeable for O_2 from the surrounding atmosphere (Figure 2.1 A). A variety of combinations of electrolyte compositions and cathode materials have been used in Li/O_2 batteries to date, of which aprotic, glycol ether based electrolytes and carbonaceous cathodes have become the most prevalent.³² An overview of used solvents in the literature is given in Figure 2.2 and of the conducting salts used in Figure 2.3. The most commonly used conducting salt is lithium bis(trifluoromethanesulfonyl)imide (LiTFSI) as it exhibits high discharge capacities, good (electro)chemical stability and considerable ionic conductivity.³² However, like all conducting salts used in Li/O_2 batteries, it undergoes partial decomposition forming LiF , among others.³³ The electrolyte also has a strong influence on the reaction mechanisms during discharging and charging. Depending on

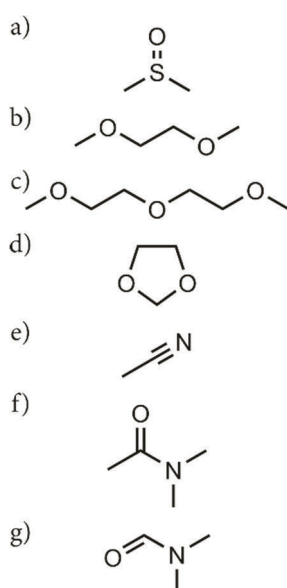


Figure 2.2. Structural formulas of commonly used organic solvents for Li/O_2 batteries. a) DMSO, b) monoglyme, c) diglyme, d) DOL, e) ACN, f) *N,N*-dimethylacetamide, g) DMF

the ability to stabilize and dissolve the intermediates of the reaction mechanism Li_2O_2 deposits as a film or as a particle on the electrode surface. This topic is further discussed in Section 2.3. At the anode, lithium metal electrodes are used since they offer theoretically higher energy densities than, e.g., graphite anodes. Lithium metal electrodes in turn come with their own challenges: The highly reactive lithium metal surface reacts with the electrolyte itself and with dissolved gases in the electrolyte, especially O_2 , CO_2 , N_2 , and H_2O .³² This can also lead to a crosstalk between electrodes, where a species is reduced at the anode, diffuses to the cathode, reacts, and diffuses back to the anode again.^{34–36} The crosstalk between electrodes can consume the lithium metal anode and leads to a reduced coulombic efficiency of the battery.³²

Alternative architectures, based on two-compartments separated by a Li^+ -conducting solid electrolyte membrane, were introduced to protect the lithium metal anode and to suppress the crosstalk between electrodes (referred to as hybrid Li/O_2 battery, Figure 2.1 B).³² Both compartments still contain a liquid electrolyte. The electrolyte membrane materials used in the literature are, e.g., $\text{Li}_{1.3}\text{Al}_{0.3}\text{Ti}_{1.7}(\text{PO}_4)_3$ (LATP), $\text{Li}_7\text{La}_3\text{Zr}_2\text{O}_{12}$ (LLZO), $\text{Li}_{1+x+y}(\text{Ti},\text{Ge})_{2-x}\text{Si}_y\text{P}_{3-y}\text{O}_{12}$ (LISICON) and $\text{Li}_{1.5}\text{Al}_{0.5}\text{Ge}_{1.5}(\text{PO}_4)_3$ (LAGP).^{37–40} While these setups suffer less from dissolved species in the liquid electrolyte, they are instead limited by the ionic conductivity of the solid electrolyte used.

In addition to hybrid approaches, all-solid-state Li/O_2 batteries are also discussed as an alternative to liquid electrolyte-based cells (Figure 2.1 C). In all-solid-state Li/O_2 batteries, the liquid electrolyte is completely replaced by a solid Li^+ -conducting electrolyte. The porous cathode consists of a mixture of solid electrolyte and carbon, which provides three-phase boundaries for the reaction of O_2 to Li_2O_2 . In contrast to liquid electrolytes, the solid electrolyte cannot be displaced from the cathode, which limits the available pore volume for the deposition of Li_2O_2 in the cathode. However, it is possible to fabricate cathodes with sufficient pore volume for the deposition of Li_2O_2 .⁴¹ So far, ceramic materials have been mainly used as solid electrolytes, such as LATP and LAGP.^{38,42} As already mentioned above, the cell performance is limited by the insufficient ionic conductivity of the solid electrolyte at the moment. Thus, further progress of such batteries is directly linked to further improvements of solid electrolytes.

One of the challenges encountered by the described aprotic Li/O_2 cell setups above is the deposition of solid Li_2O_2 , which limits the maximum capacity and rate capability of the battery. Since the deposited Li_2O_2 has a low electronic and ionic conductivity, it blocks

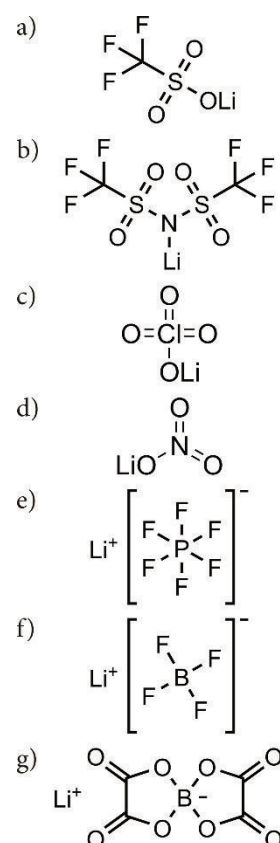
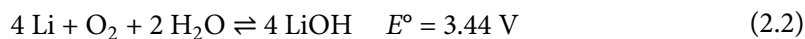


Figure 2.3. Structural formulas of commonly used conducting salts for Li/O_2 batteries.

a) LiOTf , b) LiTFSI , c) LiClO_4 , d) LiNO_3 , e) LiPF_6 , f) LiBF_4 , g) LiBOB

further electron transfer at the electrode surface. One way to overcome this limitation is to use aqueous electrolytes at the cathode (Figure 2.1 D) instead of electrolytes based on aprotic, organic solvents. In these cells, soluble lithium hydroxide is formed as discharge product:⁴³



Since the lithium metal anode reacts with water, the use of single-compartment architectures is precluded, and two-compartment architectures are always used. This approach was popularized by the PolyPlus Battery Company in 2015, but did not result in commercial applications.^{32,43–48} Unlike in aprotic Li/O₂ batteries, the electrolyte in aqueous Li/O₂ batteries participates in the discharge reaction and is consumed, and therefore more electrolyte is required to operate an aqueous Li/O₂ battery (Equation (2.2)). This leads to a higher overall weight and volume of the battery and, in return, to lower energy densities compared to their aprotic counterparts.^{49–51}

The work presented here focuses on the transport and reactions of oxygen in Li/O₂ batteries that use an aprotic electrolyte since they show better rechargeability and higher energy densities than aqueous Li/O₂ batteries. They also have attracted the most research effort in the field of metal/O₂ batteries. The limitations, fundamental reactions, and processes of aprotic Li/O₂ batteries are explained in more detail in Sections 2.2 and 2.3.

2.2 LIMITATIONS OF APROTIC LITHIUM/OXYGEN BATTERIES

The challenges and limitations prohibiting practical application of single-compartment Li/O₂ batteries with aprotic liquid electrolytes can be divided into different categories: limitations of the discharge capacity, use of Li-metal anodes, charging overvoltages, and degradation reactions, which will be discussed hereinafter in detail.

Two reasons have been identified for the poor discharge capacities of Li/O₂ batteries: On the one hand, the porous cathode structure gets clogged by deposited Li₂O₂ during discharge, preventing further diffusion of O₂ and Li⁺ into the electrode and thus limiting the amount of reactants reaching the electrode surface.^{52–54} Moreover, areas deeper inside the cathodes of metal/O₂ batteries are known to partake less in discharge reactions due to limited supply of O₂.⁵⁵ On the other hand, Li₂O₂ exhibits a low electronic and ionic conductivity, preventing charge transfer from the electrode to O₂ in the solution.¹⁶ The underlying reaction mechanisms, resulting in the deposition of Li₂O₂, are further discussed in Section 2.3.

A considered necessity in literature for high energy densities is the use of lithium metal anodes.⁵⁶ However, lithium possesses two major hurdles for application in Li/O₂ batteries. One being the tendency of lithium to form dendrites during plating, resulting in short circuits and danger of thermal runaway while charging.⁵⁷ The other being the low standard electrode potential of lithium metal, resulting in a strong reducing ability.⁵⁸ When a lithium metal electrode is brought into contact with an electrolyte, the surface will be quickly covered with a solid electrolyte interface (SEI), formed from degradation products. In addition, since the electrolyte is generally saturated with oxygen, an oxide layer is formed on the electrode surface. Assuming that a stable SEI has formed, the electrode surface is protected from further degradation reactions with the electrolyte. However, the SEI is too rigid to compensate for the volume changes of the anode during stripping and plating of lithium, which results in cracking of the SEI and exposing of pristine lithium metal to the electrolyte. Therefore, degradation reactions continuously consume lithium at the unprotected surface regions, resulting in low coulombic efficiency. The decomposition of solvents and conducting salts at the anode can also affect the processes at the carbon cathode, since at least some of the degradation products dissolve in the liquid electrolyte, diffuse to the cathode and interfere with the cathode processes.^{34,35,57-59}

In addition to degradation reactions at the anode, degradation reactions also occur at the cathode. This was experimentally shown by investigations with isotope-labelled cathodes and electrolytes.^{21,23} The starting point of the cathode degradation is the reaction of precipitated Li₂O₂, which reacts with the carbon cathode forming a lithium carbonate thin film. High electrode potentials seem to favor the decomposition of the carbon cathode, since the decomposition products are predominantly formed at the end of the charging step.²¹ To limit the degradation reactions, alternative stable electrode materials, which do not react when in contact with Li₂O₂, were investigated in the past. As proof of concept, nanoporous gold electrodes, which do not react with Li₂O₂, and titanium carbide (TiC) electrodes, which form a stable oxide layer preventing further reaction, were used.^{60,61} However, while evolution of CO₂ during charging was reduced, decomposition reactions still take place in these systems. Another approach is to reduce the charging voltage, for which various heterogeneous catalysts have been used (e.g., MnO₂, RuO₂, and Pt/Au nanoparticles).⁶²⁻⁶⁴ One problem with the application of heterogeneous catalysts is that the effect of the catalysts is limited to the direct contact

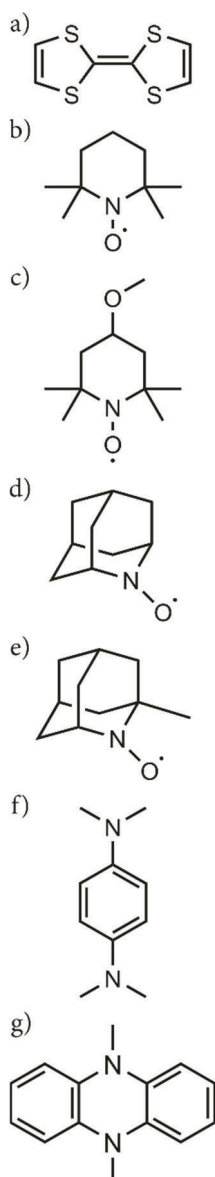


Figure 2.4. Redox mediators used in Li/O₂ batteries.
 a) TTF⁶⁵, b) TEMPO⁶⁶,
 c) 4-methoxy-TEMPO⁶⁷,
 d) AZADO⁶⁷,
 e) 1-Me-AZADO⁶⁷, f) TMPD⁶⁵,
 g) DMPZ⁶⁸

area between deposited Li₂O₂ and catalyst particles. During charging, Li₂O₂ particles inevitably lose contact with the catalyst particles, rendering the catalyst useless. The catalysts used also show low selectivity, which results in the promotion of degradation reactions in some cases.⁶⁹ In recent years, mainly redox mediators have been used, which are homogeneously dissolved in the electrolyte (see Figure 2.4). They enable indirect charge transport from the electrode surface to the deposited Li₂O₂. Important examples here are TTF⁺/TTF and TEMPO⁺/TEMPO (Figure 2.4).^{65–67} The charging voltage can thus be limited to the normal potential of the redox mediators, which is generally a few 100 mV above the normal potential of 2.96 V vs Li⁺/Li.

Although numerous aprotic solvents have been used to date, a completely stable solvent has not yet been found.^{15,18–20} Among the solvents studied, linear ethers such as diglyme are considered the most stable and were therefore selected for the experiments described in this work. The cause of the solvent decomposition during the discharge is mainly attributed to the superoxide ion (O₂^{•-}) formed, which occurs as an intermediate species.^{18,19,70} Figure 2.5 shows an example of a predicted decomposition pathway of the commonly used solvent diglyme.²⁰ In it, O₂^{•-} first abstracts an H-atom in the α-position to the ether group, forming a stabilized radical. In the presence of O₂, the radical directly forms the ether peroxide, which further decomposes. Typical decomposition products include H₂O and CO₂ as well as insoluble solids such as lithium carbonate (Li₂CO₃), lithium formate (CHO₂Li), lithium acetate (CH₃CO₂Li), polyethers and polyesters.

However, this mechanism must be considered with caution. The superoxide ion is described in the literature as a base with a pK_A of 10.6–12.3 in DMSO. A much higher pK_A is observed when a proton-induced disproportionation is considered, which removes HO₂ from the acid-base equilibrium. In this case, an effective pK_A of 23 is obtained in water.⁷¹ H-atom transfer or deprotonation of the solvent are also not observed in the mechanism of disproportionation of O₂^{•-}. Nor is superoxide a strong oxidizing agent with a standard potential of around -1.8 vs NHE in aprotic solvents.⁷² Therefore, many degradation reactions can probably be attributed to O₂ or the corresponding peroxides, the products of superoxide disproportionation. Autoxidation of ethers in the presence of oxygen was also observed and appears to play a role.⁷³ XPS studies show that the decomposition of solvents is initiated by solid Li₂O₂.⁷⁴ The conducting salts used, such as LiTFSI, are also decomposed to form insoluble LiF.^{33,75} During charging, the decomposition products are partially oxidized, releasing

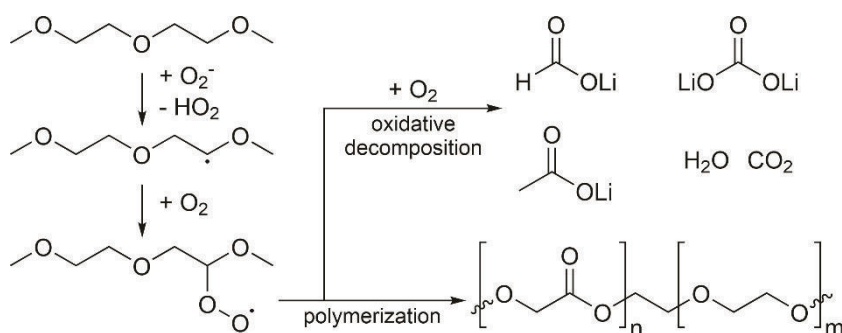


Figure 2.5. Proposed decomposition path of diglyme during discharge of Li/O₂ batteries according to Freunberger *et al.*²⁰

CO₂, which in turn reacts with Li₂O₂ and O₂⁻ in later cycles to form a variety of peroxy carbonates and Li₂CO₃.⁷⁶⁻⁷⁸ In addition, solvent decomposition seems to occur during charging due to the higher voltages used, leading to an overall accumulation of lithium carbonate, formate, and acetate on the electrodes and inside the electrolyte.^{18,21} In 2012, McCloskey *et al.* suggested that defects in the deposited Li₂O₂ play a role in the described degradation process.¹⁵ Another degradation mechanism reported in the literature is the formation of singlet oxygen.^{24,79,80} Since this mechanism has been highlighted in particular in this work, it will be discussed in detail in Publication II (Chapter 6).

2.3 FUNDAMENTAL REACTIONS IN Li/O₂ BATTERIES

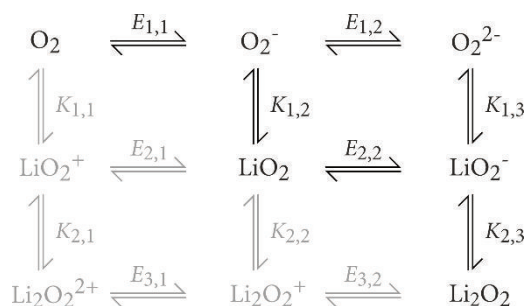
The Li/O₂ battery quickly proved to be a challenging system from a kinetic standpoint. Abraham and Jiang identified Li₂O₂ as the discharge product but the exact reaction mechanism remains unclear to this day.¹³

As in any electrochemical cell, the overall reaction can be divided into two half-cell reactions at the anode and the cathode. At the anode, lithium is stripped and plated during battery cycling. This step also comes with its own challenges (e.g., dendrite formation and formation of a solid electrolyte interface), but these are not the focus of this work.⁸¹

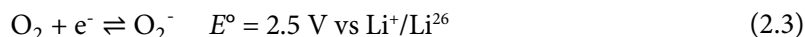
At the cathode side, reactions leading from O₂ to Li₂O₂ (during discharge) are generally summarized as oxygen reduction reaction (ORR). Their counterparts during charging, leading from Li₂O₂ to O₂, are subsumed under the term oxygen evolution reaction (OER). During ORR, starting from dissolved oxygen, it is necessary to transfer two electrons in total to form, together with two Li⁺ ions, lithium peroxide. A transfer of two electrons combined with the association of two cations can be mapped in a scheme of squares (Figure 2.6).⁸² In this scheme, a horizontal step corresponds to an electron transfer characterized by a standard electrode potential, while a vertical step represents the

Figure 2.6. Scheme of squares for the reduction of oxygen in

Li/O₂ batteries. $E_{i,j}$ are the standard electrode potentials of the various redox couples, $K_{i,j}$ are the dissociation constants. Unlikely intermediates and reaction paths are shown in gray.



association of a cation described by an equilibrium constant.* A step along a diagonal is equivalent to a concerted mechanism, in which an electron and cation are transferred in one-step (e.g., in the case of H⁺: concerted proton electron transfer (CPET)[†]).^{83,84} Before discussing the possible reaction mechanisms, the scheme can be simplified by cancelling unlikely intermediates (indicated by the gray coloring in Figure 2.6). In the case of O₂ reduction, it can be assumed that LiO₂⁺, Li₂O₂²⁺ and Li₂O₂⁺ do not play a major role. The scheme could be extended to include Li₂O, but it has never been found in Li/O₂ batteries so far. Starting from O₂, assuming only 1e⁻ transfers take place, the formation of superoxide is the first step (the case of a 2e⁻ transfer is discussed in more detail in Publication II (Chapter 6)):



Following the formation of superoxide, two reactions are possible: a further reduction to a peroxide anion or the association of a lithium cation. The formation of a peroxide anion is unlikely, since the anion is hardly stabilized in the electrolyte.⁸⁵ In contrast, the formation of LiO₂ as an intermediate is widely known in the literature.^{17,86–88}



After the formation of LiO₂, the radical may undergo various types of reactions. First, LiO₂ could be further reduced at the electrode surface, followed by association with another Li⁺ ion, forming Li₂O₂.

* The number of possible ways through such a scheme of squares can be derived from Pascal's triangle, see Appendix A.

† Caution has to be exercised, when talking about concerted electrochemical reactions, due to the different time scales of electron transfer and cation association. While the association of cations involve the movement of a nucleus, the transfer of an electron happens "instantaneously", and the involving atoms do not move in the electronic transition (Franck–Condon principle). This results in the restriction, that it is not possible to be "in between" two oxidation states, while moving along vertical lines is possible. In many cases, concerted reaction mechanisms could also be described as jumping horizontally between two adjacent vertical lines, while moving along them. They are still concerted since no intermediates occur.



Reactions (2.3)+(2.4)+(2.5) form an ECE (electrochemical-chemical-electrochemical) reaction scheme, which can be further separated into two kinetic behaviors, depending on whether (2.4) is irreversible or reversible.⁸⁹ At this point, it should be mentioned, that the reduction of LiO₂ is easier than the reduction of O₂⁻, since the additional charge is added to a neutral molecule, avoiding coulombic repulsion.⁸²

Another possibility is the reduction of LiO₂ by O₂⁻ in the solution, followed by the same association step mentioned before. This amounts to an electron transfer disproportionation, since LiO₂ and O₂⁻ have formally the same oxidation state.



The mechanism can again be further subdivided depending on the overall rate of reaction (2.4). If the backward reaction of (2.4) is slower than the following disproportionation (2.7), reaction (2.4) is also the rate-determining step. In the case, where the backwards reaction is faster than (2.7), reaction (2.4) acts as a pre-equilibrium preceding (2.7), which is then the rate-determining step.⁸⁹

Finally, two LiO₂ moieties could disproportionate to form Li₂O₂ and O₂ directly.



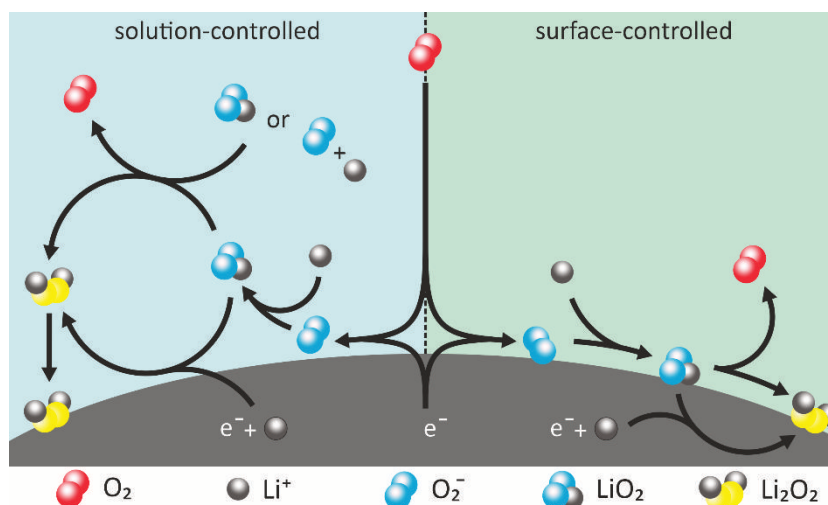
As in the case of (2.7), according to whether (2.4) or (2.8) (with (2.4) acting as a pre-equilibrium) is the rate-determining step, two different limiting behaviors are met.⁸⁹

While the intermediate LiO₂ is well-known in the literature, the exact following mechanism resulting in Li₂O₂ is unknown.^{17,86} Commonly used methods such as electrochemical impedance spectroscopy (EIS) or cyclic voltammetry (CV) are not able to decipher the underlying mechanism, since the different possible mechanisms lead to the same response in the experiment (e.g., the resulting CV curves in the case of ECE and disproportionation mechanisms are identical).^{89,90} Other methods such as XRD fail to identify short-living intermediates such as LiO₂. The problem is further complicated here by the fact that the Lewis basicity of the electrolyte solvent, typically classified by the Gutmann donor number (DN), appears to strongly influence the discharge process.^{17,91-93} Solvents with a high DN such as

Figure 2.7. Schematic representation of the reaction mechanisms leading to Li_2O_2 .

Left: O_2 is reduced to O_2^- , which diffuses into solution to form LiO_2 . LiO_2 is then reduced in solution to form Li_2O_2 . Finally, Li_2O_2 is deposited onto the electrode. Alternatively, LiO_2 is reduced at the electrode to Li_2O_2 .

Right: O_2 is reduced to O_2^- , which adsorbs onto the surface and forms LiO_2 . LiO_2 disproportionates to O_2 and Li_2O_2 or gets reduced to Li_2O_2 .



DMSO are able to dissolve and stabilize the intermediate LiO_2 , which enables the diffusion of LiO_2 away from the electrode. The dissolved LiO_2 is then further reduced to Li_2O_2 in the solution or on the surface of already existing Li_2O_2 particles, leading to larger, toroidal particles. The formation of such particles is favored at low current densities since lower concentrations of intermediates, and their respective reaction rates, allow time for diffusion away from the electrode. The aforementioned behavior is also known as the solution-controlled mechanism. In the case of low DN solvents, such as acetonitrile, the intermediate LiO_2 is hardly soluble in the electrolyte. The surface of the electrode gets covered with a thin film of Li_2O_2 , quickly blocking further charge transfer across the cathode/electrolyte interface since Li_2O_2 is an electronic insulator. This process is commonly referred to as the surface-controlled mechanism. This behavior can typically be observed at high current densities, where the electrolyte is unable to dissolve completely the LiO_2 formed.

Analogies to the processes described above can be found in related systems. In the case of the similar H_2/O_2 system, the mechanism is known for aprotic solvents and proceeds via the reduction of HO_2 by O_2^- in the solution to H_2O_2 .^{89,94}



In the case of Na/O₂ batteries, sodium superoxide (NaO₂) is the main discharge product but sodium peroxide (Na₂O₂) is also possible, if traces of water are present in the battery.⁹⁵ Moving down along the main group elements, K/O₂ batteries form exclusively KO₂ as discharge product.⁹⁶ In recent years, research on secondary Mg/O₂ and Ca/O₂ batteries started.^{97,98} In the case of Mg/O₂ batteries, magnesium peroxide (MgO₂) and magnesium oxide (MgO) are formed as discharge products.^{99,100} In Ca/O₂ batteries dissolved calcium superoxide (Ca(O₂)₂) seems to be the discharge product.¹⁰¹ However, research is still in its infancy and at the present time neither kinetic data on the systems exist nor have the reaction mechanisms involved been elucidated.⁹⁸ Similar to other metal/O₂ batteries, the initial step in both systems appears to be the reduction of O₂ to O₂⁻.^{99,101}

Coming back to the Li/O₂ system, during charging, Li₂O₂ is oxidized at the cathode to molecular O₂ and Li⁺ ions, according to reaction (2.11):



The exact mechanism during charging is again unknown and almost all literature dealing with this topic is based on theoretical calculations. However, it is widely assumed that the charging mechanism is not the reverse of the discharge mechanism and LiO₂ does not play a role.^{14,91} While the discharging process starts from dissolved O₂, charging starts from deposited Li₂O₂, which is insoluble in the electrolyte and has poor electronic and ionic conductivity (the electronic conductivity of bulk Li₂O₂ is around 10⁻⁹ – 10⁻⁸ mS cm⁻¹).^{14,102} Since no solution phase mechanism is possible, two negative charges need to be transferred from the Li₂O₂/electrolyte interface through the Li₂O₂ bulk phase to the Li₂O₂/electrode interface. Two major mechanisms are described in literature: Viswanathan *et al.* stated that the electronic conductivity of Li₂O₂ films is dominated by the tunneling of holes.¹⁶ In contrast, theoretical calculations of Radin *et al.* predicted that intrinsic point defects control the conductivity in the bulk phase of Li₂O₂. Negative lithium vacancies V_{Li}' and hole polarons, comprising of electron holes h• at oxygen dimers, have been identified as the major defects enabling the transport of Li⁺ ions and electrons, respectively.^{103,104} A theoretical and experimental study by Luntz *et al.* suggests, that the hole tunneling path seems to dominate at high current densities, while the charge transport via hole polarons dominates at low current densities.¹⁰⁵

Of course, the above-mentioned overall reactions represent ideal cases, which not describe all aspects of Li/O₂ batteries. Degradation reactions can play a major role in these batteries, which is especially

noticeable during charging. While the oxygen consumption during discharging is in most cases close to the expected value of $2e^-/\text{O}_2$ molecule, oxygen evolution during charging is significantly lower than expected. This is generally seen as an indication of a significant contribution of parasitic side reactions.^{18,20,106,107}

The reaction mechanisms discussed above have a profound influence on the energy efficiency of Li/O₂ batteries, since the overall achievable discharge capacity depends on the prevailing discharge mechanism. Batteries with electrolytes favoring the surface-controlled mechanism show lower discharge capacities than batteries favoring a solution-controlled mechanism. This is due to the blocking of the electrochemical active surface by Li₂O₂ in the case of surface-controlled mechanisms, limiting the discharge capacity. Thus, disproportionation in the solution is highly desirable for high discharge capacities but only steps of the reaction mechanism involving an electron transfer to or from an electrode can be efficiently used for energy storage. In the case of a disproportionation in solution during discharging, the released energy cannot be utilized and is lost as heat. Lost energy must be added back to the system during charging, resulting in higher charging voltages compared to systems without disproportionation. A disproportionation step can therefore be understood as an energy penalty for the battery system since such a step reduces the possible energy drawn during discharging and simultaneously increases the energy needed during charging. Disproportionation as part of discharge or charge mechanisms must be considered whenever more than one electron is transferred in total. Whether a system tends to disproportionate can be determined from its thermodynamic properties such as the standard potentials of the species involved.⁸²

In this chapter, the general cell architecture of Li/O₂ batteries investigated in the literature, as well as the limitations and challenges they face, were described. Section 2.3 highlighted the possible underlying reaction mechanisms and their impact on the battery performance. In the following, two remaining aspects of Li/O₂ batteries are discussed: first, the transport of oxygen in the electrolyte, which can be described using solubility and diffusion. And second, the description of relevant models of electron transfer at electrodes and their use in (Li/O₂) battery research.

Diffusion and Solubility of Gases in Liquids

3

Unlike most batteries, the design of Li/O₂ batteries includes a gas phase that stores and delivers one of the redox-active species. During discharging, gaseous O₂ dissolves in the electrolyte, diffuses to the electrode surface, is reduced, and forms Li₂O₂. On charging, the process is reversed, with O₂ being released from the electrolyte again. The solubility and diffusivity of O₂ play a critical role in Li/O₂ batteries since they limit the maximal amount of dissolved oxygen and the transport of O₂ within the electrolyte. Therefore, understanding and describing these parameters is essential in Li/O₂ battery research. This chapter briefly introduces the physicochemical background of the solubility of gases in liquids and their diffusion in them.

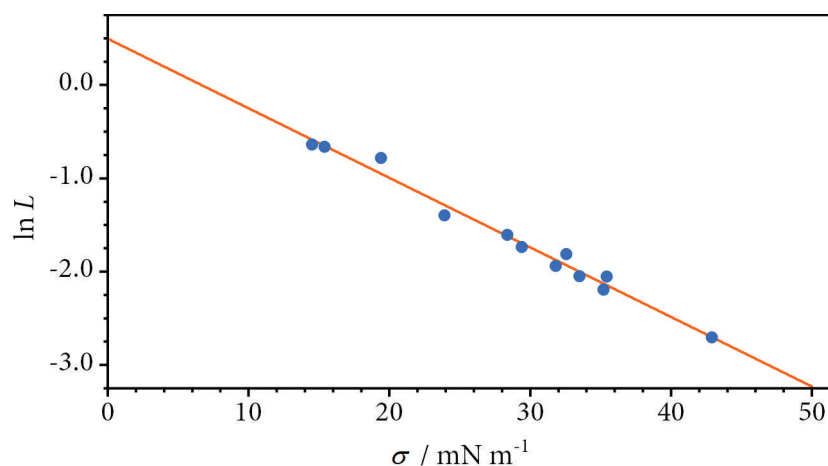
3.1 SOLUBILITY OF GASES IN LIQUIDS

Many models have been employed in literature to describe the solubility of gases in liquids. One of them is the so-called cavity model, which divides the solubility process into two steps.¹⁰⁸⁻¹¹² In the first step, a cavity of suitable size to accommodate the solute molecule is created in the solvent, which requires to do work against the surface tension σ of the liquid. In the second step, a solute molecule or atom is introduced into the cavity, which then interacts with the solvent, resulting in a gain of interaction energy E_i between solvent and the inserted molecule/atom. Strong interactions with the solvent result in larger E_i and higher solubility. The logarithm of the solubility L can be calculated from this process by Equation (3.1) for a spherical solute with radius r .¹¹² The solubility L , also known as the Ostwald coefficient, is defined as the concentration of the gas (the solute) in the liquid phase (C_g^L) divided by the concentration of the gas in the surrounding atmosphere (C_g^{atm}).^{113,114} Both concentrations are given in units of molarity. Assuming that the interaction energy E_i is independent of the solvent leads to a linear relation between $\ln L$ and the surface tension σ .

$$\ln L = \ln \frac{C_g^L}{C_g^{\text{atm}}} = - \frac{4\pi r^2 \sigma + E_i}{k_B T} \quad (3.1)$$

Although bulk surface tension might not be appropriate to calculate the energy of formation of a molecular-sized cavity, the model agrees well

Figure 3.1. Logarithm of L of O_2 as function of the surface tension for solvents used in Li/O_2 batteries. Data taken from own measurements and ref. 25,115–119. The numerical values as well as the fit parameters are given in Table B.1.



with experiments.¹⁰⁸ Figure 3.1 shows the O_2 solubility for some solvents used in Li/O_2 batteries. The positive y -axis intercept corresponds to an attractive interaction between oxygen and the solvents. Up to this point, the described theory refers to pure solvents and not electrolytes used in Li/O_2 batteries, which consist of a mixture of different solvents and salts. For electrolytes, salting in and salting out effects have to be considered to describe comprehensively the solubility of gases. Salting in/out refers to the increase/decrease of the solubility of a solute when increasing the ionic strength of a solution. The theoretical approaches to describe the effect of salting in/out can be classified into four categories: (1) hydration, (2) electrostatic, (3) van der Waals, and (4) internal pressure effects:

(1) Hydration theories assume that hydration of ions leads to effective removal of water molecules from their role as a solvent, explaining the salting out. In contrast, these theories do not provide an explanation for the salting in of solutes.

(2) Electrostatic theories relate the salt effects to the influence of the non-electrolyte on the dielectric constant of the solvent. In general, they can be divided into two approaches: On the one hand, the approach of Debye, which states that a non-electrolyte is salted in, when it increases the dielectric constant of the solvent. A non-electrolyte, which lowers the dielectric constant, is salted out.¹²⁰ For this, the non-electrolyte must have a higher total molecular polarization than the solvent. On the other hand, the approach of lyotropic salting in, which occurs when the total molecular polarization of the non-electrolyte is lower than that of the solvent and when salting out should occur according to other theories of ion-solvent interactions. Since oxygen has a low total polarization, salting in can be understood as lyotropic salting in.^{121,122}

(3) Van der Waals theories extend electrostatic theories by considering short-range forces, especially dispersion forces. These can play a significant role in the specific effects of ions.¹⁰⁸

(4) The internal pressure of a salt solution can be related to changes in the volume and compressibility of a solvent due to the dissolved salts. Both changes have been associated with salt effects.¹²³

Taking into account salting in/out effects, a comprehensive description of the solubility of O₂ (and other gases in general) in the electrolyte is possible. In the literature, instead of the solubility L , the Henry's law constant H^p (units: mol L⁻¹ bar⁻¹) is often used, which describes the pressure dependence of the [O₂] in the electrolyte. The Henry's law constant allows a direct comparison of different electrolytes at a given O₂ partial pressure and gives direct access to the [O₂] in the electrolyte and thus to the concentration of the actual active material of the battery. The next section deals with the diffusion behavior of gases in liquids to understand better the transport of oxygen in Li/O₂ batteries.

3.2 DIFFUSION OF GASES IN LIQUIDS

Diffusion, together with solubility, plays a critical role in Li/O₂ batteries. The cathode active material oxygen is not stored inside an electrode or in the electrolyte but instead in the gas phase above the electrolyte. Thus, during discharging, oxygen must be transported from the gas phase, through the electrolyte, to the electrode surface, where it is consumed (and vice versa during charging). During discharging, the electrode surface acts as a sink for oxygen, leading to a depletion of O₂ in its environment: A concentration gradient is formed, which results in a flux of O₂ to the electrode. The diffusion to the electrode surface can be described by Fick's 1st law of diffusion (here in the 1D case):⁸²

$$j_i = -D_i \frac{\partial c}{\partial x} \quad (3.2)$$

where j_i is the flux of species i in mol cm⁻²s⁻¹, corresponding to the number of moles passing through a given area in a given time, $\partial c/\partial x$ is the local concentration gradient at point x and D_i is the diffusion coefficient of species i . The negative sign in Equation (3.2) implies that the flux is down the concentration gradient. The unit of D is cm² s⁻¹ and the magnitude of D lies typically in the range of 10⁻⁶ – 10⁻⁵ cm²s⁻¹ at room temperature. Diffusion coefficients are temperature-dependent and often follow Arrhenius-type relationships:

$$D = D_{\infty} \exp\left(\frac{-E_a}{RT}\right) \quad (3.3)$$

where E_a in kJ mol^{-1} is the activation energy for diffusion and D_{∞} is the hypothetical value of D at an infinite temperature T .

As stated in Equation (3.2), Fick's 1st law assumes that the flux is driven solely by a concentration difference within the solution or electrolyte and no electric fields are involved. In the case of oxygen where the diffusion species is uncharged, the presence of an electric field does not influence the flux, but in the case of ions, such as Li^+ or O_2^- , a significant effect can be expected. However, the use of sufficient quantities of electrolyte salts eliminates this effect (except regions very close to the electrode), and even Li^+ and O_2^- move in the electrolyte via diffusion (and sometimes convection).

While Fick's 1st law describes the flux at a point x , it does not give any information on how the concentration at x will vary over time. This information is given by Fick's 2nd law (in the 1D case):

$$\frac{\partial c}{\partial t} = -\frac{\partial j}{\partial x} = D \frac{\partial^2 c}{\partial x^2} \quad (3.4)$$

where $\partial c/\partial t$ is the rate of change in concentration at point x .

Fick's law of diffusion provides a measure of the distance a molecule migrates (diffuses) over time:

$$\sqrt{\langle x^2 \rangle} = \sqrt{2Dt} \quad (3.5)$$

where $\langle x^2 \rangle$ is the mean square displacement. The equation also shows a diffusing species' motion decreases dramatically with distance from the source, meaning a small solute can only effectively diffuse a small distance in a short time.

Equation (3.5) assumes infinite space as a boundary condition, which is not met in real Li/O_2 batteries. Instead, constant diffusion through a thin film can be assumed, limited by the electrode on one side and by the atmosphere on the other side. These transport conditions can also be described by a Nernst diffusion layer model (Figure 3.2). The electrode acts as oxygen sink, resulting in $[\text{O}_2] = 0 \text{ mol L}^{-1}$ as a limiting case. The interface with the gas reservoir is held at a constant oxygen concentration, described by the Henry's law constant of oxygen in the respective electrolyte. When steady state conditions are met, Equation (3.2) can be written as:

$$j = -D \frac{\partial c}{\partial x} = D_{O_2} \frac{[O_2]^*}{\delta} \quad (3.6)$$

where δ is the thickness of the electrolyte layer and $[O_2]^*$ is the oxygen concentration at the electrolyte/atmosphere interface.

The resulting limiting current i_{lim} is given by

$$i_{lim} = \frac{nFA_s D_{O_2} [O_2]^*}{\delta} \quad (3.7)$$

where A_s is the surface area of the electrode. The Nernst diffusion layer and Equations (3.5) and (3.7) also explain why less discharge product is found in deeper regions of the cathodes of metal/ O_2 batteries. Areas further away from the electrolyte/gas reservoir interface have a larger δ and $\langle x^2 \rangle$, resulting in a smaller i_{lim} . Following the Nernst diffusion layer model, smaller δ and/or larger $[O_2]^*$ result in a larger i_{lim} . A smaller δ can be achieved by using less electrolyte, resulting in only partly flooded cathodes, optimizing oxygen flux inside the electrode. A larger $[O_2]^*$ can be achieved by higher oxygen partial pressures in the gas reservoir. Theoretically, a tenfold higher oxygen partial pressure would result in a tenfold higher limiting current.

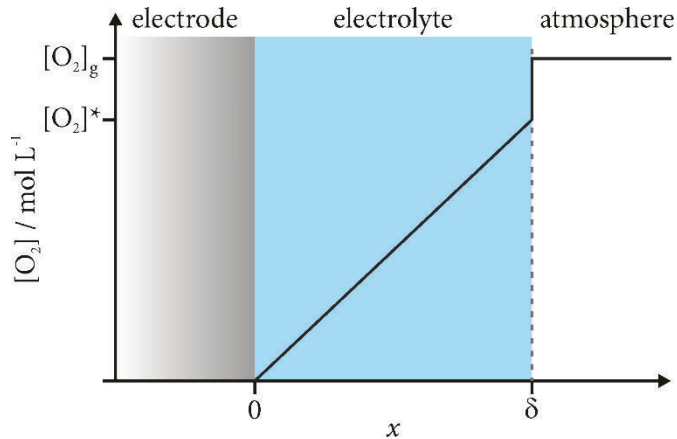


Figure 3.2. Nernst diffusion layer model of O_2 diffusion in Li/O_2 batteries. At steady state conditions, a stagnant diffusion layer in the electrolyte is formed, limiting the flux to the electrode. $[O_2]_g$ denotes the concentration of O_2 in the surrounding atmosphere. The drop in $[O_2]$ at the interface between the atmosphere and the electrolyte represent a solubility $L < 1$.

Indeed, such behaviour has been found in literature. Read *et al.* reported on the influence of oxygen solubility and D_{O_2} on the specific capacity of Li/O_2 cathodes.⁵³ Here, the capacity rose with increasing oxygen solubility and decreasing viscosity of the electrolyte. This trend is in line with the Stokes-Einstein-Equation, which relates the diffusion coefficient to the size of the solute and the viscosity of the solvent:

$$D = \frac{k_B T}{6\pi\eta_{\text{dyn}}r} \quad (3.8)$$

where η_{dyn} is the dynamic viscosity of the solvent. They also found a limiting discharge capacity for higher oxygen partial pressures. In these cases, the discharge capacity is not limited by the oxygen depletion in the electrolyte, but solely depends on the blocking of the electrode surface by deposited Li_2O_2 .

Although the theory introduced here can explain and predict the trends found in Li/O_2 batteries, real Li/O_2 batteries are much more complicated. For example, the morphology of cathodes changes during cycling, i.e., active electrode area is blocked by deposited Li_2O_2 , and the pore distribution changes towards smaller pores. The studies by Read *et al.* presented above used cathodes that were completely flooded with electrolyte, whereas studies today use partially flooded cathodes to support the diffusion of oxygen.^{52,53} To describe the diffusion of oxygen inside the cathode, more advanced models are used nowadays to include the tortuous character of the electrode.^{124–126}

Theory of Electron Transfer

4

Lithium/O₂ batteries face many challenges, one of these being their sluggish kinetics and high overvoltages. A fundamental understanding of the processes occurring in Li/O₂ batteries is essential to develop targeted solutions, such as suitable catalysts, electrolytes, or cathode materials. However, the reaction mechanisms are complex and not yet fully understood (see Section 2.3). In addition, there is a lack of theoretical models to describe fully the processes within batteries. This chapter provides a short introduction to the description of electron transfer in electrochemistry and its limitations in the case of (Li/O₂) batteries. Publication II (Chapter 6) then deals in detail with singlet oxygen from the point of electrochemical kinetics.

4.1 BUTLER–VOLMER KINETICS

One of the most widely used and versatile theories for describing electron transfers was introduced by Butler, Erdey-Grúz and Volmer, and is today known as Butler–Volmer kinetics.[‡] Although it was initially established completely empirically, today it is often derived from transition state theory or from considerations of electrochemical potentials. The following short description is based on the derivation from the transition state theory.¹²⁷ Starting from a simple 1e[−] reduction:



where O is the oxidized species and R is the reduced species. At equilibrium, both cathodic and anodic reaction have identical reaction rates, so that the concentrations of the two species remain constant (Equation (4.2)).[§] The concentrations are linked to the electrode potential E by the Nernst Equation (4.3):

$$\frac{k_c}{k_a} = K = \frac{[\text{R}]}{[\text{O}]} \quad (4.2)$$

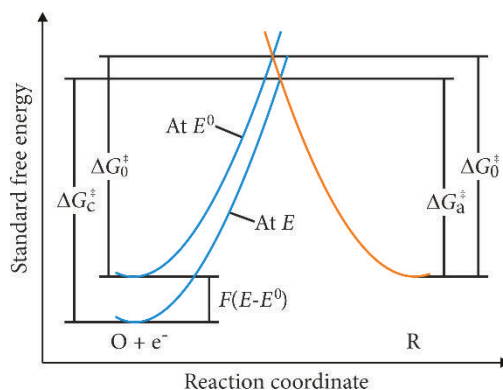
[‡] The naming of the Butler–Volmer equation was debated in the literature. A summary can be found in ref. 150 and 151.

[§] Such an agreement is required of any kinetic theory. In the limit of equilibrium, the kinetic equations must collapse to relations of the thermodynamic form; otherwise, the kinetic picture cannot be accurate. Chemical kinetics describes the evolution of mass flow throughout the system, including both the approach to equilibrium and the dynamic maintenance of that state. Thermodynamics describes only equilibrium.¹²⁷

$$E = E^{\circ} + \frac{RT}{nF} \ln \left(\frac{[O]}{[R]} \right) \quad (4.3)$$

Therefore, a change in the electrode potential leads to a change in the equilibrium and the corresponding reaction rates. To describe the impact of the potential change on the kinetics, one needs to consider the reaction coordinate, which is shown in Figure 4.1.

Figure 4.1. Effects of a potential change on the standard free energies of activation for oxidation and reduction.



The cathodic and anodic reactions have different energy barriers ΔG_c^{\ddagger} and ΔG_a^{\ddagger} for both potentials, which directly determine the corresponding rate constants. A change in the electrode potential results in a shift in the potential curve of the electrode relative to the potential curve of the solution. The Butler–Volmer approximation assumes that an increase in the driving force of the reaction is divided into two parts: one, α , to the advantage of oxidation and one, $1 - \alpha$, to the disadvantage of reduction (vice versa in the case of an oxidation). It is assumed that the transfer coefficient α is independent of the applied potential, leading to the following linear relationships for ΔG^{\ddagger} :

$$\Delta G_a^{\ddagger} = \Delta G_0^{\ddagger} - \alpha F(E - E^{\circ}) \quad (4.4)$$

$$\Delta G_c^{\ddagger} = \Delta G_0^{\ddagger} + (1 - \alpha)F(E - E^{\circ}) \quad (4.5)$$

And for the corresponding rate constants:

$$k_a = k_0 \exp \left(\frac{\alpha F}{RT} (E - E^{\circ}) \right) \quad (4.6)$$

$$k_c = k_0 \exp \left(\frac{-(1 - \alpha)F}{RT} (E - E^{\circ}) \right) \quad (4.7)$$

where k_0 is defined as the standard rate constant at $E = E^\circ$. Since the measured current i is a net current, both oxidation and reduction proceed simultaneously. The current i can be expressed as the sum of the individual currents (cathodic currents are negative by definition):

$$i = i_a + i_c = nFA(k_a[R] - k_c[O]) \quad (4.8)$$

Substitution yields the Butler-Volmer equation:

$$i = nFAk_0 \left([R] \exp\left(\frac{\alpha F}{RT}(E - E^\circ)\right) - [O] \exp\left(\frac{-(1 - \alpha)F}{RT}(E - E^\circ)\right) \right) \quad (4.9)$$

The Butler-Volmer equation is often expressed in terms of the exchange current density j_0 . At equilibrium ($E = E^{\text{eq}}$), the net current density is zero and $j_a = j_c = j_0$. In this case, j_0 can be defined as:

$$j_0 = nFk_0[R] \exp\left(\frac{\alpha F}{RT}(E^{\text{eq}} - E^\circ)\right) \quad (4.10)$$

Writing (4.3) in an exponential form and raising to the power of α gives (4.11), which can be substituted into (4.10) to yield (4.12):

$$\exp\left(\frac{\alpha F}{RT}(E^{\text{eq}} - E^\circ)\right) = \left(\frac{[O]}{[R]}\right)^\alpha \quad (4.11)$$

$$j_0 = nFk_0[O]^\alpha [R]^{1-\alpha} \quad (4.12)$$

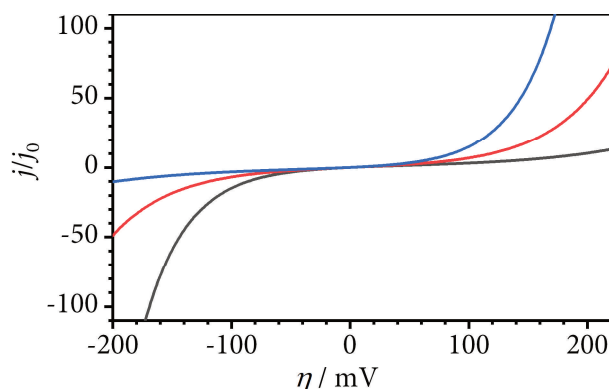
Substituting Equation (4.10) into Equation (4.9) and introducing the applied overpotential $\eta = E - E^{\text{eq}}$ finally leads to Equation (4.13):

$$j = j_0 \left(\exp\left(\frac{\alpha F}{RT}\eta\right) - \exp\left(\frac{-(1 - \alpha)F}{RT}\eta\right) \right) \quad (4.13)$$

Figure 4.2 shows corresponding current-potential profiles for different α . The absolute current density increases exponentially with increasing η . However, mass transfer becomes a limiting factor at high reaction rates resulting in a limited current density at high η (not shown).

The charge transfer kinetics is essentially characterized by the exchange current density j_0 and its standard rate constant k_0 , which mainly depend on the nature of the redox couple, the electrolyte, and the electrode material. The current profile is additionally influenced by the transfer coefficient α , which characterizes the symmetry of the activation barrier. Most redox reactions fall in the range of $0.3 < \alpha < 0.7$.

Figure 4.2. Normalized current density as a function of the applied overpotentials at 298 K for different α . Grey curve: $\alpha = 0.3$; red curve: $\alpha = 0.5$; blue curve: $\alpha = 0.7$. Calculated from Equation (4.13)(4.15).



Although extremely useful in practice, the Butler–Volmer equation is entirely empirical, with no justification of its linear character (Equation (4.4) and (4.5)) and no prediction of how the rate constants could be related to the molecular structure of the reactants and to the characteristics of the reaction medium. Thus, the Butler–Volmer equation cannot sufficiently describe and predict the processes occurring in Li/O₂ batteries. In contrast, the Marcus theory and the Gerischer model address these issues and will be described in more detail in the next chapters.

4.2 MARCUS–THEORY

The semiclassical Marcus–Hush model of outer-sphere electron transfer addresses the limitations of the Butler–Volmer model. The theory was employed initially for homogeneous electron transfer reactions, e.g., self-exchange reactions and redox reactions in solution. Later, the theory was extended to include heterogeneous, outer-sphere electron transfer on electrodes (e.g., electron transfer to and from complexed metal ions).^{90,127–130} Marcus theory starts with the description of reactants and products as parabolas along a reaction coordinate, which is shown in Figure 4.3.

The transition state is located at the intersection between the two parabolas. At this point both reactants and products have the same energy and configuration.⁸³ This satisfies both energy conservation (the electron transfer is a radiationless process) and the Franck–Condon principle (nuclear momenta and positions do not change on the time scale of the electron transfer).⁸³ The observed ΔG^\ddagger of the electron transfer also results from these conditions, since thermal activation of the reactants is necessary to reach the energy of the transition state.

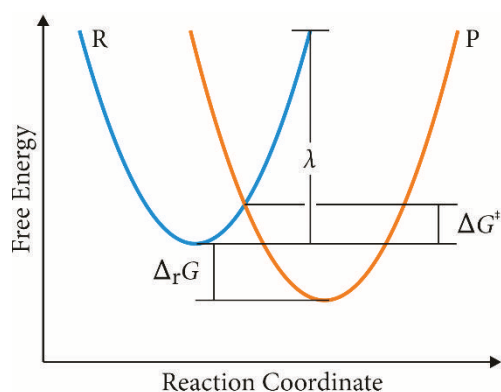


Figure 4.3. Schematic representation of the Marcus theory. The blue parabola R corresponds to the Gibbs energy of the reactants; the orange parabola P corresponds to that of the products. The energy of the reactant parabola at the minimum of the reactant parabola, the so-called reorganization energy λ , is a measure of the E_a required.

While Butler–Volmer kinetics are characterized by j_0 and α , Marcus theory describes a system with $\Delta_r G$ and λ , the so-called reorganization energy. λ represents the energy necessary to transform the nuclear configurations in the reactant and the solvent to those of the product state. It is usually separated into inner, λ_i , and outer, λ_o , components:

$$\lambda = \lambda_i + \lambda_o \quad (4.14)$$

where λ_i represents the contribution from reorganization of the reactant species, and λ_o that from reorganization of the solvent. The reorganization energy can be calculated and simulated for a given system. The activation energy for electron transfer can then be calculated by Equation (4.15). Assuming Arrhenius-type kinetics, the rate constant can be determined using (4.16). The term A depends on the nature of the electron transfer reaction (bimolecular, intramolecular, or heterogeneous) and can contain statistical factors.

$$\Delta G^\ddagger = \frac{1}{4\lambda} (\Delta G^\circ + \lambda)^2 \quad (4.15)$$

$$k = A \exp\left(-\frac{\Delta G^\ddagger}{RT}\right) \quad (4.16)$$

Besides the calculation of reaction rates, the theory's greatest value is the chemical and physical insight derived from its ability to predict and generalize electron-transfer reactions. For example, if the oxidized and reduced species are close in molecular geometry (i.e., bond lengths, bond angles), then k is large corresponding to a low activation barrier for reaction (vice versa for structurally dissimilar O and R). Also, reactions with larger $\Delta_r G$ proceed faster. One of the predictions of Marcus theory was the existence of an inverted region. In the case of

highly exothermic reactions, the intersection point between the two parabolas can cross the minimum of the reactant parabola and migrate upwards again. This results in slower kinetics than what would be expected from the high $\Delta_r G$. This prediction was later experimentally confirmed by Closs and Miller in 1984.^{131,132}

Marcus theory and the inverted region can also be used to explain chemiluminescence reactions when accompanied by electron transfer.¹³³ In chemiluminescence reactions, a very exergonic electron transfer to the ground state is substituted by a less exergonic but faster transfer to an excited state. The excited species then decays to the ground state via emission of a photon with an energy approximately equal to the difference in enthalpies. Marcus theory offers therefore a theoretical framework for generation of excited states by electron transfer reactions. Hence, it is the prime theory for describing and understanding $^1\text{O}_2$ formation in Li/O₂ batteries. A more detailed introduction into the Marcus theory, a mathematical treatment, and an analysis of the Li/O₂ system is given in Publication II (Chapter 6).

4.3 GERISCHER MODEL

An alternative theoretical approach to describe heterogeneous kinetics is based on the overlap between the electronic states of the electrode and those of the reactants in solution. The concept is illustrated in Figure 4.4 and briefly discussed in this section.^{127,134–136} This model originates from contributions by Heinz Gerischer in 1968 and is particularly useful for describing electron transfer at semiconductor electrodes, where the electronic structure of the electrode material is important. The idea is that electron transfer can occur from any occupied energy state, which matches in energy ϵ an unoccupied receiving state. If the process is a reduction, the occupied state is on the electrode and the receiving state is on a reactant O in the solution (vice versa in the case of an oxidation). In general, the states under consideration span a range of energies, and the total rate is an integral of the rates at each energy. At the electrode, the number of unoccupied and occupied electronic states can be calculated from the density of states of the material and the Fermi distribution for the given temperature. As the applied potential changes, the Fermi level shifts, leading to higher energies at more negative potentials. For a metal electrode, these changes do not occur by filling or emptying additional states, but rather by charging the metal so that all states are shifted. The charging results in a change in the total electron population on the metal, but this change is only a tiny fraction. Consequently, there is the

same number of states near the Fermi level ε_F at all potentials. States in solution are described by a similar concept, except that filled and empty states correspond to different chemical species, namely the two components of a redox couple, R and O, respectively. These states differ from those of the metal in that they are localized.

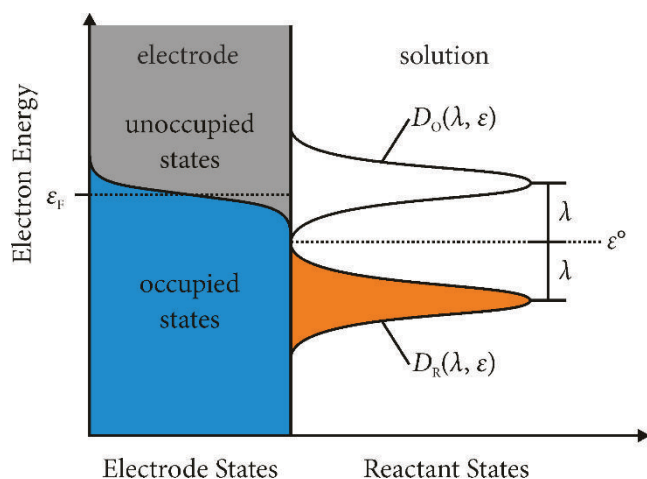


Figure 4.4. Gerischer model for a metal electrode and a solution containing equal concentrations of species O and R. On the electrode side, the Fermi level, ε_F , and the corresponding distribution of occupied states is shown in blue. On the solution side, the state density distributions are shown for O and R (occupied states in orange). The maxima of the two density distributions are located at $\varepsilon^\circ \pm \lambda$.

Knowing the distribution of the empty and occupied states in the electrode and the solution, a local (i.e., in a small energy range) reaction rate of reduction and oxidation can be calculated. Integration over all possible states leads to the rate constants of reduction and oxidation.

$$k_c = \nu \int_{-\infty}^{\infty} \gamma_{\text{red}}(\varepsilon) W_{O,\lambda}(\varepsilon) f(\varepsilon) \rho(\varepsilon) d\varepsilon \quad (4.17)$$

$$k_a = \nu \int_{-\infty}^{\infty} \gamma_{\text{ox}}(\varepsilon) W_{R,\lambda}(\varepsilon) [1 - f(\varepsilon)] \rho(\varepsilon) d\varepsilon \quad (4.18)$$

where ν is a frequency factor, $\gamma_{\text{ox}}(\varepsilon)$ and $\gamma_{\text{red}}(\varepsilon)$ are proportionality functions, $W_{O,\lambda}(\varepsilon)$ and $W_{R,\lambda}(\varepsilon)$ are the probability density functions of O and R respectively, $f(\varepsilon)$ is the Fermi distribution, and $\rho(\varepsilon)$ is the density of states.

In Figure 4.4, the distribution of states for species R does not overlap with the range of unoccupied states on the electrode, so the integrand in Equation (4.18) is virtually zero everywhere and k_a is negligible compared to k_c . The electrode is in a reducing state with respect to the O/R pair. By changing the electrode potential to a more positive value, the position of the Fermi level is shifted to lower energies where the R states begin to overlap unoccupied electrode states so that the integral in Equation (4.18) becomes significant and k_a is increased. With

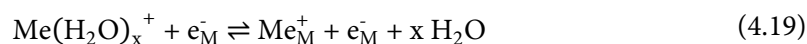
Equations (4.17) and (4.18) it is possible to account for kinetic effects due to the electronic structure of the electrode by using an appropriate density of states $\rho(\epsilon)$ for the electrode material.

The Gerischer model can also be combined with Marcus theory, which simplifies some of the mathematical concepts mentioned above. As in Marcus theory, the magnitude of the reorganization energy has a large effect on the current-potential behavior of the system under consideration. In the case of a larger λ , the distribution functions of the species in solution are broader and further apart, leading to smaller k_c and k_a . This leads, as in Marcus theory, to larger overpotentials compared to systems with small λ .

While the Gerischer model is very useful for describing electron transfer at semiconductor electrodes, and it has been used to describe the dissolution of semiconductors, the model has rarely been for batteries.^{137–139} Kurchin *et al.* used the model to account for the electronic structure of lithium metal anodes while stripping and plating. No experimental efforts have been made to date in the case of Li/O₂ batteries. Instead, Tafel analysis, Butler–Volmer kinetics and Marcus theory have been used.^{92,103,140–143}

4.4 DESCRIPTION OF ELECTRON TRANSFER IN BATTERIES

In the analysis of electrode reactions, it is usually implicitly assumed that charge transfer occurs by the transfer of electrons at the interface between the electrode and the solution.¹⁴⁴ However, this is not always the case. The simplest example is the deposition or dissolution of a metal from/into a solution:^{144,145}



The electron is either in the electrode or in the deposited metal on both sides of the reaction (designated with the index M). Therefore, the charge transfer across the interface must be through the cation. The same is true for the operation of Li-ion batteries, in which the charge is carried by the lithium ions across the electrode-electrolyte interface. Thus, it is not legitimate to assume *a priori* that charge transfer in all electrode reactions occurs by the transfer of an electron, and the mechanisms developed based on this assumption can and must be questioned. Since it is not an electron but an ion that is transferred, the reactions also occur on different time scales. While an electron transfer through the outer Helmholtz layer takes only a few femtoseconds, the diffusion of an atom would take about 10⁶ femtoseconds for the same

distance.¹⁴⁴ Therefore, the charge transfer across the interface in such a case is also not instantaneous. During the deposition process of a metal, a gradual stripping of the solvation shell can be assumed, and the charge transfer therefore does not occur in one step either. Thus, such reactions cannot be described using Marcus theory since neither the Born–Oppenheimer approximation nor the Franck–Condon principle can be applied. Moreover, it is not an outer sphere electron transfer either since the ion breaks bonds or forms new ones during the reaction under consideration. The use of the Butler–Volmer equation must also be treated with caution in such cases. In the deposition of metals, it has been assumed that electrons are transferred one at a time and adsorbed intermediates may be formed. Since these intermediates are not stable in solution, it was assumed that they are stabilized by adsorption onto the electrode surface.¹⁴⁴

In the case of Li/O₂ batteries, the Butler–Volmer equation and Marcus theory were used to describe the charge transfer.^{146,147} This seems appropriate in the case of the oxygen reduction reaction, since the charge transfer here is via an electron from the electrode to oxygen in solution. However, in the case of the charge transfer during the oxygen evolution reaction it is a charge transfer via ions, which clearly argues against the use of Butler–Volmer theory as well as Marcus theory. Caution is advisable when using these models. Clearly, the use of inappropriate models can and will lead to erroneous results and hold up progress in (Li/O₂) battery research.

Notably, Fraggedakis *et al.* proposed a new model to describe charge transfer in intercalation electrodes.¹⁴⁸ They developed a theory of coupled ion–electron transfer, in which ions and solvent molecules act cooperatively to facilitate electron transfer. In the case of lithium iron phosphate electrodes, the theory can accurately predict the concentration dependence of the exchange currents.¹⁴⁸ This appears to be an important step in describing the kinetics of battery active materials. However, up to this date, no efforts have been made in literature to implement or extend the model to Li/O₂ batteries.

Overall, the theory of electron transfer in batteries should be further advanced to improve the understanding of charge transfer processes in batteries. Then, it will be possible to manipulate and optimize processes in batteries in a targeted manner, which in turn is essential for the design and development of new of energy materials and batteries.

PART II

RESULTS AND DISCUSSION



Diffusivity and Solubility of Oxygen in Solvents for Metal/Oxygen Batteries: A Combined Theoretical and Experimental Study

One of the goals of this thesis was a better understanding and description of the Transport of oxygen inside Li/O₂ batteries. The solubility and diffusion coefficient of oxygen in the electrolyte are crucial parameters: they govern the maximal discharge current and have an influence on the achievable discharge capacity. Precise measurement of both parameters is challenging, which can also be seen in literature, where values scatter widely. This chapter compares theoretical and experimental approaches, namely oxygen uptake experiments and molecular dynamic simulations, to determine oxygen diffusion coefficients and Henry's law constants H^{cp} in several glymes and perfluorinated solvents. The experimental measurements and theoretical calculations of diffusion coefficients agree well, showing that simulation of diffusion coefficients of oxygen in solvents and electrolytes is possible.

The experiments and concepts presented in this publication were developed by the author of this thesis, under the supervision of J. Janek and D. Schröder. The manuscript was written by the first author and edited by all co-authors. A. Schürmann prepared the samples and conducted the measurements of diffusion coefficients and Henry's law constants. R. Haas conducted some of the measurements of diffusion coefficients and Henry's law constants under the supervision of A. Schürmann. M. Murat, N. Kuritz and A. Natan performed the molecular dynamic simulations. M. Balaish and Y. Ein-Eli contributed to the scientific discussions.

Reprinted with permission from A. Schürmann, R. Haas, M. Murat, N. Kuritz, M. Balaish, Y. Ein-Eli, J. Janek, A. Natan, and D. Schröder, Diffusivity and Solubility of Oxygen in Solvents for Metal/Oxygen Batteries: A Combined Theoretical and Experimental Study, *Journal of The Electrochemical Society* **2018**, 165, A3095–A3099. DOI: 10.1149/2.0601813jes. Copyright 2018 The Electrochemical Society.

5





Diffusivity and Solubility of Oxygen in Solvents for Metal/Oxygen Batteries: A Combined Theoretical and Experimental Study

Adrian Schürmann,^{1,2} Ronja Haas,¹ Michael Murat,^{3,4} Natalia Kuritz,³ Moran Balaish,⁵ Yair Ein-Eli,^{5,*} Jürgen Janek,^{1,2,*} Amir Natan,^{3,z} and Daniel Schröder^{1,2,z}

¹Institute of Physical Chemistry, Justus Liebig University Giessen, 35392 Giessen, Germany

²Center for Materials Research (LaMa), Justus Liebig University Giessen, 35392 Giessen, Germany

³Department of Physical Electronics, Tel-Aviv University, Tel-Aviv 69978, Israel

⁴Soreq NRC, Yavne 81800, Israel

⁵Department of Materials Science and Engineering and The Grand Technion Energy Program, Technion - Israel Institute of Technology, Haifa 3200003, Israel

The solubility and the diffusion constant of oxygen in the electrolyte are crucial parameters in the kinetics of metal/oxygen batteries since they govern the discharge current that can be achieved. However, both parameters are often unknown or scatter widely in literature. Evaluating these parameters in typical solvents and electrolytes is therefore essential toward better quantitative understanding and improvement of metal/oxygen batteries. Using oxygen uptake experiments and molecular dynamics simulations, we compare theoretical and experimental approaches to determine oxygen diffusion coefficients in several molecular solvents that are commonly used. We report diffusion coefficients and Henry's law constants of oxygen for a series of glymes with different chain length and perfluorinated solvents, and discuss the benefit of using both experiment and simulation to determine these parameters. In all nine investigated solvents, the difference between simulated and measured diffusion coefficients is small in comparison to the magnitude of the coefficients. The methodology and the reported values for oxygen solubility and diffusivity form a solid starting point for further investigations into more complex electrolyte solutions. Ultimately, they might help to propel research on metal/oxygen batteries even further.

© The Author(s) 2018. Published by ECS. This is an open access article distributed under the terms of the Creative Commons Attribution Non-Commercial No Derivatives 4.0 License (CC BY-NC-ND, <http://creativecommons.org/licenses/by-nc-nd/4.0/>), which permits non-commercial reuse, distribution, and reproduction in any medium, provided the original work is not changed in any way and is properly cited. For permission for commercial reuse, please email: oa@electrochem.org. [DOI: 10.1149/2.0601813jes]



Manuscript submitted July 25, 2018; revised manuscript received September 10, 2018. Published September 28, 2018.

Despite serious challenges, rechargeable metal/oxygen batteries are still considered as highly promising electrochemical energy storages for future applications, primarily because of their high theoretical energy density.^{1–6} Even if their practical use is currently out of reach, metal/oxygen batteries are excellent research subjects, as they combine some of the most difficult issues in electrochemistry: a) Their use requires reversible and dendrite-free metal dissolution and deposition in liquid electrolytes at sufficiently high current densities – which has yet not been demonstrated unequivocally.^{7,8} b) Their use also requires reversible oxygen reduction and oxidation with sufficient rates at low overpotentials at room temperature.⁴ c) The electrolyte components and the cathode material(s) need to be long-term stable against attack by reactive oxygen species.⁴

Most of the research on non-aqueous metal/oxygen batteries has focused on the cathode side, where oxygen is reduced sequentially to superoxide and peroxide species during discharge, and where these species may react with electrolyte components or the cathode surface.^{9–13} As important side aspect of the cathode studies, the stability of electrolyte components, i.e. solvents and conducting salts, as well as the diffusion and solubility of oxygen and other ions and molecules in the electrolyte have been investigated. These are important parameters in any micro-kinetic model of metal/oxygen batteries (see papers by Gröbl et al.).^{14–18}

The role of the electrolyte is quite different for the two general types of electrodes that exist in state-of-the-art batteries: In the case of intercalation-type electrodes, the electrolyte mainly transports lithium ions, but may also contain dissolved functional additives. The redox process at the electrode itself relies on the transport and transfer of lithium ions from the liquid electrolyte. In the case of electrodes with mobile redox species, such as oxygen gas electrodes or sulfur electrodes, the electrolyte acts as transport (and storage) medium for lithium ions and redox-active species (see Fig. 1). Thus, its role for efficient electrode kinetics is even more important. Indeed, the choice of the electrolyte has been proven to influence e.g. the reaction mech-

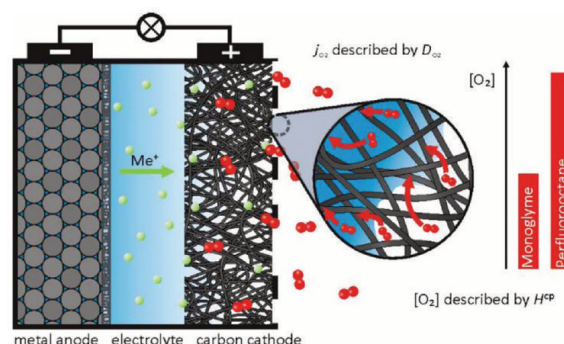


Figure 1. Schematic representation of a metal/oxygen battery with detailed depictions of the path for oxygen diffusion inside the cathode. The oxygen concentration $[O_2]$ depends on the used solvent and can be described with the help of the Henry's law constant. The flux of oxygen j_{O_2} to the electrochemical active site depends on the diffusion coefficient inside the solvent and on the reaction rate at the electrochemical active surface of the cathode.

anism in non-aqueous Li/O_2 and Na/O_2 batteries.^{19–28} In addition, it was shown that the solubility and transport of oxygen (O_2) in these cells have a direct impact on the capacity and the upper limit of the current density, as well as on the distribution of the discharge product in the porous cathode.^{29–37}

Formulating non-aqueous electrolytes with excellent oxygen mobility properties is a challenging task, which could be eased through the introduction of additives. Perfluorocarbons (PFCs), liquids with superior oxygen solubility and diffusivity, are advocated as the perfect oxygen-carrier additives with extraordinary chemical stability, fast dissolution kinetics and high oxygen solubility.^{38–40} Given their distinct chemical and physical properties, PFCs could neither dissolve lithium salt nor are they miscible with most organic solvent, thus could only be used as a part of a hybrid organic-electrolyte/PFC system.

*Electrochemical Society Member.

^zE-mail: amiratan@post.tau.ac.il; daniel.schroeder@phys.chemie.uni-giessen.de

The promising properties and successful first-phase implementation of PFCs in Li/O₂ batteries encourages further evaluation and understanding of oxygen transportation in electrolyte and PFCs components, both separately and combined.^{41–44} Recently, the intriguing interplay between both components in a porous carbonaceous material at the cathode was reported and could serve as a fertile ground for further investigation and understanding of oxygen mobility in more complex structures.^{44,45} The second-phase implementation of PFC in organic electrolyte is envisioned through PFC nanodroplets architectures to obtain better distribution of molecular oxygen inside the porous structure of cathodes. Modelling and measuring oxygen solubility and diffusion coefficients as a function of PFC's size and distribution could largely assist to tailor desired parameters for optimized Li/O₂ batteries.

The solubility of oxygen in solvents is usually described by Henry's law, introducing Henry's law constant H^{cp} ,

$$H^{\text{cp}} = [\text{O}_2] \cdot p_{\text{O}_2}^{-1}, \quad [1]$$

where H^{cp} is Henry's law constant in mol L⁻¹ bar⁻¹, [O₂] is the concentration of oxygen in mol L⁻¹ and p_{O_2} the pressure of oxygen above the solvent in bar. From the practical point of view, Henry's law constant is a measure of the maximum concentration of oxygen that can be achieved in metal/oxygen batteries in the cathode electrolyte at a given pressure and temperature. Together with the diffusivity of oxygen, an upper limit of operating current, i.e. the mass transport-limiting current, can be calculated from the equation,⁴⁶

$$I_{\text{lim}} = nFA D_{\text{O}_2} [\text{O}_2] \delta^{-1} \quad [2]$$

for an idealized planar electrode, where n is the number of electrons in the rate limiting reaction, F is Faraday's constant, A is the surface area of the electrode, D_{O_2} is the reactant diffusion coefficient and δ is the cell-specific thickness of the Nernst layer across which the reactant oxygen must diffuse.

Accordingly, the selection of an appropriate electrolyte is critical to realizing the full potential of metal/oxygen batteries. In the field of metal/oxygen batteries, the concentration of molecular oxygen has been measured successfully in e.g. DMSO-, tetraglyme- and carbonate-based solvents and electrolytes.^{20,29,32,43,47–53} In addition, the influence of different Li-containing conducting salts and fluorinated ethers on the solubility was examined. Nevertheless, both Henry's law constant and the diffusion coefficient are still seldom known, and if, reported data scatter over a wide range.

Striving for a long-term systematic and precise approach toward a comprehensive data set, we combine molecular dynamics simulations and oxygen uptake experiments to determine diffusion coefficients and Henry's law constants for O₂ in a series of different glycol ethers (glymes) and perfluorinated solvents (PFC). Pure solvents – without conducting salt – were chosen as a reasonable and straightforward starting point for the comparison of theoretical and experimental results. Pure solvents can be seen as a test case for theory and are well suited to properly predict diffusivity and solubility. In fact, we show that both methods applied in this work are equally valid to evaluate diffusion coefficients and that the results agree well. The reported values for oxygen solubility and diffusivity will be helpful for further research on metal/oxygen batteries.

Experimental

Chemicals.—All pressure measurements in this work were carried out using a PAA-33X absolute pressure sensor, a K104B USB computer adapter, and the Software Control Center Series 30 (all from KELLER Gesellschaft für Druckmesstechnik mbH). All chemicals were purchased from Sigma-Aldrich: perfluorohexane (99%), perfluorooctane (98%), perfluorononane (97%), perfluorodecaline (95%), 2-methoxyethanol (99.8%), sodium hydride (NaH, 95%) and tri(ethylglycol) ditosylate (98%). Pentaglyme was synthesized in-house as described by Akazome et al.⁵⁴ ¹H NMR (CDCl₃, 400 MHz): $\delta = 3.64\text{--}3.59$ (m, 16 H, CH₂), $\delta = 3.58\text{--}3.53$ (m, 4 H, CH₃-O-CH₂-CH₂), $\delta = 3.36$ (s, 6 H, CH₃-O). Solvents were dried

over molecular sieves (0.3 nm) prior use. Oxygen (5.0/99.999%) from Praxair was used.

Determination of gas volumes.—The volumes of the different gas reservoirs were determined by parallel use of the pressure sensor and a calibrated syringe (Hamilton). Further information and data plots are provided in the Supporting Information.

Oxygen uptake experiments for Henry's law constants.—A modified setup, previously described by Hartmann et al. and Bergner et al. was used.^{47,55} For the bulk electrolyte experiments, a glass cell (approximately 12 cm³) with magnetic stirrer was used. The cell was connected to a stainless steel cross fitting (Swagelok). To this cross fitting, the pressure sensor, oxygen gas container, and vacuum pump were connected as well, each separated by a manual ball valve (Swagelok). Further information and data plots are provided in the Supporting Information.

Oxygen uptake experiment for diffusion coefficients.—A modified setup, previously described by Hou et al. and Hartmann et al. was used.^{47,56} A stainless steel container of cylindrical shape (19.8 mm diameter) with a total volume of approximately 8.5 cm³ was used. A vacuum pump and the above-mentioned pressure sensor were mounted to the cylindrical cell via separate connectors. Oxygen supply was controlled using a manual ball valve and a small oxygen reservoir. Further information and data plots are provided in the Supporting Information.

Molecular dynamic simulations.—Molecular Dynamics (MD) simulations of glymes and perfluorinated carbon solvents with varied molecular length were performed using the LAMMPS package.⁵⁷ Initial structures and LAMMPS input files were constructed using Packmol and Moltemplate packages respectively.^{58,59} The OPLS-AA⁶⁰ force field (FF) was adopted for PFC⁶¹ and glymes.⁶² This force field was shown to give reasonable densities and heats of vaporization for perfluoroalkanes⁶³ and other organic liquids.⁶⁴ For glymes, we used the torsion parameters given in Table IV of Anderson and Wilson,⁶² in rows corresponding to the DME force field.⁶² These force field parameters were chosen as they resulted in densities and self-diffusion coefficients that had better agreement with the experimental values compared to the other parameters that were suggested in the same reference. For oxygen we used a force field after Arora and Sandler.⁶⁵ Optimization, equilibration and diffusion coefficient calculation were done according to the procedure that was presented and described in a recent work published by some of the authors for the mixing of perfluorinated carbons and triglyme.⁶⁶ For oxygen diffusion we used time averaging of a single oxygen molecule movement; this is because the size of the simulation cell allowed to have only a single oxygen molecule for a realistic concentration value.⁶⁶

Viscosity calculations were based on the Green-Kubo formula, from the time autocorrelation functions of the off-diagonal components of the pressure tensor - P_{xy} , P_{xz} and P_{yz} as described in Eq. 3. The runs were performed in the NVT ensemble, starting from an equilibrated configuration.

$$\eta = V/(k_B T)^{-1} \int_0^\infty \langle P_{\alpha\beta}(0) P_{\alpha\beta}(t) \rangle dt, \quad [3]$$

where V is the volume of the system, T is the temperature, k_B is the Boltzmann constant and the brackets indicate the ensemble average.

Results and Discussion

Diffusion coefficients and Henry's law constants of oxygen.—We calculated the diffusion coefficient for O₂ inside each of the solvents with MD (Table I). With realistic values of oxygen pressure and solubility, the simulation cell, which contains few hundred solvents molecules, would only contain a single oxygen molecule. Hence, it is not possible to calculate the ensemble average for the mean square displacement (MSD). Instead, we have calculated a sliding time average of the oxygen displacement as described by Kuritz et al.⁶⁶ Since we estimate the diffusion coefficient by tracking a single O₂ molecule,

Table I. Calculated and experimental diffusion coefficients D_{O_2} of oxygen in different solvents at 25°C. All diffusion coefficients are given in $\text{cm}^2 \text{s}^{-1}$.

molecule	our calculations	our experiments
monoglyme	$7.43 \cdot 10^{-5}$	$(6.0 \pm 0.5) \cdot 10^{-5a}$
diglyme	$2.95 \cdot 10^{-5}$	$(4.6 \pm 0.3) \cdot 10^{-5*}$
triglyme	$2.38 \cdot 10^{-5}$	$(3.5 \pm 0.3) \cdot 10^{-5*}$
tetraglyme	$1.23 \cdot 10^{-5}$	$(2.6 \pm 0.3) \cdot 10^{-5a}$
pentaglyme	$1.19 \cdot 10^{-5}$	$(2.7 \pm 0.5) \cdot 10^{-5*}$
C ₆ F ₁₄	$7.30 \cdot 10^{-5}$	$(7.9 \pm 0.6) \cdot 10^{-5*}$
C ₈ F ₁₈	$5.10 \cdot 10^{-5}$	$(7.3 \pm 1.0) \cdot 10^{-5*}$
C ₉ F ₂₀	$4.20 \cdot 10^{-5}$	$(6.7 \pm 0.6) \cdot 10^{-5*}$
<i>t</i> -C ₁₀ F ₁₈	$2.25 \cdot 10^{-5}$	$(3.9 \pm 0.2) \cdot 10^{-5*}$

*this work.

^asee Reference 47.

the result can be heavily affected by the simulation and integration lengths, we estimate this to cause a statistical error of 15% at most in our calculated diffusion coefficients. The resulting diffusion coefficient corresponds to the infinitely dilute solution of O₂ in the solvents. The behavior of this property is shown in Fig. 2 for both the PFC molecules and the glymes.

It is evident that the longer the molecule is, the lower the diffusion coefficient becomes – this trend holds for both the PFC molecules and the glymes that were calculated and also agrees well with the self-diffusion trends. The experimental values were determined by a method described by Hartmann et al. and Hou et al.^{47,56} We modified the method to compensate for solvent loss during preparation of the

Table II. Henry's law constants $H_{O_2}^{\text{cp}}$ for the different solvents. Data are given in units of $\text{mmol L}^{-1} \text{bar}^{-1}$. The applied temperature was 25°C if not otherwise stated.

solvent/electrolyte	$H_{O_2}^{\text{cp}}$ ($\text{mmol L}^{-1} \text{bar}^{-1}$)
monoglyme	$10.0 \pm 0.3^*$
diglyme	$7.1 \pm 0.3^*$
triglyme	$5.0 \pm 0.4^*$
tetraglyme	$4.3 \pm 0.2^*$
pentaglyme	na
C ₆ F ₁₄	$20.6\text{--}21.1^a$
C ₈ F ₁₈	$20.1\text{--}21.7^b$
C ₉ F ₂₀	$19.7\text{--}20.3^a$
<i>t</i> -C ₁₀ F ₁₈	$16.1\text{--}16.6^a$
0.1 M LiTFSI in diglyme	$6.6 \pm 0.1^*$
1 M LiTFSI in diglyme	$5.5 \pm 0.1^*$

*this work.

^asee Reference 70.^bsee Reference 62.

experiment (for details see ESI). The used Henry's law constants are shown in Table II. Nevertheless, the same trend between simulated and measured diffusion coefficients is only achieved if the experimental diffusion coefficients are carefully evaluated and corrected for volume, temperature and vapour pressure, as seen by the wide spreading of diffusion coefficients that can be found in literature for the same system.

While acceptor and donor number are often used for the scaling of solvation effects in metal/oxygen batteries, a clear-cut correlation between these numbers and oxygen solubility has yet not been found.^{11,28} This lack of correlation is reasonable, since the acceptor number describes the Lewis acidity and the donor number describes the Lewis basicity of the solvent. These parameters can well be used to describe how anions, such as superoxide, and cations, such as Li⁺, are stabilized in the electrolyte. In contrast, oxygen is a non-polar, uncharged molecule and its solubility should not be affected by a parameter describing the stabilization of ions.

Electrolytes for metal/oxygen batteries necessarily contain conducting salts, in comparison to the pure solvents we analyzed in this work. Therefore, we also tested the impact of LiTFSI on the solubility of oxygen (see Table II, and Fig. S5 in the ESI). As expected, the Henry constant for oxygen drops significantly for higher concentrations of LiTFSI, which was also reported by Gittleston et al.²⁹ This finding emphasizes that our experimental setup is capable of testing both pure solvents and electrolytes, whereas electrochemical methods can only be applied with conducting salt included.

Self-diffusion and viscosity of solvents.—We also calculated the self-diffusion coefficients and viscosity parameters. Self-diffusion coefficients are usually determined experimentally by NMR measurements but are often difficult to perform and so are not always available.^{67,68} Viscosity measurements are much easier to perform and hence more experimental data is available. The mean square displacement (MSD) behavior as a function of time is shown in the ESI for the PFC molecules and the glymes. The resulting self-diffusion coefficients are given in Table III. The calculation of self-diffusion coefficients is performed for the ensemble of molecules and hence the statistical error is significantly lower (less than 5%) than the error for the O₂ diffusion coefficients. Comparison to experimental results (when available) and to other calculations is also stated. The experimental data for self-diffusion coefficients of diglyme and triglyme by Hayamizu et al. are two times higher than the calculated ones but show exactly the same trend: the greater the chain length, the lower the self-diffusion coefficient.⁶⁹

An example for the time average in the viscosity calculation is shown in Fig. 3 for tetraglyme; Tables IV shows our calculated viscosity values and some experimental data for both glymes and PFCs.

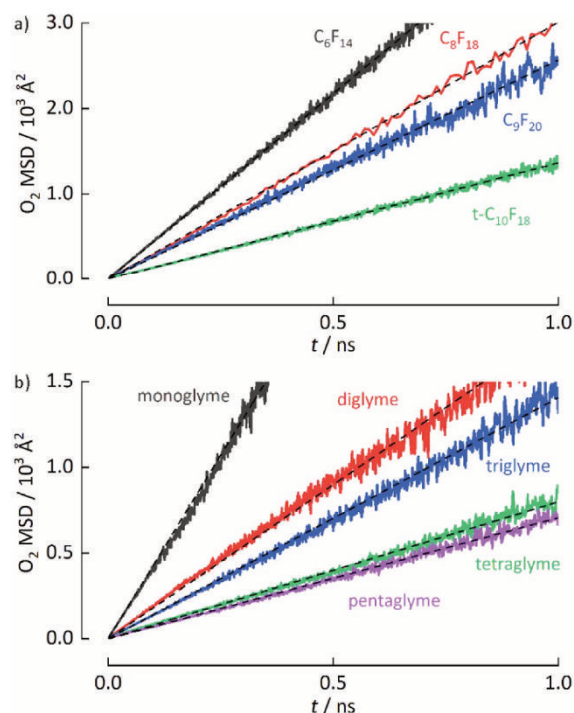


Figure 2. Sliding time averages of the oxygen mean square displacement determined by simulation: a) results for PFC molecules, b) results for glymes. The diffusion coefficient is calculated from the slope of the line using the relation $\langle r^2 \rangle = 6Dt$.

Table III. Calculated self-diffusion coefficients D_{solvent} for different solvent molecules. Data are given in units of $\text{cm}^2 \text{s}^{-1}$. The applied temperature was 25°C if not otherwise stated.

solvent	our calculations	experimental (literature)
monoglyme	$2.15 \cdot 10^{-5}$	
diglyme	$6.90 \cdot 10^{-6}$	$13 \cdot 10^{-6}$ at $30^\circ\text{C}^{\text{a}}$
		$2 \cdot 10^{-6}$ at $30^\circ\text{C}^{\text{b}}$
triglyme	$3.28 \cdot 10^{-6}$	$6.1 \cdot 10^{-6}$ at $30^\circ\text{C}^{\text{a}}$
tetraglyme	$1.41 \cdot 10^{-6}$	
pentaglyme	$6.56 \cdot 10^{-7}$	
C_6F_{14}	$1.85 \cdot 10^{-5}$	$1.2 \cdot 10^{-5}$ – $4.3 \cdot 10^{-5}$ at 25°C (calculated) ^c
C_8F_{18}	$6.53 \cdot 10^{-6}$	
C_9F_{20}	$5.60 \cdot 10^{-6}$	
$t\text{-C}_{10}\text{F}_{18}$	$1.61 \cdot 10^{-6}$	

^asee Reference 69.

^bsee Reference 71.

^csee Reference 72.

As is evident from the table, the calculated viscosity values for glymes are very close to experimentally obtained values for the shorter glymes and start to have larger differences in the case of the longer glymes, however, the trend is very similar. In the case of the PFC, the experimentally measured data are twice as high as the calculated ones, but again the trend with the chain length is similar in experiment and calculation.

Conclusions

Detecting oxygen accessibility trends in liquids may assist to formulate advantageous hybrid electrolyte-additive systems for future metal/oxygen batteries. A selection based merely on ionic conductivity, oxygen solubility and electrochemical stability seems acute, yet incomplete for advancing metal/oxygen batteries from their research phase onward. Numerous publications explored the effect of oxygen solubility on the cell performance; however, oxygen diffusion in common electrolytes has been relatively overlooked. We have performed both calculations and measurements for oxygen diffusion coefficients in a series of perfluorinated alkane and glyme molecules with varied length. This allowed us to derive both specific predictions and to identify trends of the diffusion coefficients as a function of chain length and of solvent type.

If one is aiming for high current densities, our studies show that shorter chain length are better suited, seeing that both D_{O_2} and $H_{\text{O}_2}^{\text{cp}}$

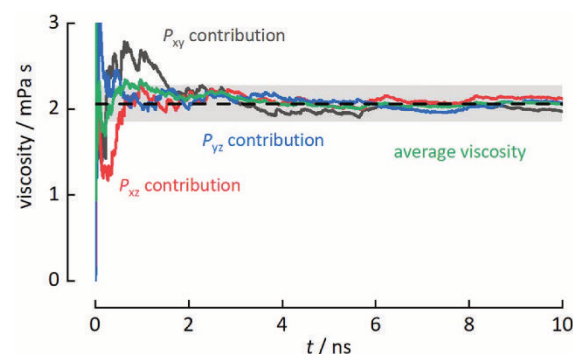


Figure 3. Exemplary calculation of the viscosity of tetraglyme from MD simulations. The black dashed line shows the overall average of $2.06 \text{ mPa} \cdot \text{s}$ with an interval of $\pm 10\%$. It is evident that convergence is achieved after $2 \cdot 10^9 \text{ fs}$ in all different pressure tensor contributions.

Table IV. Viscosity values (η) in $\text{mPa} \cdot \text{s}$ for the different glymes and PFC molecules. Comparison to experimental values is given when available. All calculations were performed at $T = 25^\circ\text{C}$.

solvent	our calculations	experimental (literature)
monoglyme	0.42	$0.41\text{--}0.42^{\text{a}}$ $0.42\text{--}1.1$ at $20^\circ\text{C}^{\text{b}}$
diglyme	0.98	$0.98\text{--}1.14$ at $20^\circ\text{C}^{\text{b}}$
triglyme	1.47	$1.95\text{--}2.16$ at $20^\circ\text{C}^{\text{b}}$
tetraglyme	2.05	$3.3\text{--}4.2$ at $20^\circ\text{C}^{\text{b}}$
pentaglyme	2.73	
C_6F_{14}	0.394	0.700 at $25^\circ\text{C}^{\text{d}}$
C_8F_{18}	0.641	1.256 at $25^\circ\text{C}^{\text{d}}$
C_9F_{20}	0.75	1.789 at $25^\circ\text{C}^{\text{d}}$
$t\text{-C}_{10}\text{F}_{18}$	1.32	5.412 at $25^\circ\text{C}^{\text{d}}$

^asee Reference 73.

^bsee Reference 74.

^csee Reference 75.

^dsee Reference 76.

are higher compared to longer chains. Limiting current is governed by concentration of oxygen and diffusivity thereof. While concentration can be easily raised by use of elevated oxygen pressure, diffusivity is a constant in a given system. Consequently, we think D_{O_2} is the limiting factor, compared to $H_{\text{O}_2}^{\text{cp}}$ and should be in the scope of further studies.

The experimental measurements and theoretical calculations completely agree in the qualitative trends, i.e. the larger the solvent molecule, the lower the diffusion coefficient. Furthermore, both methods show that PFC have larger diffusion coefficients of oxygen in comparison to the larger n -glymes ($n > 1$). Quantitatively there are still differences but they are not large, and hence we can assume that the agreement of theory and experiment strengthens the validity of both. To our knowledge, this is the first consistent set of measurements and calculations of oxygen diffusion coefficients for both the n -glymes and PFC molecules.

Evaluating oxygen diffusion coefficients in well-established electrolytes and PFC liquids are the missing pieces in the puzzle toward a defined selection of electrolytes, suitable for metal/oxygen batteries. One can build upon the knowledge gained in this work, combined with previously reported parameters (e.g. solubility, ionic conductivity, thermodynamic data), and provide a strong base to further enhance oxygen accessibility e.g. through the use of a mixed PFC-electrolyte.

Moreover, modelling and measuring oxygen diffusion in nano-sized PFC architectures may assist to develop novel electrolytes with tailored oxygen solubility, diffusion and distribution inside the complex porous cathode structure.

Acknowledgments

A.S., D.S. and J.J. gratefully acknowledge financial support by the BMBF (Federal Ministry of Education and Research) within the project ‘BenchBatt’ (03XP0047D) and ‘MeLuBatt’ (03XP0110A). A.S. thanks Peter Schmitz for help while setting up the diffusion cell. A.N. acknowledge the support of Planning & Budgeting Committee/ISRAEL Council for Higher Education (CHE) and Fuel Choice Initiative (Prime Minister Office of ISRAEL), within the framework of ‘Israel National Research Center for Electrochemical Propulsion (INREP)’.

ORCID

Jürgen Janek <https://orcid.org/0000-0002-9221-4756>

Daniel Schröder <https://orcid.org/0000-0002-2198-0218>

References

1. K. M. Abraham and Z. Jiang, *J. Electrochem. Soc.*, **143**, 1 (1996).
2. J. Christensen et al., *J. Electrochem. Soc.*, **159**, R1 (2012).

3. P. G. Bruce, S. A. Freunberger, L. J. Hardwick, and J.-M. Tarascon, *Nat. Mater.*, **11**, 19 (2012).
4. D. Aurbach, B. D. McCloskey, L. F. Nazar, and P. G. Bruce, *Nat. Energy*, **1**, 1 (2016).
5. N. Feng, P. He, and H. Zhou, *Adv. Energy Mater.*, **6**, 1 (2016).
6. G. Girishkumar, B. McCloskey, A. C. Luntz, S. Swanson, and W. Wilcke, *J. Phys. Chem. Lett.*, **1**, 2193 (2010).
7. L. Medenbach et al., *Energy Technol.*, **5**, 2265 (2017).
8. B. Sun et al., *Adv. Mater.*, 1801334 (2018).
9. Y. C. Lu, H. A. Gasteiger, and Y. Shao-Horn, *J. Am. Chem. Soc.*, **133**, 19048 (2011).
10. Y.-C. Lu et al., *J. Am. Chem. Soc.*, **132**, 12170 (2010).
11. N. B. Aetukuri et al., *Nat. Chem.*, **7**, 50 (2015).
12. M. Balaish, A. Kraysberg, and Y. Ein-Eli, *Phys. Chem. Chem. Phys.*, **16**, 2801 (2014).
13. M. M. Ottakam Thotiyil, S. A. Freunberger, Z. Peng, and P. G. Bruce, *J. Am. Chem. Soc.*, **135**, 494 (2013).
14. D. Gröbl, T. Danner, V. P. Schulz, A. Latz, and W. G. Bessler, *ECS Trans.*, **62**, 137 (2014).
15. D. Gröbl, J. Janek, and W. G. Bessler, *J. Electrochem. Soc.*, **163**, A599 (2016).
16. D. Gröbl, B. Bergner, J. Janek, and W. G. Bessler, *ECS Trans.*, **69**, 11 (2015).
17. D. Gröbl, B. Bergner, D. Schröder, J. Janek, and W. G. Bessler, *J. Phys. Chem. C*, **120**, 24623 (2016).
18. D. Gröbl and W. G. Bessler, *J. Power Sources*, **297**, 481 (2015).
19. L. Johnson et al., *Nat. Chem.*, **6**, 1091 (2014).
20. C. O. Laoire, S. Mukerjee, K. M. Abraham, E. J. Plichta, and M. A. Hendrickson, *J. Phys. Chem. C*, **114**, 9178 (2010).
21. D. G. Kwabi et al., *Angew. Chemie - Int. Ed.*, **55**, 3129 (2016).
22. C. M. Burke, V. Pande, A. Kheitan, V. Viswanathan, and B. D. McCloskey, *Proc. Natl. Acad. Sci.*, **112**, 9293 (2015).
23. D. Zheng, Q. Wang, H. S. Lee, X. Q. Yang, and D. Qu, *Chem. - A Eur. J.*, **19**, 8679 (2013).
24. D. Sharon et al., *ACS Appl. Mater. Interfaces*, **8**, 5300 (2016).
25. Y. Zhang et al., *J. Phys. Chem. C*, **122**, 15276 (2018).
26. I. M. Aldous and L. J. Hardwick, *Angew. Chemie - Int. Ed.*, **55**, 8254 (2016).
27. L. Lutz et al., *J. Phys. Chem. C*, **120**, 20068 (2016).
28. I. Landa-Medrano, I. Ruiz de Larramendi, and T. Rojo, *Electrochim. Acta*, **263**, 102 (2018).
29. F. S. Gittleton, R. E. Jones, D. K. Ward, and M. E. Foster, *Energy Environ. Sci.*, **10**, 1167 (2017).
30. B. D. Adams et al., *Energy Environ. Sci.*, **6**, 1772 (2013).
31. R. Younesi, G. M. Veith, P. Johansson, K. Edström, and T. Vegge, *Energy Environ. Sci.*, **8**, 1905 (2015).
32. J. Read et al., *J. Electrochem. Soc.*, **150**, A1351 (2003).
33. X. Yang and Y. Xia, *J. Solid State Electrochem.*, **14**, 109 (2010).
34. E. Joseph Nemanick and R. P. Hickey, *J. Power Sources*, **252**, 248 (2014).
35. D. Schröder et al., *Sci. Rep.*, **6**, 1 (2016).
36. J. Read, *J. Electrochem. Soc.*, **153**, A96 (2006).
37. C. Xia, C. L. Bender, B. Bergner, K. Peppler, and J. Janek, *Electrochem. Commun.*, **26**, 93 (2013).
38. L. Gomes and E. R. Gomes, *Rev. da Fac. Ciências da Saúde (Artigos em Inglês)*, **4**, 58 (2007).
39. K. C. Lowe, *Comp. Biochem. Physiol. - Part A Physiol.*, **87A**, 825 (1987).
40. R. B. Hirschl, *Crit. Care*, **4**, 67 (2000).
41. Y. Nishikami et al., *J. Mater. Chem. A*, **3**, 10845 (2015).
42. M. Balaish, A. Kraysberg, and Y. Ein-Eli, *ChemElectroChem*, **1**, 90 (2014).
43. O. Wijaya et al., *J. Mater. Chem. A*, **3**, 19061 (2015).
44. M. Balaish and Y. Ein-Eli, *J. Power Sources*, **379**, 219 (2018).
45. M. Balaish and Y. Ein-Eli, *ACS Appl. Mater. Interfaces*, **9**, 9726 (2017).
46. A. J. Bard and L. R. Faulkner, *Electrochemical methods: fundamentals and applications*, p. 833, Wiley, (2001).
47. P. Hartmann et al., *J. Phys. Chem. C*, **118**, 1461 (2014).
48. M. Khodayari et al., *ChemPhysChem*, **17**, 1647 (2016).
49. I. Gunasekara, S. Mukerjee, E. J. Plichta, M. A. Hendrickson, and K. M. Abraham, *J. Electrochem. Soc.*, **161**, A381 (2014).
50. I. Gunasekara, S. Mukerjee, E. J. Plichta, M. A. Hendrickson, and K. M. Abraham, *J. Electrochem. Soc.*, **162**, A1055 (2015).
51. W. Xu, J. Xiao, D. Wang, J. J.-G. Zhang, and J. J.-G. Zhang, *J. Electrochem. Soc.*, **157**, A219 (2010).
52. J. Herranz, A. Garsuch, and H. A. Gasteiger, *J. Phys. Chem. C*, **116**, 19084 (2012).
53. W. Xu, J. Xiao, J. Zhang, D. Wang, and J.-G. Zhang, *J. Electrochem. Soc.*, **156**, A773 (2009).
54. M. Akazome, T. Takahashi, R.-I. Sonobe, and K. Ogura, *Supramol. Chem.*, **13**, 109 (2001).
55. B. J. Bergner, A. Schürmann, K. Peppler, A. Garsuch, and J. Janek, *J. Am. Chem. Soc.*, **136**, 15054 (2014).
56. H. Ying and R. E. Baltus, *Ind. Eng. Chem. Res.*, **46**, 8166 (2007).
57. S. Plimpton, *J. Comput. Phys.*, **117**, 1 (1995).
58. L. Martínez, R. Andrade, E. G. Birgin, and J. M. Martínez, *J. Comput. Chem.*, **30**, 2157 (2009).
59. A. Jewett, *Moltemplate Manual*, p. 1, (2017).
60. W. L. Jorgensen and J. Tirado-Rives, *J. Am. Chem. Soc.*, **110**, 1657 (1988).
61. M. Tsige and G. S. Grest, *J. Phys. Chem. C*, **112**, 5029 (2008).
62. P. M. Anderson and M. R. Wilson, *Mol. Phys.*, **103**, 89 (2005).
63. E. K. Watkins and W. L. Jorgensen, *J. Phys. Chem. A*, **105**, 4118 (2001).
64. W. L. Jorgensen, D. S. Maxwell, and J. Tirado-Rives, *J. Am. Chem. Soc.*, **118**, 11225 (1996).
65. G. Arora and S. I. Sandler, *Langmuir*, **22**, 4620 (2006).
66. N. Kuritz, M. Murat, M. Balaish, Y. Ein-Eli, and A. Natan, *J. Phys. Chem. B*, **120**, 3370 (2016).
67. V. V. Krishnan, K. H. Thornton, and M. Cosman, *Chem. Phys. Lett.*, **302**, 317 (1999).
68. J. E. Tanner, *J. Chem. Phys.*, **52**, 2523 (1970).
69. K. Hayamizu, Y. Aihara, S. Arai, and C. G. Martinez, *J. Phys. Chem. B*, **103**, 519 (1999).
70. A. M. A. Dias, M. Freire, J. A. P. Coutinho, and I. M. Marrucho, *Fluid Phase Equilib.*, **222-223**, 325 (2004).
71. K. Hayamizu and W. S. Price, *J. Magn. Reson.*, **167**, 328 (2004).
72. C. McCabe, D. Bedrov, O. Borodin, G. D. Smith, and P. T. Cummings, *Ind. Eng. Chem. Res.*, **42**, 6956 (2003).
73. M. N. Caro et al., *J. Chem. Eng. Data*, **58**, 909 (2013).
74. S. Tang and H. Zhao, *RSC Adv.*, **4**, 11251 (2014).
75. A. Henni, A. Naami, and P. Tontiwachwuthikul, *J. Chem. Eng. Data*, **50**, 1038 (2005).
76. M. G. Freire, A. G. M. Ferreira, I. M. A. Fonseca, I. M. Marrucho, and J. A. P. Coutinho, *J. Chem. Eng. Data*, **53**, 538 (2008).

Singlet Oxygen in Electrochemical Cells: A Critical Review of Literature and Theory

The Li/O₂ battery currently suffers from rapid degradation and thus a short lifetime. Older works held the superoxide ion responsible, which can serve as both an oxidizer and a strong base. Another possible cause frequently referred to was the high charging voltage observed, which favors the degradation of the cathode and electrolyte. In recent publications, this degradation was attributed to singlet oxygen, which is formed either as a product of the disproportionation of superoxide to peroxide and oxygen or electrochemically during the oxidation of Li₂O₂. The first experimental demonstration of ¹O₂ formation in Li/O₂ batteries by Wandt *et al.* in 2016 was followed by several experimental and theoretical works since then. Nevertheless, the discussion in literature was also plagued by missing relevant citations, especially when they contradicted the formation of ¹O₂ in electrochemical cells.

Chapter 6 represents the first complete review of the relevant literature on the subject and presents the various theories needed to describe the phenomenon. The review also addresses in detail the proton-induced disproportionation of superoxide, since H⁺ is a known contaminant in Li/O₂ batteries, but also the systems and reactions are similar (e.g., the corresponding superoxides are instable but the peroxides and oxides are stable). Marcus(-Hush-Chidsey) theory can describe reactions at electrodes as well as electron transfer reactions leading to excited states. Thus, it is used to determine whether and how ¹O₂ is a possible reaction product in Li/O₂ batteries. In addition, side reactions and challenges in the detection of ¹O₂ are also addressed.

The concepts presented in this publication were compiled by the author of this thesis, under the supervision of J. Janek and D. Schröder. The manuscript was written by the first author. All co-authors commented on and edited the manuscript.

Reprinted with permission from A. Schürmann, B. Luerßen, D. Mollenhauer, J. Janek, and D. Schröder, Singlet Oxygen in Electrochemical Cells: A Critical Review of Literature and Theory, *Chemical Reviews* **2021**, *121*, 20, 12445–12464. DOI: 10.1021/acs.chemrev.1c00139 Copyright 2021 American Chemical Society.

6



Singlet Oxygen in Electrochemical Cells: A Critical Review of Literature and Theory

Adrian Schürmann, Bjoern Luerßen, Doreen Mollenhauer, Jürgen Janek,* and Daniel Schröder*

Cite This: *Chem. Rev.* 2021, 121, 12445–12464

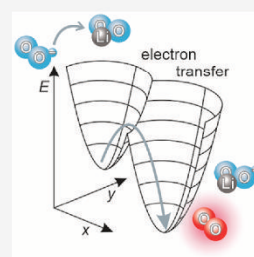
Read Online

ACCESS |

Metrics & More

Article Recommendations

ABSTRACT: Rechargeable metal/O₂ batteries have long been considered a promising future battery technology in automobile and stationary applications. However, they suffer from poor cyclability and rapid degradation. A recent hypothesis is the formation of singlet oxygen (¹O₂) as the root cause of these issues. Validation, evaluation, and understanding of the formation of ¹O₂ are therefore essential for improving metal/O₂ batteries. We review literature and use Marcus theory to discuss the possibility of singlet oxygen formation in metal/O₂ batteries as a product from (electro)chemical reactions. We conclude that experimental evidence is yet not fully conclusive, and side reactions can play a major role in verifying the existence of singlet oxygen. Following an in-depth analysis based on Marcus theory, we conclude that ¹O₂ can only originate from a chemical step. A direct electrochemical generation, as proposed by others, can be excluded on the basis of theoretical arguments.



CONTENTS

1. Introduction	12445
2. Background and Literature Review	12446
3. Theoretical Considerations	12449
3.1. Molecular Orbital Description	12449
3.2. Deactivation of Singlet Oxygen	12450
3.3. Spin Conservation and Wigner's Rules	12451
3.4. Marcus Theory	12452
4. Reaction Mechanisms Leading to Singlet Oxygen	12456
4.1. Discharging Me/O ₂ Cells: Singlet Oxygen from Chemical Reactions	12456
4.2. Charging Me/O ₂ Cells: Singlet Oxygen from Electrochemical Reactions	12457
4.3. Singlet Oxygen from Side Reactions	12458
4.4. Specificity of Singlet Oxygen Traps	12458
5. Conclusions	12459
Author Information	12460
Corresponding Authors	12460
Authors	12460
Notes	12460
Biographies	12460
Acknowledgments	12461
References	12461

1. INTRODUCTION

For quite some time, metal/O₂ batteries were regarded as one of the electrochemical energy storage devices of the future. Their high theoretical energy density was seen as a key to widespread long-range electromobility.^{1–3} While progress has been made, there are still numerous problems such as poor rechargeability, cycle life, and high overvoltages, all currently preventing

commercial use.^{4–8} In recent experimental works, singlet oxygen was identified as a possible root for these problems by Wandt et al. and Mahne et al. in the case of lithium/O₂ batteries.^{9–13} While this seems to be an important step forward, a theoretical analysis of the formation of singlet oxygen on the basis of electrochemical fundamentals is still pending. In-depth understanding is not only important for the development of suitable strategies against the formation of the highly reactive singlet oxygen species or the root thereof. It also could give hints to a deeper understanding of the underlying (electro)chemistry in metal/O₂ batteries and electrochemical cells in which oxygen redox reactions are involved in general.

The following analysis of the different aspects of singlet oxygen in battery systems will be split into three parts: first, a broad literature survey, reviewing the most important publications up to date including the disproportionation of superoxide and highlighting experimental pitfalls. We also included the proton-induced disproportionation of superoxide, since proposed reaction mechanisms in metal/O₂ batteries often contain superoxide as an intermediate and water is a known contamination.^{6,8} This review covers the relevant literature to this topic starting from 1963 to the end of March 2021. Second, an analysis of the theoretical background consisting of molecular orbital diagrams, deactivation and reactions of singlet oxygen, spin conservation and Wigner-Witmer rules in (electro)-

Received: February 16, 2021

Published: July 28, 2021



chemical reactions and Marcus theory. Third, we discuss possible reaction mechanisms leading to singlet oxygen and their implications for metal/O₂ batteries.

In doing so, we show that the experimental evidence is yet not fully conclusive and side reactions can play a major role in verifying the existence of singlet oxygen. The theoretical considerations show that ¹O₂ can originate from a chemical reaction step, and direct electrochemical generation is, according to the Marcus–Hush–Chidsey, theory not possible.

2. BACKGROUND AND LITERATURE REVIEW

When the term singlet oxygen is used in the remainder of this paper, it refers to the first electronic excited state of dioxygen, also denoted as ¹O₂ (cf. section 3.1). In the following, we highlight some of the important reports needed for revisiting the recent findings in electrochemical cells and batteries. For a more general overview on singlet oxygen, we refer to the reviews of Schweitzer and Schmidt as well as Adam, Kazakov, and Kazakov.^{14,15}

Singlet molecular oxygen was first discovered and identified as a product of a chemical reaction by Khan and Kasha in 1963 in the reaction of hydrogen peroxide with sodium hypochlorite in aqueous solution.^{16,17} The exact circumstances, which led to the discovery, starting from a coffee between Robert Mulliken and Ahsan Khan, can be found in an anecdotal paper by Khan.¹⁸ In the following years, research on singlet oxygen expanded quickly, dealing with the physical, chemical, and biological impact of the newly found molecular species. A summarizing timeline of the reviewed literature is shown in Figure 1.

Mayeda and Bard showed that singlet oxygen can be formed from the oxidation of superoxide with suitable substrates.^{19,20}

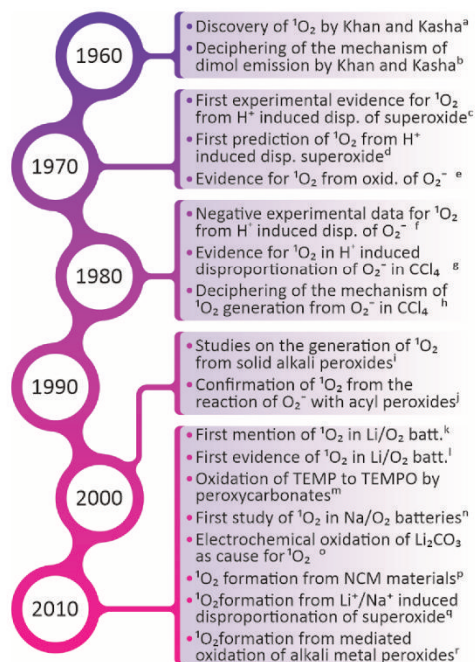


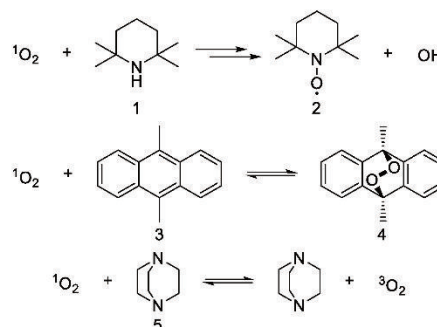
Figure 1. Summarizing timeline of the reviewed literature: (a) refs 16, 17; (b) ref 22; (c) ref 19; (d) refs 23–25; (e) refs 20, 26; (f) refs 27–30; (g) ref 31; (h) ref 32; (i) refs 33–35; (j) ref 36; (k) ref 37; (l) ref 9; (m) ref 38; (n) ref 39; (o) ref 12; (p) ref 10; (q) ref 40; (r) ref 41.

They found that the reaction of the ferrocenium cation with superoxide leads to singlet oxygen. In addition, they found that the proton-induced disproportionation leads to singlet oxygen by using the spin trap 1,3-diphenylisobenzofuran. In general, spin traps react with singlet oxygen and form stable molecules. In the ideal case, they react fast, selectively, and form a stable product, which can be easily detected. Spin traps are consumed while reacting, which is part of the analytical strategy. An often-used spin trap utilizes the reaction of 2,2,6,6-tetramethylpiperidine (TEMP, 1) to (2,2,6,6-tetramethylpiperidin-1-yl)-oxyl (TEMPO, 2) or the reaction of 9,10-dimethylantracene (DMA, 3) to 9,10-dimethyl-9,10-epidioxyanthracene (DMAO₂, 4) (see Table 1 and Scheme 1). In contrast, quenchers catalyze

Table 1. Names and Abbreviations of Traps and Quenchers Used in Singlet Oxygen Chemistry

name	abbreviation	#
2,2,6,6-tetramethylpiperidine	TEMP	1
(2,2,6,6-tetramethylpiperidin-1-yl)oxyl	TEMPO	2
9,10-dimethylantracene	DMA	3
9,10-dimethyl-9,10-dihydro-9,10-epidioxyanthracene	DMAO ₂	4
1,3-diphenylisobenzofuran	DPBF	
1,4-diazabicyclo[2.2.2]octane	DABCO	5

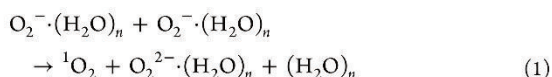
Scheme 1. Exemplary Reactions of Spin Traps and Quenchers with ¹O₂



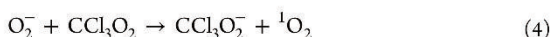
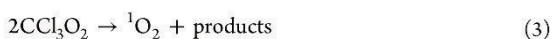
the deactivation of singlet oxygen to triplet oxygen. Ideally, they are chemically stable, and therefore not consumed while catalyzing, and react fast. The use of furans as trapping agents is generally problematic since they also react with other oxidizing agents, resulting in similar products (see also *Specificity of Singlet Oxygen Traps*).²¹

Khan predicted, using electron transfer theory, the generation of singlet oxygen from the disproportionation of superoxide in aqueous solutions in 1976 and 1978.^{23–25} He found a strong dependence on the surrounding number of water molecules present, yielding in some cases singlet oxygen as the only product of the reaction. Since then, numerous reports dealt with the generation of singlet oxygen from superoxide in different media and the results of these experimental works vary from positive via inconclusive to negative. Following the work of Khan and Mayeda and Bard, Foote et al. investigated the disproportionation of superoxide in water at pH values ranging from 6 to 10, using a spin trap.²⁷ Foote et al. used cholesterol as a specific ¹O₂ trap and found that singlet oxygen is not produced in fractions of more than 0.2% compared to the used amount of tetramethylammonium superoxide as starting material. Further studies by Aubry (1981), Nanni (1981), and Arudi (1984)

supported the absence of singlet oxygen in the proton-induced disproportionation of superoxide.^{28–30} This result was again questioned by a work of Khan in 1981.³¹ He observed the luminescence of singlet oxygen at 1268 nm in the water-induced disproportionation of KO₂ in CCl₄. The setup used contained a continuous stream of finely suspended KO₂ in CCl₄ flowing through a gap between a wetted glass frit and an infrared detector. He proposed eq 1 as cause of the observed luminescence:

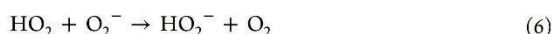


While he indeed found singlet oxygen, the root cause was falsely claimed to be the disproportionation of superoxide. Kanofsky found spectral proof for the generation of singlet oxygen by mixing carbon tetrachloride and carbon tetrabromide with potassium superoxide in absence of water.³² He proposed the reaction mechanism shown in eqs 2–4:



Chloroform was less reactive but infrared emission at 1268 nm could be observed when the concentration of superoxide ions in the halocarbon phase was increased by 18-crown-6. The disproportionation of superoxide ions in deuterium oxide was not accompanied by chemiluminescence. In addition, the emission intensities did not differ under either dry or wet conditions. Kanofsky concluded that less than 0.02 mol of singlet oxygen per mole of superoxide ion was produced. These findings were also supported by the work of Roberts and Sawyer showing a fast reaction between electrogenerated superoxide and different chloromethane substrates in dimethylformamide resulting in oxygenated products and the corresponding chloride anion.⁴² The observed kinetics were first order in O₂^{·-} and first order in the chloromethane substrates, and the first step was rate limiting. The overall reactions found for the chloromethane substrate are multistep processes that consume one or more superoxide ions per chloride ion to yield oxygenated products. Finally, Corey et al. showed spectral evidence for the generation of singlet oxygen from water-induced superoxide disproportionation in Freon 113, CCl₄, and perfluorohexane.⁴³ Bursts of infrared radiation were found when the prepared KO₂ solutions were brought in contact with water. The authors also excluded the above-mentioned reactions found by Roberts and Sawyer, as Kanofsky who excluded these reactions due to the lower rate constants compared to disproportionation. In contrast, it was shown by Kanofsky et al. in 1988 that the addition of D₂O to a solution containing CCl₄, like the reaction system described of Corey et al., does not increase the yield of singlet oxygen.⁴⁴ These results are consistent with prior reports but in conflict with the results of Corey et al. However, alternative explanations exist for the data of Corey et al. The addition of large amounts of water to the KO₂-halocarbon suspensions will induce the dissolution of KO₂ and cause enhanced reactivity with the halocarbon and will lead to the rapid decomposition of KO₂. The oxygen evolution from the KO₂ particles will increase the reactant mixing rate, which will increase the rate of the surface reaction between KO₂ and the halocarbon. The water-induced decomposition of KO₂ may also heat the reaction mixture and

thereby increase the rate of the superoxide-halocarbon reaction. MacManus-Spencer and McNeill studied the formation of singlet oxygen in the reaction of H₂O₂ with O₂^{·-} in toluene, which can essentially be described as proton-induced disproportionation of superoxide when H₂O₂ serves as the proton source (eqs 5 and 6).⁴⁵ They found that less than 0.2% singlet oxygen was formed based on the amount of potassium superoxide used:



In view of all these results and to the best of our knowledge, there is still no unequivocal proof for direct singlet oxygen generation from the proton-induced disproportionation of superoxide whether in aqueous or organic solvents.

Conversely, the reaction between the ferrocenium cation and superoxide does lead to singlet oxygen as was shown by Nanni et al. They observed luminescence as a result of the oxidation of superoxide. They proposed that the formation of singlet oxygen depends on the specific properties of substrates, which favor singlet transition states in the electron transfer process. Reactions involving either adiabatic electron transfer or triplet transition states form directly triplet ground state oxygen.²⁸ Calculations by Koppenol and Butler supported these findings.⁴⁶ These findings leave room for potential singlet oxygen generation from reactions with byproducts, if the reaction involves a transition state with singlet spin. Danen and Arudi detected evidence for ¹O₂ in the reaction of dibenzoyl peroxide and superoxide (resulting in benzoate and oxygen) by using 1,2-dimethylcyclohexene as a trap.²⁶ These results were confirmed in 2005 by MacManus-Spencer et al., who also found that the reaction only produced ¹O₂ in the case of diacyl peroxides, with an average yield of 5% ¹O₂.³⁶ The used potassium superoxide acted as a nucleophile and reducing agent. Less than 0.1% singlet oxygen was found in the case of alkyl peroxides like di-*tert*-butyl peroxide or *tert*-butyl hydroperoxide.

The formation of ¹O₂ from solid super- and peroxides was also investigated for the use in chemical oxygen iodine lasers (COIL). Alfano and Christie used Li₂O₂ and Na₂O₂ in combination with HCl and HBr, resulting in emissions at 1270 nm.³³ Li et al. used Li₂O₂, Na₂O₂, and KO₂ as starting materials and wetted chlorine gas as an oxidizing agent.^{34,35} In these cases, emission at 1270, 703, and 634 nm was observed. It can be assumed that the mixing of these superoxides and peroxides will result in the formation of H₂O₂, and depending on the conditions, hypochlorous acid (HOCl) or chlorine gas *in situ*. The following reactions will form HCl and ¹O₂ quantitatively, which is well-known in literature.

In recent years, singlet oxygen was also mentioned as a possible culprit for the poor performance of Li/O₂ batteries. It was first mentioned as a possible charging product in Li/O₂ batteries by Hassoun et al. in 2011.³⁷ They assumed that the observed charging potential of 3.2 V vs Li⁺/Li is a mixed potential of triplet oxygen formation at 2.91 V vs Li⁺/Li and singlet oxygen generation at 3.9 V vs Li⁺/Li. An experimental proof of the statement was not given. McCloskey et al. also discussed briefly the possibility of ¹O₂ from the OER in Li/O₂ batteries but deemed the scenario overall unlikely given that the onset potential of electrolyte degradation did not fit the thermodynamic threshold for singlet oxygen formation.⁴⁷ The first experimental evidence was later given by Wandt et al. in

2016, and follow-up studies have focused since then on mainly two points: (a) detection of singlet oxygen via spin traps and (b) deactivation of singlet oxygen via quenchers.^{9–13,39,48,49}

Wandt et al. detected singlet oxygen in Li/O₂ batteries through a reaction with a spin trap, which forms a stable radical (4-oxo-TEMP to 4-oxo-TEMPO). The radical was then observed by time- and voltage-resolved operando EPR spectroscopy. The lower limit for the fraction of evolving singlet oxygen (¹O₂) was estimated to be 0.5% of the total amount of oxygen formed. The standard potential at which this process occurs was estimated to be 3.9 V vs Li⁺/Li or 3.5 V vs Li⁺/Li, depending on the assumed number of transferred electrons (*n* = 1 or 2).⁹ Mahne et al. found evidence that ¹O₂ forms while discharging and charging applying the trap DMA. They used quenchers to improve cycle life and found higher fractions of ¹O₂ with rising concentrations of trace water.¹¹ In addition, they found the characteristic emission of singlet oxygen at 1270 nm while charging in deuterated acetonitrile. Mahne et al. later examined Li₂CO₃-packed working electrodes and found generation of DMAO₂ when applying voltages above 3.8 V vs Li⁺/Li.¹² This is also likely to happen in Li/O₂ batteries, since Li₂CO₃ is a well-known side product in these batteries. Wandt et al. evidenced the formation of singlet oxygen evolution from different types of NCM and correlated also the findings with the oxidation of Li₂CO₃ using another characteristic emission of singlet oxygen at 633 nm.¹⁰ Schafzahl et al. reported singlet oxygen formation also during cycling of aprotic Na/O₂ batteries. They used DMA as ¹O₂ trap and reported that water has a significant impact on the formation of ¹O₂.³⁹ Mourad et al. could link the generation of singlet oxygen to the disproportionation of superoxide and found a correlation with the counteraction (H⁺, Li⁺, Na⁺, K⁺, TBA⁺).⁴⁰ They stated that the strong Lewis acids H⁺, Li⁺, and Na⁺ stabilize the respective peroxide relative to the respective superoxide and hence drive the disproportionation reaction. Weaker Lewis acids tend to stabilize intermediates in the reaction path less, leading to reduced barriers toward singlet oxygen. The proton H⁺ yielded only insignificant ¹O₂ fractions, while ¹O₂ fractions increased strongly with Li⁺ (2%) and Na⁺ (12%) containing electrolytes. Vice versa, they also suggested a dependence of the spin state of the released dioxygen on the spin state of the reacting species along the reaction path. DFT calculations were also performed to further unravel the reaction mechanism, but these results must be reviewed carefully. The shown Δ*G* values refer to a thermodynamic characterization of reactants, intermediates, and products. Possible energy barriers in the framework of kinetic considerations have not been presented. It must be noted that naturally endothermic reactions have at least an activation energy corresponding to the Gibbs energy of the considered reaction. However, a comparison of activation energies is only possible for a number of very similar reactions under the same conditions. It must be demonstrated whether this is the case here and whether the reactants and energetically higher-lying products are necessarily linked by electronic state transitions that would allow the formation of singlet oxygen.

Nevertheless, the aforementioned experimental proofs of ¹O₂ formation must be considered carefully. Zhang et al. demonstrated that it is possible to oxidize 4-oxo-TEMP to 4-oxo-TEMPO without an applied potential by adding CO₂ to a solution of 4-oxo-TEMP and finely dispersed Li₂O₂.³⁸ The addition of CO₂ gives rise to a mixture of different peroxydicarbonates and peroxydicarbonates, which act as strong oxidizing agents (see Figure 2). These results render at least 4-

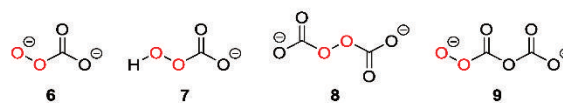


Figure 2. Possible peroxydicarbonates formed from Li₂O₂ in contact with CO₂, as proposed by Zhang et al. From left to right: peroxydicarbonate 6; hydroperoxydicarbonate 7; symmetrical peroxydicarbonate 8; unsymmetrical peroxydicarbonate 9.³⁸

oxo-TEMP as an unsuitable trap for singlet oxygen in Li/O₂ batteries since CO₂ and CO₃²⁻ are commonly found in metal/O₂ batteries. DMA on the other hand was found to be stable against combinations of Li₂CO₃, Li₂O₂, and CO₂.¹² Since singlet oxygen was found both during discharging and charging, different mechanisms must be considered. This also includes reactions with byproducts, which may provide false positive proofs for mechanisms under consideration.

A possible reaction path for the formation of singlet oxygen from the dissociation of the lithium superoxide as simplest model system was investigated by Zaichenko et al. on the basis of multireference CASSCF/CASPT2 calculations in the gas phase.⁵⁰ The reaction path for singlet oxygen generation is about 0.9 eV higher in energy than the reaction path to triplet oxygen considering the dissociation curves, which show no additional barrier. They discussed that the solvent can strongly influence the potential energy curves and that this could determine whether the singlet oxygen reaction path can be reached at all. Houchins et al. calculated reaction rates for the disproportionation of superoxide and lithium superoxide based on Marcus theory. They found that singlet oxygen formation is highly preferred in the case of disproportionation of free superoxide. The specific rate constants depend to a small degree on the electron donor and acceptor properties of the solvents used.⁵¹ Pierini et al. modeled thermodynamic and kinetic data of the lithium and proton induced disproportionation reaction of superoxide using multireference CASSCF/NEVPT2 calculations.⁵² They found qualitatively similar reaction profiles for both cases and stated that the presented activation energy of 1.5 eV shows the inaccessibility of purely chemical pathways in the case of Li⁺. They attributed the detected singlet oxygen to either stem from the proton-induced disproportionation or an electrochemical reaction. The interaction of redox mediators/catalysts and singlet oxygen was also investigated. Kwak et al. attributed the slow degradation of redox mediators during the cycling of Li/O₂ batteries to oxidation reactions with singlet oxygen.⁵³ Reduced forms of redox mediators were particularly susceptible due to the higher electron affinity of singlet oxygen compared to triplet oxygen. Liang et al. investigated the influence of redox mediators on the formation of singlet oxygen in Li/O₂ batteries. In nonmediated batteries, they found a fraction of up to 27% ¹O₂ of the total evolved oxygen, while in the case of mediated batteries, the formation of ¹O₂ was suppressed. They hypothesize that redox mediators promote the rate of intersystem crossing, which accelerates the relaxation of singlet oxygen to triplet oxygen.⁵⁴ Petit et al. investigated the reaction mechanism of mediated oxidation of (su)peroxides by redox mediators.⁴¹ They found that the oxidation of peroxides leads to superoxides in the first step. Subsequent oxidation of superoxides with redox mediators with a standard potential >3.5 V vs Li⁺/Li formed significant amounts of ¹O₂. They found that the extent to which ¹O₂ or ³O₂ is generated is determined by the relative kinetics of superoxide oxidation versus ¹O₂ generation by disproportionation, the redox mediator concentration, and

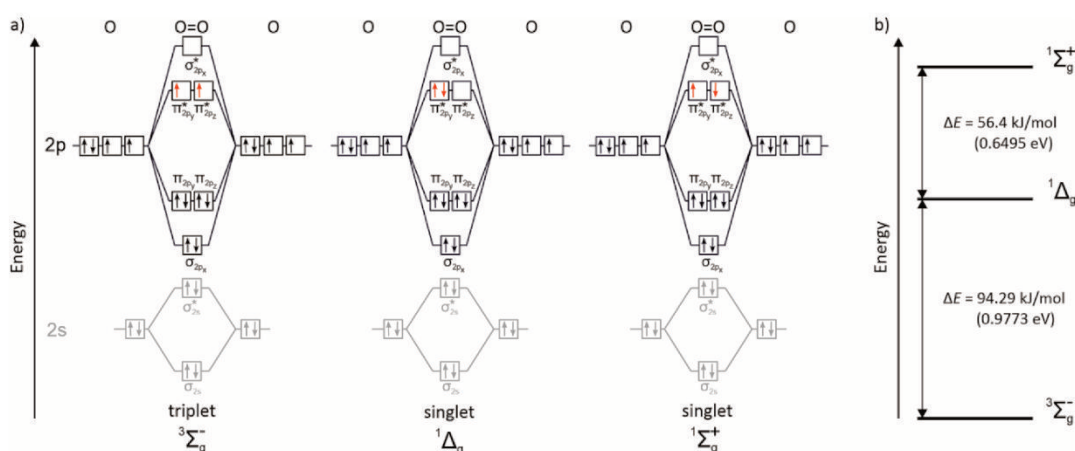


Figure 3. (a) Molecular orbital diagrams of different spin states of dioxygen and the corresponding term symbols. From left to right: oxygen in the ground state, exhibiting two unpaired electrons with parallel spin in the two highest occupied molecular orbitals (HOMO) due to Hund's rule. Spin inversion of one of the unpaired electrons, and additional pairing of them, leads to the first electronic excited state with the term symbol ${}^1\Delta_g$ (middle). This spin state is referred to as singlet oxygen or ${}^1\text{O}_2$. Spin inversion of one unpaired electron leads to the second electronic excited state ${}^1\Sigma_g^+$, sometimes referred to as high-energy singlet oxygen. The ${}^3\Sigma_g^-$, ${}^1\Delta_g$, and ${}^1\Sigma_g^+$ electronic states are triple-, double- and nondegenerate, respectively.⁵⁸ (b) Transition between the ground state and ${}^1\Delta_g$ or ${}^1\Sigma_g^+$ is spin-forbidden and therefore kinetically hindered. In comparison, transition between ${}^1\Sigma_g^+$ and ${}^1\Delta_g$ is spin allowed and therefore fast.

the ${}^1\text{O}_2$ quenching efficiency of the mediator. The apparent reaction rate between mediator and solid (su)peroxides showed a maximum around 3.2 V vs Li⁺/Li for the standard potential of used redox mediators, which was attributed to the Marcus inverted region (cf. section 3.4). However, caution must be exercised here since the Marcus theory was originally developed for homogeneous reactions. Samojlov et al. studied the influence of different solid catalysts (Pd, Co₃O₄, MnO₂, and TiC) on the generation of ${}^1\text{O}_2$ in Li/O₂ batteries.⁵⁵ They found that catalysts that can release ${}^1\text{O}_2$ from H₂O₂ can also lead to increased amounts of ${}^1\text{O}_2$ in Li/O₂ batteries. Córdoba et al. used fluorescence quenching of DMA as a probe for ${}^1\text{O}_2$.⁵⁶ They detected a decay in fluorescence during electrochemical oxygen reduction in a 0.1 M LiTFSI/DMSO electrolyte. The decay could also be detected when a solution containing superoxide anions was mixed with a solution containing Li⁺ ions, hinting that the measured decay originates from the Li⁺-induced disproportionation of superoxide. The overall amount of formed ${}^1\text{O}_2$ was not further quantified. Lozano et al. detected singlet oxygen by fluorescence quenching of DMA also during the O₂ reduction in NaOTf/diglyme electrolytes.⁵⁷ Ammonium trifluoromethanesulfonate (NH₄OTf) was also used as an acid and catalyst for proton induced disproportionation of superoxide. The quenching of DMA fluorescence was enhanced when NH₄OTf was used. They ascribed the detected ${}^1\text{O}_2$ to the proton induced disproportionation of superoxide. The used setup did not allow to quantify the formed amount of ${}^1\text{O}_2$.

As with proton-induced disproportionation, there is so far no clear evidence for the formation of singlet oxygen in metal/O₂ batteries from the proposed causes (namely disproportionation or direct electrochemical generation). In addition, reported values of the fraction of ${}^1\text{O}_2$ compared to the overall evolved amount of oxygen scatter widely. This is due to the complex nature of the systems under consideration and the short life span of singlet oxygen, which makes detection difficult. False positive results cannot be excluded as the studies of Zhang et al. show. The found potential dependence together with the reported

influence of water and Li₂CO₃ could also be interpreted as an indication for a side reaction resulting in ${}^1\text{O}_2$. Future studies must take advantage of the characteristic luminescence of singlet oxygen or show that a false positive result from a side reaction mimicking singlet oxygen can be excluded. Extensive kinetic studies will be required to find the root cause of the singlet oxygen found.

3. THEORETICAL CONSIDERATIONS

Obviously, the experimental observations of singlet oxygen and its formation are not conclusive, and questions on possible reaction mechanisms remain unanswered. In the following, theoretical considerations of molecular orbital diagrams, singlet oxygen, spin conservation, Wigner-Witmer rules in (electro)-chemical reactions, and Marcus theory are summarized using examples and reactions to explain their fundamental nature. These fundamental rules and considerations are then transferred in the next section to the oxygen electrode in electrochemical metal/O₂ cells.

3.1. Molecular Orbital Description

The molecular orbital diagrams of oxygen provide an insight into the energetics of the molecular orbital energies. The molecular orbitals are occupied by electrons in the sense of the Pauli principle, noting that the antibonding π_{2p}^{*}-orbitals are doubly degenerate. In molecular oxygen, these two antibonding π_{2p}^{*}-orbitals are occupied by two electrons. An important consequence of the Aufbau principle for molecules is that molecular oxygen has a triplet ground state. This is due to the fact that according to Hund's rule the two electrons have parallel spin. Typical for configurations with nonclosed shells is that there are several states for a configuration, which can be characterized by term symbols. For linear molecules, these terms are characterized by the total spin *S*, the component *M_L* of *L* in the direction of the molecular axis, and the behavior of the total wave function with respect to inversion at the center of symmetry (if one exists). The terms for the ground state configuration of O₂ can be determined by considering only the

open shell (π_{2p}^* -orbitals) and setting up the corresponding six possible Slater determinants. The Slater determinants can be assigned to term symbols and result in $^3\Sigma_g^-$, $^1\Delta_g$ and $^1\Sigma_g^+$ with a 3-fold, 2-fold, and no degeneracy. A more detailed discussion can be found in ref 58. The molecular orbital diagrams and the corresponding term symbols are shown in Figure 3: unpaired electrons with parallel spin (triplet ground state, $^3\Sigma_g^-$, often denoted as 3O_2), paired electrons (singlet state, $^1\Delta_g$, first electronic excited state, here denoted as 1O_2) and unpaired electrons with antiparallel spin (singlet state, $^1\Sigma_g^+$, second electronic excited state, here labeled as high energy 1O_2 or HE- 1O_2). In most cases, the $^1\Delta_g$ configuration is referred to as singlet oxygen (this also applies here in the following). The energy difference between 1O_2 and 3O_2 is roughly 1 eV, and the energy difference between HE- 1O_2 and 3O_2 is roughly 1.6 eV.¹⁴

Both singlet oxygen species are stronger oxidizing agents than triplet oxygen. One reason is the higher electron affinity of the excited states; reactions with singlet oxygen are therefore more exothermic compared to reactions with triplet oxygen.⁵⁹ The higher electron affinity of the excited states corresponds also to a higher standard potential in electrochemical cells.^{60,61} Another reason is the spin state of the singlet oxygen molecule. Most organic molecules are in the singlet state and therefore do not react readily with triplet oxygen but with singlet oxygen.⁶² This behavior roots in spin conservation and is discussed in detail below.

Although the states differ in their energy and reactivity, the corresponding oxygen molecules still have comparable bond lengths (3O_2 , 120.752 pm; 1O_2 , 121.156 pm; HE- 1O_2 , 122.688 pm).⁶² In addition, the emission wavelength for the transition back into ground state triplet oxygen does only slightly depend on the solvent (e.g., gas-phase, 1270 nm; acetone-*d*₆, 1273 nm; pentane, 1275 nm).⁵⁹ Therefore, ground state triplet and excited singlet oxygen probably have similar solvation energies in solvents and electrolytes. Conversely, this means that the energies required for a transition between two states are directly related to half-cell potentials in electrochemical cells, at least in a first approximation.^{59,63} The lifetime of singlet oxygen depends highly on the used solvent and can vary over several orders of magnitude (e.g., $\tau_{\Delta, H_2O} = 3.1 \mu\text{s}$; $\tau_{\Delta, \text{acetone-}d_6} = 992 \mu\text{s}$).^{14,64,65}

Dioxygen can exist in metal/ O_2 batteries in different oxidation states. The reduction reaction during discharge of a metal/ O_2 battery leads via superoxide (O_2^-) to peroxide (O_2^{2-}) species as discharge product. A direct two-electron pathway is also under consideration (cf. Aurbach et al.).⁶ The reduction is accompanied by a decrease of the bond order (O_2 , 2; O_2^- , 1.5; O_2^{2-} , 1) and an increase of the bond length. This is due to the additional electrons in antibonding π_{2p}^* states. Further reduction of molecular oxygen to the trianion is not experimentally known, instead further reduction leads to bond breaking and the formation of atomic oxygen radical mono- (e.g., O^-) and dianions (O^{2-}).

3.2. Deactivation of Singlet Oxygen

Compared to triplet oxygen, singlet oxygen is very reactive and can be deactivated in three ways depending on the chemical environment (e.g., gaseous 1O_2 or dissolved 1O_2):¹⁴

1. Nonradiative deactivation:¹⁴ singlet oxygen relaxes into the triplet state, and the released energy is transferred to surrounding molecules. The term nonradiative deactivation covers various competing reaction mechanisms. These are, in the order of increasing rate for the deactivation, electronic-to-vibrational energy transfer,

charge transfer induced quenching, and common electronic energy transfer. Electronic-to-vibrational energy transfer is a general deactivation process of singlet oxygen, which converts electronic excitation energy of the oxygen molecule into vibration of oxygen and quencher and occurs during any di- or polyatomic collision in the gas or liquid phase. In most liquids, the lifetime of singlet oxygen is limited by electronic-to-vibrational deactivation to the range of micro- to milliseconds. Figure 4 shows the

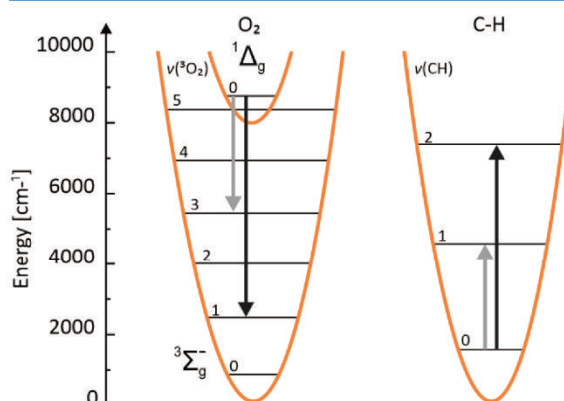


Figure 4. Electronic-to-vibrational energy transfer from $O_2(^1\Delta_g)$ to a C–H bond. The potential energy curves of the $^3\Sigma_g^-$ and $^1\Delta_g$ states of O_2 and the ground-state potential curve of a C–H bond as deactivating bond are shown, together with their corresponding vibrational levels. Since only very weak temperature effects have been determined for electronic-to-vibrational deactivation, only exothermic deactivation paths should be relevant. Two different possible coupled transitions of $O_2(^1\Delta_g)$ and C–H are shown: the first one starting from $\nu(^1O_2) = 0$ and $\nu(\text{CH}) = 0$ to the final state $\nu(^3O_2) = 3$ and $\nu(\text{CH}) = 1$. The second one starting again from $\nu(^1O_2) = 0$ and $\nu(\text{CH}) = 0$ to the final state $\nu(^3O_2) = 1$ and $\nu(\text{CH}) = 2$. Lengths of arrows correspond to transition energies E_{O_2} and E_{CH} , respectively. Data from Schmidt and Afshari. Adapted with permission from ref 66. Copyright 1992 Deutsche Bunsen-Gesellschaft für physikalische Chemie e.V. and Wiley-VCH.

coupled transition of 1O_2 to 3O_2 with the excitation of a C–H bond. Electronic-to-vibrational energy transfer shows a pronounced H-D isotope effect, which leads to longer lifetimes in deuterated solvents, often by more than one order of magnitude (e.g., $\tau_{\Delta, H_2O} = 3.1 \mu\text{s}$; $\tau_{\Delta, D_2O} = 68 \mu\text{s}$; $\tau_{\Delta, \text{acetone}} = 51.2 \mu\text{s}$; $\tau_{\Delta, \text{acetone-}d_6} = 992 \mu\text{s}$).^{14,64–66}

2. Radiative deactivation:¹⁴ The excess energy that is released during the change from singlet to triplet oxygen state is emitted as photon. This transition is spin-forbidden for the given selection rules, which explains the long half-life time of 1O_2 in the gas phase of 72 min. Collisions with other atoms or molecules induce perturbations of the electronic structure, which weakens the strong forbiddenness of the radiative processes. This is especially true for condensed matter. There is a multitude of possible emitted photons, which are summarized in Table 2 (including an approximation of the perceived color of the photon⁶⁷).¹⁵
3. Chemical reactions: Since most organic compounds are molecules in the singlet state, reactions with 1O_2 are spin allowed, in contrast to reactions with triplet oxygen.

Table 2. Radiative Routes for Deactivation of Singlet Oxygen and Corresponding Photon Wavelengths^a

initial state	final state	wavelength
$(^1\Delta_g)_{\nu=0}$	$(^3\Sigma_g^-)_{\nu=1}$	1580 nm
$(^1\Delta_g)_{\nu=0}$	$(^3\Sigma_g^-)_{\nu=0}$	1270 nm
$(^1\Delta_g)_{\nu=1}$	$(^3\Sigma_g^-)_{\nu=0}$	1070 nm
$(^1\Sigma_g^+)_{\nu=0}$	$(^3\Sigma_g^-)_{\nu=1}$	865 nm
$(^1\Sigma_g^+)_{\nu=1}$	$(^3\Sigma_g^-)_{\nu=1}$	770 nm
$(^1\Sigma_g^+)_{\nu=0}$	$(^3\Sigma_g^-)_{\nu=0}$	762 nm
$(^1\Delta_g)_{\nu=0}(^1\Delta_g)_{\nu=0}$	$(^3\Sigma_g^-)_{\nu=2}(^3\Sigma_g^-)_{\nu=0}$	786 nm
$(^1\Delta_g)_{\nu=0}(^1\Delta_g)_{\nu=0}$	$(^3\Sigma_g^-)_{\nu=1}(^3\Sigma_g^-)_{\nu=0}$	703 nm
$(^1\Delta_g)_{\nu=0}(^1\Delta_g)_{\nu=0}$	$(^3\Sigma_g^-)_{\nu=0}(^3\Sigma_g^-)_{\nu=0}$	633 nm
$(^1\Delta_g)_{\nu=1}(^1\Delta_g)_{\nu=0}$	$(^3\Sigma_g^-)_{\nu=0}(^3\Sigma_g^-)_{\nu=0}$	578 nm
$(^1\Sigma_g^+)_{\nu=0}(^1\Delta_g)_{\nu=0}$	$(^3\Sigma_g^-)_{\nu=0}(^3\Sigma_g^-)_{\nu=0}$	477 nm
$(^1\Sigma_g^+)_{\nu=0}(^1\Sigma_g^+)_{\nu=0}$	$(^3\Sigma_g^-)_{\nu=0}(^3\Sigma_g^-)_{\nu=0}$	381 nm

^aSubscript ν describes the vibrational mode of the oxygen molecule. Higher vibrational modes in the initial states lead to the emission of photons with higher energy, while higher vibrational modes in the final state lead to the emission of photons with lower energy.¹⁵ The observed wavelengths differ only slightly in different media and allow to identify the generated singlet oxygen.¹⁴ The coloring in the table indicates an approximation for the perceived color of the photon.

Possible reactions are for example ene-reactions and [4 + 2] and [2 + 2] cycloadditions.⁶⁸

3.3. Spin Conservation and Wigner's Rules

Wigner's spin conservation rule states that the total angular momentum of a system does not change during an allowed electronic energy transfer.^{61,69–71} The rule applies both during an electronic transfer between different energy states of the same molecule or atom and during a transfer between molecules or atoms, regardless of ground state or excited state. From Wigner's spin conservation rule, it follows that there must be a correlation of the spins of the electrons involved between the reactants and the products in an allowed reaction. These reactions are also called (electronically) adiabatic.⁷² If one considers a reaction of the reactants A and B with the respective spins S_A and S_B , the possible total spins can be determined with the help of the vector addition rule $|S_A + S_B|$, $|S_A + S_B - 1|$, ..., $|S_A - S_B|$. Both the transition state passed through and the resulting products must have a total spin that corresponds to the values determined from the reactants. In this situation, reactants, transition state, and products are on the same potential energy surface. The Wigner rule can also be illustrated by looking at the individual spins of the type α (\uparrow) and of the type β (\downarrow). In the combined initial and final state of the system, the number of spins of type α and β remains the same, regardless of how they are combined in the final state (see Table 3). The reaction of two reactants in the singlet state ($\uparrow\downarrow + \uparrow\downarrow$) can therefore lead to products in the singlet ($\uparrow\downarrow + \uparrow\downarrow$) or triplet ($\uparrow\uparrow + \downarrow\downarrow$) state but not to a combination of triplet and singlet ($\uparrow\uparrow + \uparrow\downarrow$).

Another example for the role of spin conservation represents the reactions of organic and biological molecules with O_2 , which are typically highly exergonic, whereas they do not occur spontaneously. The standard Gibbs energy of reaction for the reaction of O_2 in the triplet state with the double bond of ethene to formaldehyde is calculated from the standard Gibbs energy of formation (data taken from M. W. Chase⁷³):

Table 3. Examples of Wigner Spin Correlation Rules for Combination of Different Spin State Reaction Partners and Resulting Spin States of Potential Energy Surfaces^{61,69,71a}

reactant A	reactant B	products
Singlet ($S = 0$)	Singlet ($S = 0$)	Singlet ($S = 0$) Singlet ($S = 0$) + Singlet ($S = 0$) Doublet ($S = 1/2$) + Doublet ($S = 1/2$) Triplet ($S = 1$) + Triplet ($S = 1$)
Singlet ($S = 0$)	Doublet ($S = 1/2$)	Doublet ($S = 1/2$) Singlet ($S = 0$) + Doublet ($S = 1/2$) Triplet ($S = 1$) + Doublet ($S = 1/2$)
Singlet ($S = 0$)	Triplet ($S = 1$)	Triplet ($S = 1$) Triplet ($S = 1$) + Singlet ($S = 0$) Doublet ($S = 1/2$) + Doublet ($S = 1/2$) Triplet ($S = 1$) + Triplet ($S = 1$)
Doublet ($S = 1/2$)	Doublet ($S = 1/2$)	Singlet ($S = 0$) Triplet ($S = 1$) Singlet ($S = 0$) + Singlet ($S = 0$) Triplet ($S = 1$) + Singlet ($S = 0$) Doublet ($S = 1/2$) + Doublet ($S = 1/2$) Triplet ($S = 1$) + Triplet ($S = 1$)

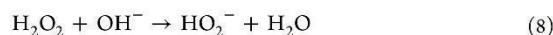
^aReactions are of the type $A + B \rightarrow C + D$.

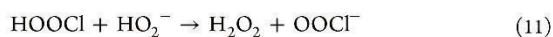


Although this oxygenation reaction is highly exergonic, it does not occur spontaneously due to spin conservation.^{62,74} Ethene, like other typical organic and biologic molecules, is a singlet multiplicity molecule ($S = 0$); the direct reaction of a molecule with $S = 0$ with triplet oxygen (3O_2 ; $S = 1$) would tend to proceed via a reaction surface with $S = 1$ to yield an oxygenation product with $S = 1$ (cf. Table 3). Thereby, reaction rate theory predicts a low probability for any reaction that involves a change in multiplicity.⁷⁴ In contrast, the same reaction with 1O_2 occurs spontaneously since there is no change in multiplicity.⁷⁵ Furthermore, the driving force of the reaction rises due to the excited state of oxygen to $\Delta G^\circ = -382.5$ kJ/mol, making the reaction even more favorable.

Nevertheless, a low probability for a reaction does not exclude the reaction completely and the terms allowed and forbidden must be used carefully. When the term forbidden is used, it usually implies that along a reaction path an additional barrier is encountered. The barrier stems from the unfavorable orbital properties (symmetry) of the system and is sometimes called an electronic barrier. To avoid the electronic barrier, a reaction must proceed via a different reaction path (for example, stepwise instead of concerted). Similarly, a reaction that is allowed is simply one that does not have such an additional electronic barrier. However, this does not mean that an allowed reaction is *per se* favorable. Steric interactions, energetic conditions, spin-orbit-coupling, or other factors could slow down the reaction. In many cases, the additional electronic barrier reduces the observed reaction rate by a significant value.^{76,77} Assuming an Arrhenius-like behavior, an additional activation energy of 5.7 kJ mol⁻¹ results in a 10-fold slower reaction.

Another example for the importance of spin conservation in reactions is the oxidation of H_2O_2 with elemental chlorine, which generates singlet oxygen:^{22,78–80}





Starting with molecules in the singlet state, the reaction proceeds to OOCl^- in the singlet state. OOCl^- finally decomposes to ${}^1\text{O}_2$ and Cl^- . Since the total spin is $S = 0$ and does not change, the oxygen molecule formed must be ${}^1\text{O}_2$, and indeed, it is formed quantitatively. Such a behavior is observed with many strong $2e^-$ -oxidants, as this can lead to a direct transition from singlet to singlet.⁸¹

Spin conservation and Wigner's rule are also assumed to be obeyed in electron transfer reactions on electrode surfaces. Marcus theory, which is one of the most important kinetic models for electron transfer reactions, assumes an adiabatic behavior and therefore spin conservation.⁸²

3.4. Marcus Theory

The Marcus theory was developed to explain the rates of electron transfer reactions between two molecules or ions in a homogeneous solution (e.g., disproportionation of superoxide).⁸³ It can also be used to rationalize electron transfer reactions and is used to describe reactions yielding products in excited states or reactions leading to chemiluminescence. While the Marcus theory *per se* was not intended to describe electron transfer reactions at an electrode, the theory was later extended to include them.⁸³

First, a simple, single electron transfer from one species to another is considered:



Marcus originally only considered outer sphere electron transfer, meaning reactions in which an electron is transferred between two chemical species that remain separate and intact before, during, and after the electron transfer. In the case of inner sphere electron transfer, the two species become connected via a chemical bridge, for example, a ligand or solvent molecule. Electron transfer between two reacting species is a radiationless electronic rearrangement of these species whether it is homogeneous or heterogeneous. Since the transfer is radiationless, the electron must move from its initial state with a given energy to a receiving state with the same energy. This is usually called isoenergetic electron transfer, and it is assumed that the Born–Oppenheimer approximation can be applied to the system. In addition, the Franck–Condon principle is assumed, stating that nuclear momenta and positions do not change on the time scale of the actual act of electron transfer or electronic excitation. This is sometimes also called “optical conditions”, referring to the origin of the Franck–Condon principle. We assume in the following that the assumptions made by the Marcus theory are valid and applicable and the described cases below fall well within these limits. Oxygen reduction and superoxide oxidation in aprotic media are often considered as outer sphere electron transfers, but there are also cases in which significant inner sphere contributions or inner sphere mechanisms are observed, for example, in electrocatalysis involving oxygen or superoxide.^{13,84–86} However, it is known in literature that these assumptions are not always valid, for example, the Born–Oppenheimer approximation (or also adiabatic approximation) breaks down in the case of large distance electron transfer⁸⁷ or when two electronic states are close to each other.⁸⁸

Any reaction proceeds on a multidimensional surface defining the standard Gibbs energy of the systems and includes reactants, products, and solvent. Finally, it is assumed that the free energies of reactants and products depend quadratically on the reaction coordinate, which gives rise to the two shown parabolas in Figure 5. These are essentially diabatic surfaces of the system, as

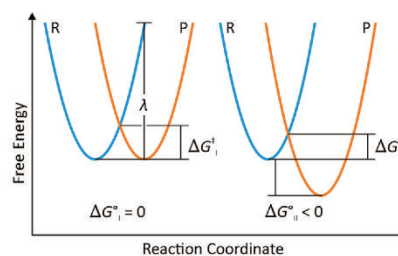


Figure 5. Schematic representation of the Marcus theory for two different systems. The blue parabola R corresponds to the Gibbs energy and the electronic structure of the reactants; the orange parabola P corresponds to that of the products. Both represent diabatic surfaces. On the left side, a self-exchange reaction is shown whose reactants and products are in sum identical (e.g., $\text{Fe}^{3+} + \text{Fe}^{2+} \leftrightarrow \text{Fe}^{2+} + \text{Fe}^{3+}$) and $\Delta G^0 = 0$ kJ/mol. The energy of the reactant parabola at the position of the minimum of the product parabola, the so-called reorganization energy λ , is a measure of the activation energy required. The reaction on the right side is exothermic, the product parabola is therefore shifted downward, and a lower activation energy is observed (e.g., $\text{Fe}^{2+} + \text{Ce}^{4+} \leftrightarrow \text{Fe}^{3+} + \text{Ce}^{3+}$). This is also known as the Bell–Evans–Polanyi principle, which states that in a family of similar reactions, the activation energy decreases with increasing exergonicity. In addition, the position of the transition state shifts toward the reactants and becomes therefore more reactant-like in energy and structure. This is known as the Hammond postulate. In both cases, the mentioned examples are spin allowed (adiabatic) reactions.

they cross each other, opposite to adiabatic surfaces, which avoid those intersections. The transition state of the reaction is at the crossing of the two parabolas, where both states have the same configuration and energy. Electron transfer, essentially a tunnel process between two states, can only occur at this point, in line with the Franck–Condon principle.⁸⁹

The energy of the reactant parabola at the position of the minimum of the product parabola is the so-called reorganization energy λ and is a measure of the activation energy required. It represents the energy needed to transform the nuclear configuration in the reactant state to those of the product state. The model relates the activation barrier to the nuclear reorganization that accompanies the electron transfer. Within the Marcus theory, it is a constant for a given system. The reorganization energy λ is composed of the solvational or outer component λ_o (here given for the case of homogeneous reactions) and vibrational or inner component λ_i :

$$\lambda = \lambda_o + \lambda_i \quad (14)$$

$$\lambda_o = \frac{n^2 e^2}{4\pi\epsilon_0} \left(\frac{1}{D_{\text{op}}} - \frac{1}{D_s} \right) \left(\frac{1}{2a_1} + \frac{1}{2a_2} - \frac{1}{r} \right) \quad (15)$$

where n is the number of transferred electrons, D_{op} is the optical dielectric constant (equal to the square of the refractive index), D_s is the static dielectric constant, a_1 and a_2 are the radii of the two spheres exchanging the charge, and r is the separation between the spheres.

$$\lambda_i = \frac{1}{2} \sum_j k_j (Q_j^r - Q_j^p)^2 \quad (16)$$

where Q_j^r and Q_j^p are equilibrium values for the j th normal mode coordinate Q , and k_j is a reduced force constant, originating from the force constants of reactants and products.

Together with the Gibbs energy of reaction, the activation energy of the reaction can be calculated according to eq 17. The reaction rate can then be determined using eq 18. The term A depends on the nature of the electron transfer reaction (bimolecular, intramolecular, or heterogeneous) and can also contain statistical factors. For further details, see the works by Marcus and others.^{82,83,90–92}

$$\Delta G^* = \frac{1}{4\lambda} (\Delta G^\circ + \lambda)^2 \quad (17)$$

$$k = A \exp\left(-\frac{\Delta G^*}{RT}\right) \quad (18)$$

According to Marcus theory, reactions with increasing exothermic character show decreasing activation energy until a virtually activationless reaction occurs (Figure 6). If the

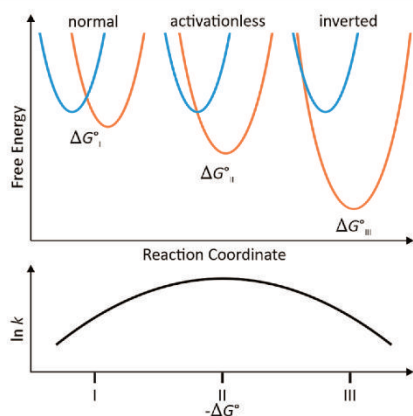


Figure 6. Simplified potential energy curves for an exothermic electron transfer reaction according to the Marcus theory. While the exothermic character of the reaction rises from left to right, the rate constant of the reaction passes through a maximum (bottom). This behavior can be explained by looking at the point of intersection between the reactant and product parabola: with increasing released energy, the point of intersection approaches the minimum of the reactant parabola and passes through it in very strongly exergonic reactions. Up to this point, a rise in exergonicity leads to a higher reaction rate via a larger reaction constant k (I \rightarrow II). This area is also called normal region. At this point, the reaction has no activation barrier; the rate constant is at its maximum. With a further increased exergonicity, the activation barrier rises again, and the reaction slows down again (II \rightarrow III). This region is also known as “Marcus inverted region”. The resulting rate constant k for the different cases can be determined via eqs 14–18.

exothermic character is increased further (ΔG becomes more negative), the activation energy increases again.⁸³ This behavior can be explained by looking at the point of intersection between the reactant and product parabola: with increasing released energy, the point of intersection approaches the minimum of the reactant parabola, which is also known as Bell-Evans–Polanyi principle. In addition, the transition state becomes more reactant-like, which is known as the Hammond postulate. If the position of the transition state reaches the minimum of the

reactant parabola, the reaction is considered activationless and reaches its maximum rate. A further increase in exergonicity does not lead to a higher rate and decreased activation energy as proposed by the Bell-Evans–Polanyi principle. Instead, the crossing point migrates upward again, and the activation energy rises. The region where an increase in exergonicity leads to a higher reaction rate is also called the normal Marcus region. A renewed increase in activation energy despite increasing exergonicity is also referred to as the “Marcus inverted region”. The validity of the theory was successfully experimentally confirmed for intramolecular long-distance electron transfer in organic molecules by Closs and Miller in 1984.^{93,94}

The Marcus theory can also be used to rationalize chemiluminescence reactions if they are accompanied by an electron transfer.⁹⁵ In a chemiluminescence reaction, an electronically excited state is generated by kinetically shunting a would-be highly exergonic electron transfer by a much less exergonic one. The excited species then decays to a lower energy level through the emission of a photon with an energy that is close to that of the difference in enthalpies. The excited product can be shown as additional, upward shifted parabola in comparison to a ground state or unexcited product (Figure 7).

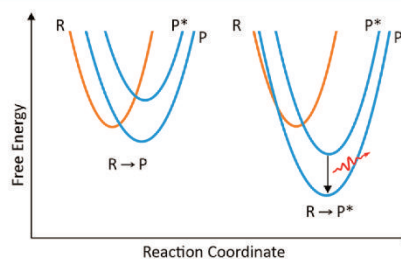


Figure 7. Potential energy curves for an exothermic electron transfer reaction with two possible products, one leading to chemiluminescence.⁹⁶ In a chemiluminescence reaction, an electronically excited state is generated by kinetically shunting a would-be highly exergonic electron transfer by a much less exergonic one. The excited species then decays to a lower energy level through the emission of a photon, the energy of which is close to that of the difference in enthalpies. The excited product can be shown as additional, upward shifted parabola in comparison to a ground state or unexcited product. Left: The reactant parabola intersects with both possible product parabola but due to a lower activation energy only product P in the ground state is formed. No chemiluminescence can be observed. Right: A shift to a sufficiently higher exergonic character leads to the Marcus inverted region for the reaction $R \rightarrow P$ and therefore to an overall higher activation energy. At the same time, product P is accessible in its excited state with a lower activation energy. The reaction proceeds via $R \rightarrow P^*$, in the following deactivation of P^* , back to its ground state P, chemiluminescence can be observed.

In the case of $^1\text{O}_2$, the product parabola would be shifted upward by ≈ 1 eV. In a sufficiently exothermic electron transfer reaction to reach the Marcus inverted region, the region where the surface of ground state products intersects that of reactants is not readily accessible and becomes less accessible with increasing exothermicity.

Under these conditions, the region where the potential energy surface involving an excited product intersects that for the unexcited reactants may be readily accessible within the Marcus theory.⁹⁶ The formation of an excited product can then occur easily, and it should be possible to generate $^1\text{O}_2$ from (molecular) Li_2O_2 . This could be possible with strong $2e^-$

oxidizing agents, like chlorine gas, while assuming a spin allowed reaction. Indeed, as already mentioned above, it is possible to produce $^1\text{O}_2$ from H_2O_2 , which is comparable to Li_2O_2 regarding the oxidation state of oxygen and bond order of the O–O bond even though the chemical nature of the O–H bond is covalent, and the O–Li is more ionic in character. At this point, the question arises whether the formation of $^1\text{O}_2$ is also electrochemically possible or whether the oxidation of peroxides leads to products in the ground state.

At this point, the definition of term adiabatic in electrochemistry must be discussed since it differs from the definition given above.^{61,89} For an electron transfer to occur, some mixing of the two states at the position of the transition state must exist, which results in a splitting of the curves (Figure 8).^{90,91}

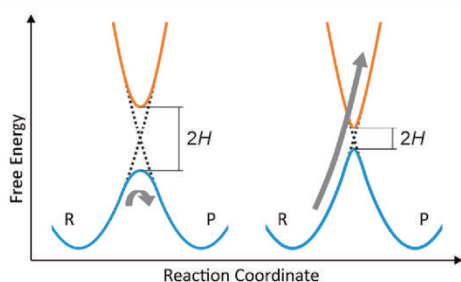


Figure 8. Splitting of the energy surfaces in the region of the transition state. Left: A strong interaction between the reactants leads to a well-defined, continuous energy surface connecting initial and final state of the system. If the reacting system reaches the transition state, the probability is high that it will proceed into the valley corresponding to the products (P), as indicated by the curved arrow. The splitting is greater than kT and the reaction is said to be adiabatic. Right: A weak interaction, less than kT , leads to a small splitting in the region of the transition state. When the reacting system approaches the transition state from the left, it has a tendency to remain on the reactant parabola, as indicated by the straight arrow. The probability of a transition to the product state is small and the system will most likely return to its initial state. The probability of an electron transfer at the intersection of the two diabatic states is described by the electronic transmission factor κ_{el} .

Otherwise the system will remain on its initial diabatic surface, pass over the intersection region, and fall again back to the reactants, therefore excluding the conversion into product. The probability that the reactant is converted into the product on passing the activation barrier is an increasing function of the electronic coupling energy H between the two states at the intersection of the two diabatic surfaces. When resonance between the two states at the transition state is sufficient for the reaction probability to reach unity, the reaction is said to be adiabatic. In this case, the electron transfer proceeds via the energetically favorable surface continuously from reactants to products. The coupling energy H needed to ensure adiabatic behavior is also a function of the reorganization energy λ , but in general a value around kT is deemed to be sufficient. This argument is taken into account by introducing a pre-exponential factor κ_{el} (electronic transmission factor). If $\kappa_{\text{el}} \ll 1$, or the splitting is less than kT , the reaction is said to be diabatic (or nonadiabatic, a double negation). Strictly speaking, the coupling energy H should be subtracted from the derived activation free energy. However, in most cases, H is small enough for this correction to be negligible but large enough for adiabaticity to be ensured. The electronic transmission factor κ_{el} can be calculated

using eq 19 and the passage from a diabatic to an adiabatic behavior is shown in Figure 9:⁹⁰

$$\kappa_{\text{el}} = \frac{2 - 2 \exp\left[-\frac{\pi^{3/2} H^2}{\lambda^{1/2}} \left(\frac{F}{RT}\right)^{3/2}\right]}{2 - \exp\left[-\frac{\pi^{3/2} H^2}{\lambda^{1/2}} \left(\frac{F}{RT}\right)^{3/2}\right]} \quad (19)$$

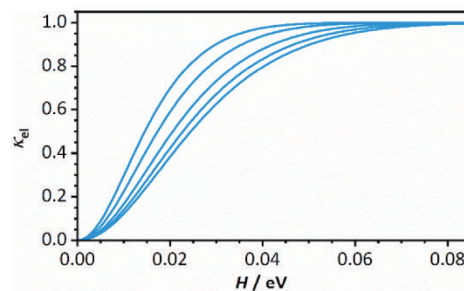


Figure 9. Passage from nonadiabatic to adiabatic conditions. Variations of the transmission coefficient κ_{el} with the electronic coupling energy H for various values of the reorganization energy. From left to right, $\lambda_i = 0.5, 1, 2, 3, 4$ eV; temperature: 25 °C. Formula for calculation taken from Savéant.⁹⁰

Up to this point, the Marcus theory only applies to electron transfer in homogeneous solution. The Marcus–Hush–Chidsey theory extends this concept to electrochemical reactions between metal electrodes and reactants in solution. Since solid electrodes are considered, their band structure is taken into account (Figure 10). In contrast to the classical Marcus theory, there are now not only two potential energy surfaces, which are approximated by harmonic parabola, but combinations of harmonic parabolae including the (simplified) band structure of the bulk phase of the metal electrode.

The energy states within the band structure are only considered if these are occupied by electrons: in case of an oxidation on the product side or in case of a reduction on the reactant side. The consideration of the band structure leads to completely different kinetic results than with individual molecules reacting in homogeneous solution, as in the classical Marcus theory. To calculate the resulting rate constants in such a case, the approach is to use the forward and backward rate constant expressions of the individual rate constants (eqs 17 and 18) and sum these individual rate constants over all electronic states. The contribution of each state to the resulting rate constant is weighted according to the Fermi–Dirac distribution. Assuming that H_i and the density of states and therefore $\kappa_{\text{el},i}$ are independent of the energy of the electronic states, the results are expressed by eqs 20 and 21:

$$k_f(E) = \frac{k_{\infty}}{\sqrt{4\pi\lambda_i}} \int_{-\infty}^{\infty} \frac{\exp\left[-\frac{RT}{4E\lambda_i} \left\{ \frac{F}{RT} |\lambda_i + (E - E^0)| - \zeta \right\}^2\right]}{1 + \exp(\zeta)} d\zeta \\ = \frac{k_{\infty}}{\sqrt{\pi}} \int_{-\infty}^{\infty} \frac{\exp[-v^2] dv}{1 + \exp\left\{ \frac{F}{RT} |\lambda_i + (E - E^0)| \right\} \exp\left(\sqrt{\frac{4E\lambda_i}{RT}} v\right)} \quad (20)$$

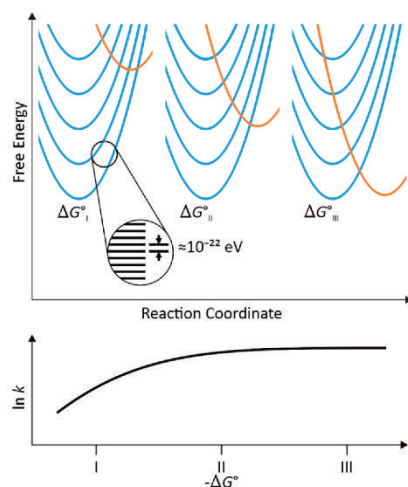


Figure 10. Schematic, simplified representation of an electrode reaction by the Marcus–Hush–Chidsey theory. The blue group of reactants parabolae consists of individual parabolae with energy intervals of about 10^{-22} eV. This corresponds to a parabola for every possible state of an electron in the conducting band of the metal electrode. Since the electron occupies a band state at the beginning of the reaction, the shown reaction is a reduction (e.g., $\text{Fe}^{3+} + \text{e}^- \rightarrow \text{Fe}^{2+}$). With increasing exergonicity, additional lower states of the band structure are accessible, which is kinetically favorable. The exergonicity of a reaction can be tuned by applying a potential to the electrode. Contrary to Figure 6, an increase in exergonicity as shown from II to III does not lead to a lower reaction rate and a Marcus inverted region. Instead, a limiting behavior is found after reaching a sufficient potential since there is always a state without a barrier through which the reaction can take place. Overall, the reaction still proceeds via states on the band edge since holes in lower states are quickly filled with electrons from states near the Fermi level in case of a reduction. Energy conservation is therefore given overall, despite a limiting kinetic behavior.

$$\begin{aligned}
 k_i(E) &= \frac{k_\infty}{\sqrt{4\pi\lambda_t}} \int_{-\infty}^{\infty} \frac{\exp\left[-\frac{RT}{4\lambda_t} \left\{ \frac{F}{RT} |\lambda_t - (E - E^0)| - \zeta \right\}^2\right]}{1 + \exp(\zeta)} d\zeta \\
 &= \frac{k_\infty}{\sqrt{\pi}} \int_{-\infty}^{\infty} \frac{\exp[-v^2] dv}{1 + \exp\left\{ \frac{F}{RT} [\lambda_t - (E - E^0)] \right\} \exp\left(\sqrt{\frac{4F\lambda_t}{RT}} v\right)}
 \end{aligned} \quad (21)$$

The most important consequence of taking all electrode electronic states into account is the disappearance of the inverted region that is predicted by the classical Marcus theory. Since the band structure of the metal contains quasi-continuous states for receiving or releasing electrons, the reaction can proceed without a barrier after a sufficient potential is reached in case of a reduction via states below the Fermi level or above the Fermi level in case of an oxidation (Figures 10 and 11). The inverted region is therefore wiped out by the interference of other electronic states in the electrode, which are thermodynamically unfavorable but kinetically advantageous. This results in a limiting behavior for electrode reactions.⁹⁰ In other words, due to the large width of the band structure of the metal electrode, the system can easily reduce the exothermic character of an electron transfer by electron transfer from/into such a filled/unfilled level. Energy conservation is also given overall, despite a limiting kinetic behavior. The reaction proceeds quasi

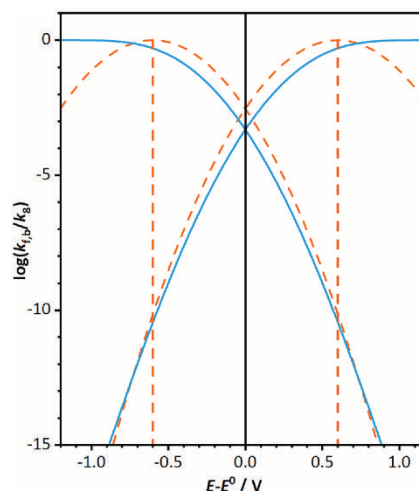


Figure 11. Effect of taking into account all electrode electronic states in the case of an electrochemical reaction ($\lambda = 0.6$ eV; temperature: 25 °C). The dotted, orange lines represent the rate constants as predicted by classical Marcus theory (eqs 17 and 18). A maximum is observed at $E - E^0 = \pm\lambda$ and the corresponding inverted regions at values $E - E^0 < -\lambda$ in the case of the forward rate constant and $E - E^0 > \lambda$ in the case of the backward rate constant. The inverted region vanishes when all electrode electronic states are taken into account (solid, blue lines, eqs 20 and 21).

via states on the band edge since holes in lower states are quickly filled with electrons from states near the Fermi level in case of a reduction (vice versa in the case of an oxidation).

A direct comparison between an electrode reaction with and without taking all electronic states into account is shown in Figure 11. The computation can be further refined by using for example calculated density of states as was shown by Kurchin and Viswanathan.⁹⁷ The integrals shown in eqs 20 and 21 can also be approximated with small errors for ease of computation.^{98,99}

Spin conservation is still applied in the Marcus–Hush–Chidsey theory since adiabatic behavior of the reaction is assumed. This is not in conflict with the absence of an inverted region: formed products are in the lowest energetic state possible since a higher exergonicity simply cannot lead to a higher activation energy compared to a reaction path leading to an excited state. Thus, unless the formation of the excited state of an ion by electron transfer to or from the electrode has an exceedingly small activation barrier, it cannot compete with the formation of the ground state of an ion or molecule.⁹⁶ There is also experimental evidence showing that it is not possible to reach excited states by direct electron transfer at electrodes.^{100,101}

Albeit it is not possible to reach excited states via direct 1e^- or 2e^- electron transfer reactions at a metal electrode, it is still possible that electrochemical reactions lead to chemiluminescence if they are coupled with homogeneous chemical reactions. This concept is called electrochemiluminescence (ECL) or sometimes electrogenerated chemiluminescence, which we consider as a better term in this case. An often-shown example is the so-called annihilation ECL of $\text{Ru}(\text{bipy})_3^{2+}$. First, $\text{Ru}(\text{bipy})_3^+$ and $\text{Ru}(\text{bipy})_3^{3+}$ are generated electrochemically.¹⁰² A following comproportionation reaction in solution leads to an excited product, which relaxes into the ground state with

emission of a photon. A generalized scheme for this reaction is shown as follows:



The Marcus theory can also be applied to electron transfer reactions at semiconductor–liquid interfaces. In the case of narrow bandwidth semiconductors, only few states of the electrode need to be considered. In principle, this leads back to the Marcus theory for homogeneous electron transfer. Again, this gives rise to a Marcus inverted region for the electron transfer reaction.⁹⁶ This behavior was indeed found in some cases, notably in metal oxide semiconductor/inorganic dye systems.^{103,104} This case was treated extensively by Gerischer.^{105,106}

4. REACTION MECHANISMS LEADING TO SINGLET OXYGEN

As summarized in the literature review section, the generation of singlet oxygen requires specific experimental conditions and often has led to contradictory results. As summarized in the previous section, quantum-chemical considerations and their application in reaction dynamics also lead to conditions that are required for realistic reactions paths. In the final section, we will discuss whether these conditions are fulfilled in cathodes of metal/O₂ batteries.

4.1. Discharging Me/O₂ Cells: Singlet Oxygen from Chemical Reactions

Singlet oxygen can obviously only stem from reactions that release molecular oxygen. Conversely, this means that in the case of oxygen reduction reactions (ORR) at electrodes singlet oxygen can only be observed if the superoxide formed in the first step is not the final product. In this case, a disproportionation can occur (a purely chemical reaction), which forms, for example, a peroxide under the release of oxygen. This reaction is known for the case of proton and lithium cation induced disproportionation of superoxides. To some extent, this reaction is also known from Na/O₂ batteries, but in these cases, water seems to play a role and the overall thermodynamic driving force is small.¹⁰⁷ Strictly speaking, only a reduction of oxygen to superoxide is necessary, the electron transferred does not need to stem from an electrode, but of course this will be the main route in electrochemical cells. Different mechanisms leading to oxygen evolution during an overall reduction reaction, which finally leads to a peroxide, can be proposed based on a scheme of squares (Figure 12). The scheme shows possible intermediates starting from molecular oxygen. Steps in horizontal direction correspond to electron transfers, which can be described by a redox or electrode potential. Vertical steps correspond to dis- or association reactions with a cation, which can be described by an equilibrium constant. It is unlikely that the oxygen species under consideration, in solution and with the given conditions, will undergo a significant equilibrium with their positively charged counterparts. The species XO₂⁺, X₂O₂²⁺, and X₂O₂⁺ can hence be neglected. As can be seen from the scheme, the first step in all possible cases is, assuming a 1e⁻-reaction, the reduction of oxygen to superoxide. If suitable cations are present in the

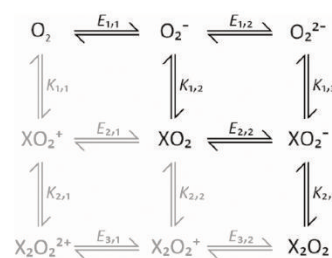
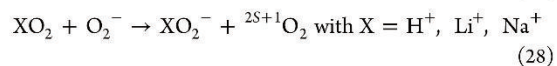
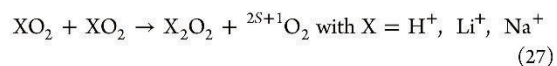
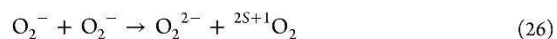


Figure 12. Scheme of squares for the reduction of molecular oxygen to the corresponding peroxide with X = H⁺, Li⁺, Na⁺ in aprotic solvents. A horizontal step corresponds to electron transfer, which can be described by a standard potential $E_{x,y}$. Therefore, moving to the right is equal to a reduction step. A vertical step adds or removes a cation, which can be described by an equilibrium constant $K_{x,y}$. Compounds in gray do not play a major role in the systems under consideration.

solution, the superoxide formed will associate with the cation, resulting in XO₂.

The only possible species that can participate in a disproportionation are O₂⁻ and XO₂, as they can be both reduced and oxidized. Vice versa, the reaction between two species at the edges corresponds to a comproportionation. This leads to three general possible reactions, which can release oxygen (the spin state will not be stated and instead the general term for the multiplicity (2S + 1) is used):



The disproportionation of pure superoxide to the peroxide dianion does not seem to play a role since it is highly unfavorable in aprotic solvents.¹⁰⁸ The stability of tetramethylammonium superoxide in aprotic solutions is also known in literature. It is stable as long as solvent and used tetramethylammonium superoxide are dry and free of impurities.¹⁰⁹ Therefore, at least one cation must be involved. This is also the case for the disproportionation of superoxide in water, where the dianion is also nonexistent and not relevant in the mechanism, instead protons enable the formation of HO₂ and subsequently HO₂⁻, which is finally protonated to form H₂O₂.^{108,110} A general ECL mechanism, which could explain the observed singlet oxygen, can be proposed based on an EC mechanism. When describing electrochemical reactions an “E” and “C” formalism is often employed. The E represents an electron transfer at an electrode; the C represents a chemical reaction which can be any elementary reaction step. If a process in which a chemical step must occur first and is followed by an electron transfer, it is referred as a CE mechanism, whereas an electron transfer followed by a chemical step is an EC mechanism and so on. For further details, see the works by Testa and Reimuth.¹¹¹ For the two remaining reactions, oxygen is reduced to superoxide in the first step. In further steps, the formed superoxide associates with the corresponding cation and disproportionates into peroxide and oxygen (eqs 27 and 28). Both types of superoxides, with or without associated cation, are in a doublet spin state. According to Wigner’s rules, the reaction of two doublets can return products in singlet state (Table 3). This type of reaction is called

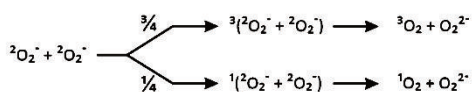
doublet–doublet-annihilation and could be the root of the found singlet oxygen, at least in theory. However, these reactions would also be spin allowed if they generate $^3\text{O}_2$, which would be the thermodynamically favorable product. As proposed by Nanni et al., the generation of $^1\text{O}_2$, whether by disproportionation of superoxide or oxidation thereof, seems to depend on the spin of the transition state, which is in line with Wigner's rule of spin conservation.²⁸ As mentioned above, both the transition state passed through and the resulting products must have a total spin that corresponds to the spins of the reactants. In this situation, reactants, transition state, and products are on the same potential energy surface. On the basis of semi empirical SCF-MO-INDO calculations and experiments, Nanni et al. found that the transition state of the redox reaction involving O_2^- dictates the multiplicity of the released oxygen. They stated that if the mechanism involves a triplet transition state, for example, electron transfer from O_2^- to HO_2 , then triplet oxygen should be favored.²⁸

The reaction energies of eqs 27 and 28 for the corresponding different spin state products differ only by the difference of energy of $^3\text{O}_2$ to $^1\text{O}_2$ in a first approximation. Assuming that eqs 27 and 28 are elementary step reactions, it can therefore be expected that the activation barrier is smaller in the case of $^3\text{O}_2$ since it is the thermodynamically lower lying product. In addition, the position of the transition state on the reaction coordinate, leading to triplet oxygen, should be shifted toward the reactants. If eqs 27 and 28 are elementary step reactions, it could be assumed that the fraction of singlet oxygen generated would only depend on the difference in activation energy of the two different reaction paths.

Other spin statistical effects could also play a role. The parameter A in eq 18 can be extended to include a spin statistical factor σ , accounting for different possible spin factors. At collision of two reactants in solution, a precursor complex (also called encounter complex) is formed that can undergo electron transfer. The total number of possible total spin angular momentum quantum numbers S of such a complex is given by the product of the multiplicity of the reactants. Again, to achieve a correlation and an allowed reaction, both the transition state passed through and the resulting products must have a total spin magnitude that belongs to the values determined from the reactants.

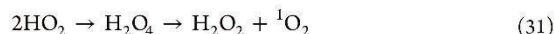
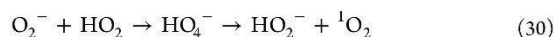
Considering the possible total spin S of eq 27 and 28, starting from $S_{\text{LiO}_2} = S_{\text{O}_2^-} = 1/2$, four different spin states of the precursor complex result. Each of four spin states is then expected to form with equal probability upon collision of the two reactants. Three of these would be sublevels of the encounter complex with triplet multiplicity, $S = S_{\text{LiO}_2} + S_{\text{O}_2^-} = 1$, $2S + 1 = 3$, and the fourth is a singlet encounter complex, $S = S_{\text{LiO}_2} - S_{\text{O}_2^-} = 0$, $2S + 1 = 1$ (see Scheme 2). Only the latter could undergo a reaction to $^1\text{O}_2$, leading to a spin statistical factor $\sigma = 1/4$, suggesting that the rate constant for the electron transfer will not exceed one-third of the reaction rate leading to $^3\text{O}_2$, even in the case of similar activation

Scheme 2. Probability of Different Multiplicities for a Precursor Complex Consisting of Two Doublets, In This Case Superoxide Ions



energies for the corresponding reactions.¹¹² In reality, the rate constant in the case of $^1\text{O}_2$ will be even lower since the exergonicity of the reaction leading to $^1\text{O}_2$ is lower in comparison to the reaction leading to $^3\text{O}_2$, suggesting a higher activation energy in the case of $^1\text{O}_2$.

Mahne et al. found a correlation between the fraction of generated singlet oxygen and the concentration of trace water. They assumed that H_2O or other proton sources will protonate superoxide ions to form the HO_2 radical. The following reactions finally lead to $^1\text{O}_2$ (see eqs 29–31).¹¹ These reaction were also proposed by Corey et al. in 1987.⁴³ Corey et al. and Mahne et al. did not specify if they assume H_2O_4 or HO_4^- to be intermediates or transition states of the reactions. In addition, the calculations of Zaichenko et al. indicate that during the dissociation of HO_2 the singlet oxygen path cannot be reached at least in the gas phase:⁵⁰



This reaction path would also fall into the category of electrogenerated chemiluminescence and as described above, these reactions do not lead to singlet oxygen in the case of protons. In addition, the exact mechanism is known for the case of H^+ : the disproportionation proceeds via eq 28 in aprotic organic solvents, as was shown by Andrieux et al.¹¹³ In the case of lithium peroxide, various reaction mechanisms are discussed. The exact reaction mechanism is unclear and seems to depend on the electrolyte used.⁶ It is not known if the disproportionation proceeds exclusively via LiO_2 (eq 27) or if O_2^- (eq 28) is also involved.

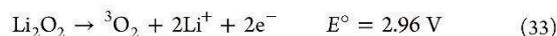
4.2. Charging Me/O₂ Cells: Singlet Oxygen from Electrochemical Reactions

Finally, the question arises whether, in addition to the disproportionation of superoxides, the oxygen evolution reaction is also a possible source of singlet oxygen. Different cases should be distinguished here: on the one hand the oxidation of dissolved super- and peroxides (whether dissociated or ion pair), on the other hand the oxidation of the super- and peroxides deposited on the electrode. In these cases, different models need to be applied.

Looking at the oxidation of a dissolved peroxide at a metallic electrode one starts at the right edge of the scheme of squares (Figure 12). A $1e^-$ -oxidation would lead to a superoxide species (example given in eq 32), which could then disproportionate via eqs 27 and 28 and would overall generate $^1\text{O}_2$ in the oxidation of Li_2O_2 :



The same train of thought as in the case of the oxygen reduction reactions applies here, and again these reactions would fall into an EC-mechanism scheme. Besides this mechanism, a direct oxidation of the peroxide to oxygen is conceivable:



The released oxygen could be $^1\text{O}_2$ at first sight, but several arguments speak against it. First, it should be noted that a widely

held concept in electrochemistry is that truly elementary electron-transfer reactions always involve the exchange of one electron.^{91,114} To observe true two-electron transfer reactions, no coupled chemical steps are possible in the reaction path. This is clearly not the case in the oxidation of lithium peroxide, which is accompanied by decomposition in different products in completely different solvation shells. It can therefore be assumed that the oxidation consists of several elementary steps and some type of lithium superoxide-like species is involved in the oxidation of lithium peroxide to oxygen. In addition, the standard potentials of the reactants involved and their relative position to each other must be considered. The oxidation of the peroxide occurs at potentials of more than 3 V vs Li⁺/Li while the standard potential of LiO₂ is unknown due to its transient character. A possible range for the standard potential is below 2.96 V vs Li⁺/Li and above the standard potential of O₂/O₂⁻, which is at around 2.5 V vs Li⁺/Li in organic aprotic solvents.^{108,115–117} It is therefore more difficult to oxidize lithium peroxide than lithium superoxide, which is described as “potential inversion”.^{114,118} Consequently, lithium superoxide is not stable in the potential range needed to oxidize lithium peroxide and is thus oxidized immediately, a two-electron oxidation should be observed. LiO₂ could be an intermediate while charging but its lifetime is small, and it is difficult to detect it experimentally. The existence of lithium superoxide as an intermediate during charging is also discussed in the literature.^{119–123} The same train of thought can be applied to almost all electrode reactions for which more than one electron is transferred. As an example, the reduction of Fe²⁺ to Fe⁰ is assumed to proceed via Fe⁺.¹²⁴ Two electrons are transferred, while the intermediate Fe⁺ is yet not known experimentally. Second, the Marcus theory predicts a four times higher λ₀ in the case of a 2e⁻ transfer (eqs 14 and 15). This leads to higher activation energies and slower kinetics in these cases, rendering 2e⁻ transfers unlikely. Third, the Marcus–Hush–Chidsey theory predicts, that it is not possible to reach excited states via direct electron transfer reactions (cf. section 3.4). On the basis of these theoretical considerations and the related arguments it should, for example, not be possible to form ¹O₂ directly from dissolved peroxides by a direct 2e⁻ electrochemical reaction at a metal electrode/solution interface. Therefore, the observed ¹O₂ must originate from a chemical reaction, for example, the disproportionation of superoxide or a side reaction. The same argument shows that it is also not possible to generate ¹O₂ from a superoxide via a direct 1e⁻ electrochemical reaction (eq 35) because here again the Marcus–Hush–Chidsey theory predicts that the generation of excited states is not possible:



Notably, the differences in the standard potentials of a reaction resulting in triplet or singlet oxygen are 0.96 V in the case of one transferred electron (e.g., eq 35) and 0.48 V in the case of two transferred electrons (e.g., eqs 33 and 34).

The dissolution processes of the precipitated oxides are quite different to the solution-mediated processes mentioned above. The general situation consists of an ion-blocking metallic electrode in contact with an insulating or wide band gap oxide. The oxide is also in contact with the solution. The exact oxidation mechanisms for the respective super- and peroxides are unknown and only some theoretical papers exist on this topic. It can be assumed that a hole is generated on the interface between the oxide and the electrode during oxidation. The hole then moves probably via hole hopping or tunneling of electrons

to the surface.^{125–129} At the surface, disproportionation of superoxide like species or oxidation by holes thereof releases oxygen. If the precipitated oxide is indeed a semiconductor, the dissolution would depend on the hole migration to the surface as described by Gerischer and others.^{105,130,131} It could be argued that the observed luminescence by Wandt et al. stems from an anodic dissolution process of a carbonate, but they found a dependence on the state of charge of the used electrodes. The luminescence roots therefore in a chemical reaction of the electrode material, which is independent of the applied potential. Therefore, luminescence from anodic (semiconductor) dissolution is not known in literature to our best knowledge.

4.3. Singlet Oxygen from Side Reactions

In addition to the generation of singlet oxygen during oxygen reduction or oxygen evolution reaction, the possibility of a side reaction leading to singlet oxygen must be considered. The prime example for such a case is the above-mentioned detection of singlet oxygen from superoxide in CCl₄ by Khan et al., where singlet oxygen is produced but was erroneously contributed to the disproportionation of superoxide.

Nanni et al. have shown that the reaction of one-electron oxidizers with the superoxide anion could lead to singlet oxygen, if a singlet transition state is possible.²⁸ In this regard, the use of redox mediators must be carefully considered. Used redox mediators, such as TEMPO, tetrathiafulvalene (TTF), 2-azaadamantane-*N*-oxyl (AZADO), LiI, LiBr, ferrocene, and others, are one-electron oxidizers.^{132–136} In the reaction of the ferrocene cation and the superoxide anion, singlet oxygen is a reaction product. Other strong oxidizers are evidenced *in situ* in metal/O₂ batteries, for example, the peroxycarbonate radical anion, peroxydicarbonate anion, and the carbonate radical anion, which were found by Zhang et al. as a result of the reaction between CO₂ and superoxide. They also seem to play a major role in the formation of carbonate from ether- and carbonate-based electrolytes.³⁸ Danen and Arudi and MacManus et al. detected singlet oxygen in the reaction of diacyl peroxides with superoxide.^{26,36} It could be argued that symmetrical peroxydicarbonate (8) is akin to diacyl peroxides, possibly resulting in singlet oxygen when reacting with superoxide anions.

Besides, the reactivity of the individual intermediates and products needs to be considered. The superoxide anion is a strong base and good nucleophile.¹⁰⁸ Together with proton sources, it disproportionates to hydrogen peroxide, which is a good oxidant. Traces of water can practically always be expected in the systems under consideration.

4.4. Specificity of Singlet Oxygen Traps

Another, sometimes overlooked, problem is the specificity of the singlet oxygen traps used. Ideally, a suitable trap should only react with singlet oxygen or the product should be a chemical fingerprint specific for singlet oxygen. Metal/O₂ batteries can contain a variety of different reactive oxygen species, like triplet oxygen, superoxide anions, and peroxide anions, but might also contain peracids, peroxy radicals, and hydrogen peroxide.

The use of 4-oxo-TEMP as a trap has already proven to be such an example, as peroxycarbonates occurring in the batteries are also able to oxidize 4-oxo-TEMP to 4-oxo-TEMPO, as shown by Zhang et al.³⁸ The CO₂ required for this reaction is practically always present in metal/O₂ batteries during charge due to the decomposition of the organic electrolyte.¹³⁷ This is also in line with the findings of Mahne et al., who observed a

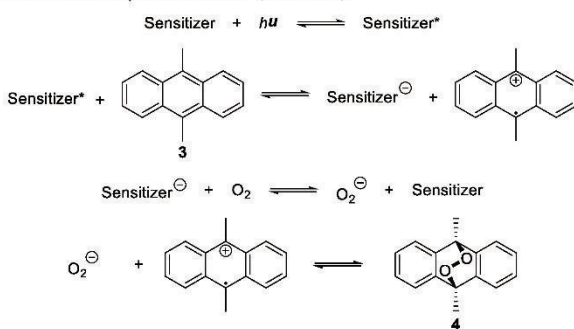
connection between the oxidation of lithium carbonate and $^1\text{O}_2$.¹²

Another problematic class of traps are furans, which were used by Mayeda and Bard for trapping in superoxide disproportionation experiments.²⁰ While furans react with singlet oxygen via an endoperoxide to a diketone, it is also possible to form the diketone from the starting furans with the help of peracids, peroxy radicals, H_2O_2 , triplet oxygen, or electrochemical oxidation.²¹

A general class of reactions, which need to be considered, are electron-transfer oxygenations, which do not involve singlet oxygen but mimic many of its reactions.

Scheme 3 shows the case of photoinduced electron-transfer oxygenations, where an electron-poor sensitizer (for example,

Scheme 3. Photoinduced Electron-Transfer Oxygenation of 9,10-Dimethylanthracene (DMA, 3)



9,10-dicyanoanthracene¹³⁸ or 9-mesityl-10-methylacridinium¹³⁹) is excited and reacts with an electron donor to give a radical ion pair.¹⁴⁰ The reduced sensitizer is oxidized by oxygen back to its ground state resulting in a superoxide anion. Finally, the donor cation and superoxide anion react to an oxygenated product. Importantly, this reaction yields endoperoxides in the case of dienes and aromatic systems.^{141,142}

Similar reactions are also possible electrochemically, where donor cation and superoxide are directly produced on two closely placed electrodes. This behavior was shown by Amatore et al. in the case of anthracene.¹⁴³ The question therefore arises as to the origin of the DMAO_2 4 found since it is at least conceivable that DMA 3 reacts to form DMA^+ through oxidants formed *in situ* in metal/ O_2 batteries (for example, by reacting with peroxy carbonate radical anions or carbonate radical anions). A further reaction with superoxide resulting in DMAO_2 4 cannot be ruled out then (here).

The above discussion shows that the reliable detection of singlet oxygen is difficult. One possible way out of this dilemma is to use quantitative methods, for example, a combination of a singlet oxygen trap and a quencher. The amount of inhibition detected with an inhibitor should be quantitatively compared to that expected, based on known rate constants. This technique was discussed in further detail by Foote.²¹ Another useful technique could be the use of deuterated solvents, which exhibit a longer lifetime of $^1\text{O}_2$, thus reactions involving $^1\text{O}_2$ are generally more efficient in deuterated solvents. A kinetic isotope effect can be expected for reactions involving singlet oxygen, but the magnitude of the effect can vary, depending on the kinetics of the system. A kinetic isotope effect for other possible reactions must also be considered. A particularly important example is the disproportionation of the superoxide anion in water, which has

been shown to have a kinetic isotope effect $k_{\text{H}}/k_{\text{D}}$ of 3.5.¹⁴⁴ Luminescence can also be used to detect singlet oxygen, but unfortunately is often not suitable for quantification. Besides, luminescence is extremely inefficient with a quantum yield around 10^{-9} . Obviously, it is not sufficient to detect only the light emission of a reaction, but the wavelength of the emitted light must be determined.

One problem remains with the techniques listed above, which is that they can be applied mainly in homogeneous systems since the simple kinetics may not apply in heterogeneous systems. Another problem with heterogeneous systems is that it is difficult to know where reagents are located; they may be inhomogeneously concentrated (e.g., in pores of an electrode). Thus, either less or more of a trap or quencher may be present in a given region than the average concentration in the bulk solution would suggest, making quantification even more difficult. The detection of luminescence is also made more complicated in these systems.

5. CONCLUSIONS

In light of all reviewed results, we conclude that there is still no unambiguous proof of singlet oxygen formation (originating from the proposed mechanisms in literature) in metal/ O_2 electrochemical cells.

Singlet oxygen satisfies the thirst for an explanation for the observed degradation of electrolyte components in metal/ O_2 batteries, but it may be too simple an explanation after all. Singlet oxygen formation is inherently a complex subject both in its theoretical description and in its experimental detection. Extraordinary claims require extraordinary evidence, and the past has shown that not all evidence can stand up to scrutiny.

First, the disproportionation of superoxide induced by metal cations like Li^+ and Na^+ is considered. In this case, the existing data originate from trapping and quenching experiments and no luminescence was observed. The found singlet oxygen could therefore also result from side reactions or it could be a false positive result, as already described in the literature by Zhang et al. resulting in no singlet oxygen at all.³⁸ To exclude the possibility of a side reaction, the choice of a suitable trap is essential and careful, extensive search for possible side reactions is necessary.

Second, the proton-induced disproportionation of superoxide ions as a source of singlet oxygen seems unlikely, whether in aqueous solution or in organic solvents, especially in the light of reported results by Kanofsky, Sawyer, Koppenol, and others.^{28–30,32,42,44,46}

In general, from a spin conservation point of view, both triplet and singlet oxygen are possible as reaction products of a disproportionation reaction, while triplet oxygen would be preferred due to the lower Gibbs energy of reaction compared to singlet oxygen. The fraction of generated singlet oxygen would therefore be determined by the difference in the overall rate of the reactions, depending largely on the difference in activation energy and the electron transfer probability for the different paths.

Third, the direct electrochemical generation of singlet oxygen as proposed by Hassoun et al., Wandt et al., and Mahne et al. needs to be considered, which appears not to be possible when considering the oxidation of superoxides and peroxides in the framework of the Marcus–Hush–Chidsey theory: $1e^-$ and $2e^-$ transfer reactions at a metal (or metal-like) electrode are considered not to lead to excited states for dissolved reactants. Instead, using the Marcus–Hush–Chidsey theory, a limiting

kinetic behavior must be assumed for electrochemical reactions, leading to ground state products. While singlet oxygen luminescence was found in electrochemical experiments, they were also linked to Li_2CO_3 and H_2O , suggesting a side reaction leading to electrogenerated chemiluminescence. In the case of semiconductors and isolators, excited states are, based on the Marcus–Hush–Chidsey theory, accessible but these cases are specific and scarce and only a few examples are discussed in literature.^{103,104}

The discussion of singlet oxygen in metal/ O_2 batteries is hampered by a lack of thermodynamic and kinetic data, for example, standard potentials, equilibrium constants, and rates of reaction. This is especially true in the case of Li/O_2 batteries, in which transient intermediates are involved. A better understanding of the underlying reaction mechanisms, and the interplay of the many reactive species in metal/ O_2 batteries, is necessary to enable further progress. However, it is also clear that most observations will be understood based on the mechanisms established using simple or simplified systems. Thus, any study of singlet oxygen in heterogeneous systems will require an excellent comprehension of the individual mechanism of generation, deactivation, and reaction of singlet oxygen. The argument above can also be extended to metal/ O_2 batteries in general and especially to the superoxide chemistry within these systems.

In any case, methods that are more specific or a combination of several techniques should be used to provide unequivocal experimental evidence for singlet oxygen. The use of deuterated solvents to increase the half-life of singlet oxygen could be useful, and if possible, detection by luminescence should be used. The combination of traps and quenchers has also been found to be adequate. Even in cases where singlet oxygen is found, correct source identification remains a challenge, especially in complex, heterogeneous matrices such as metal/ O_2 batteries. Other reactive oxygen species may also play a role and need to be considered in the experiments.

We do not intend to rule out the possibility that singlet oxygen occurs in the reported experiments. However, the analytical methods used in future experiments must also demonstrate that side reactions leading to false positive results can be clearly excluded or quantified. The challenges posed by $^1\text{O}_2$ require fundamental work to understand the chemistry that occurs. This will ultimately lead to a better fundamental understanding of electrochemistry in general and oxygen electrochemistry in particular and will provide a solid foundation for future metal/ O_2 batteries.

AUTHOR INFORMATION

Corresponding Authors

Jürgen Janek – *Institute of Physical Chemistry, Justus Liebig University Giessen, 35392 Giessen, Germany; Center for Materials Research (LaMa), Justus Liebig University Giessen, 35392 Giessen, Germany; orcid.org/0000-0002-9221-4756; Email: juergen.janek@phys.chemie.uni-giessen.de*

Daniel Schröder – *Institute of Energy and Process Systems Engineering (InES), Technische Universität Braunschweig, 38106 Braunschweig, Germany; orcid.org/0000-0002-2198-0218; Email: d.schroeder@tu-braunschweig.de*

Authors

Adrian Schürmann – *Institute of Physical Chemistry, Justus Liebig University Giessen, 35392 Giessen, Germany; Center for*

Materials Research (LaMa), Justus Liebig University Giessen, 35392 Giessen, Germany

Bjoern Luerßen – *Institute of Physical Chemistry, Justus Liebig University Giessen, 35392 Giessen, Germany; Center for Materials Research (LaMa), Justus Liebig University Giessen, 35392 Giessen, Germany*

Doreen Mollenhauer – *Institute of Physical Chemistry, Justus Liebig University Giessen, 35392 Giessen, Germany; Center for Materials Research (LaMa), Justus Liebig University Giessen, 35392 Giessen, Germany; orcid.org/0000-0003-0084-4599*

Complete contact information is available at:

<https://pubs.acs.org/10.1021/acs.chemrev.1c00139>

Notes

The authors declare no competing financial interest.

Biographies

Adrian Schürmann received his master's degree in 2016 from the University of Giessen, where he studied chemistry. He is currently a Ph.D. student in the research group of Prof. Jürgen Janek at the Institute of Physical Chemistry. His research interests mainly focus on the fundamental understanding of the chemistry of nonaqueous Li/O_2 batteries.

Bjoern Luerßen studied chemistry at the University of Hannover and received his doctorate from the Justus Liebig University in 2003. Since 2006, he has been employed as a senior lecturer at the Institute of Physical Chemistry in Gießen. His research interests are in the field of kinetics of interfacial reactions, in particular the reduction/oxidation of oxygen at metal/solid electrolyte interfaces but also interfacial layer (SEI) formation in lithium-ion batteries.

Doreen Mollenhauer is a chemist and studied at Friedrich-Schiller University Jena, Germany. In 2011, she received her doctoral degree in theoretical chemistry at Freie Universität Berlin. After research stays as postdoctoral fellow in Wellington, New Zealand, and Berlin, in 2014, she was appointed a junior professor and in 2020 professor at Justus Liebig University Gießen. Her research focuses on the theoretical investigation of energy materials, nanomaterials, and surface phenomena.

Jürgen Janek received his Dr. rer. nat. in Physical Chemistry in 1992 from Leibniz University in Hannover under the supervision of Prof. Hermann Schmalzried. He has a chair for Physical Chemistry at Justus Liebig University in Giessen (JLU), is director of the JLU Center for Materials Research, and is Scientific Director of the BELLA lab at KIT, Karlsruhe. He was visiting professor at Seoul National University (South Korea), Tohoku University (Sendai, Japan), and Aix-Marseille (France). His research interests focus on the physical chemistry of inorganic solids, solid-state ionics, and reactivity, specifically on the properties of mixed ionic-electronic conductors, solid electrolytes, defect chemistry of ionic materials, kinetics of solid-state reactions, and solid–solid interfaces.

Daniel Schröder is head of the Institute of Energy and Process Systems Engineering at TU Braunschweig. There he received his Ph.D. with distinction in 2015 and stayed afterward at the Justus Liebig University Giessen as a junior group leader until the beginning of 2021. In 2017, he had a brief research stay at Kyoto University, Japan. His research focuses on the fundamental understanding and improving of metal oxygen batteries and redox flow batteries as well as fuel cells and electrolyzers by using a combination of model-based and operando techniques.

ACKNOWLEDGMENTS

We thank Dr. Dennis Gerbig, Prof. Hermann A. Wegner, and Prof. Herbert Over for having shared their expertise in many fruitful discussions. A.S., D.S., and J.J. gratefully acknowledge financial support by the BMBF (Federal Ministry of Education and Research) within the project "BenchBatt" (03XP0047D) and "MeLuBatt" (03XP0110A).

REFERENCES

- (1) Girishkumar, G.; McCloskey, B.; Luntz, A. C.; Swanson, S.; Wilcke, W. Lithium–Air Battery: Promise and Challenges. *J. Phys. Chem. Lett.* **2010**, *1*, 2193–2203.
- (2) Lu, Y. C.; Gallant, B. M.; Kwabi, D. G.; Harding, J. R.; Mitchell, R. R.; Whittingham, M. S.; Shao-Horn, Y. Lithium–Oxygen Batteries: Bridging Mechanistic Understanding and Battery Performance. *Energy Environ. Sci.* **2013**, *6*, 750–768.
- (3) Abraham, K. M.; Jiang, Z. A Polymer Electrolyte-Based Rechargeable Lithium/Oxygen Battery. *J. Electrochem. Soc.* **1996**, *143*, 1–5.
- (4) Christensen, J.; Albertus, P.; Sanchez-Carrera, R. S.; Lohmann, T.; Kozinsky, B.; Liedtke, R.; Ahmed, J.; Kojic, A. A Critical Review of Li/Air Batteries. *J. Electrochem. Soc.* **2011**, *159*, R1–R30.
- (5) Bruce, P. G.; Freunberger, S. A.; Hardwick, L. J.; Tarascon, J.-M. Li–O₂ and Li–S Batteries with High Energy Storage. *Nat. Mater.* **2012**, *11*, 19–29.
- (6) Aurbach, D.; McCloskey, B. D.; Nazar, L. F.; Bruce, P. G. Advances in Understanding Mechanisms Underpinning Lithium–Air Batteries. *Nat. Energy* **2016**, *1*, 1–11.
- (7) Feng, N.; He, P.; Zhou, H. Critical Challenges in Rechargeable Aprotic Li–O₂ Batteries. *Adv. Energy Mater.* **2016**, *6*, 1–24.
- (8) Kwak, W.-J.; Rosy, Sharon, D.; Xia, C.; Kim, H.; Johnson, L. R.; Bruce, P. G.; Nazar, L. F.; Sun, Y.-K.; Frimer, A. A.; Noked, M.; Freunberger, S. A.; Aurbach, D. Lithium–Oxygen Batteries and Related Systems: Potential, Status, and Future. *Chem. Rev.* **2020**, *120*, 6626–6683.
- (9) Wandt, J.; Jakes, P.; Granwehr, J.; Gasteiger, H. A.; Eichel, R.-A. Singlet Oxygen Formation during the Charging Process of an Aprotic Lithium–Oxygen Battery. *Angew. Chem., Int. Ed.* **2016**, *55*, 6892–6895.
- (10) Wandt, J.; Freiberg, A. T. S.; Ogrodnik, A.; Gasteiger, H. A. Singlet Oxygen Evolution from Layered Transition Metal Oxide Cathode Materials and Its Implications for Lithium-Ion Batteries. *Mater. Today* **2018**, *21*, 825–833.
- (11) Mahne, N.; Schafzahl, B.; Leybold, C.; Leybold, M.; Grumm, S.; Leitgeb, A.; Strohmaier, G. A.; Wilkening, M.; Fontaine, O.; Kramer, D.; Slugovc, C.; Borisov, S. M.; Freunberger, S. A. Singlet Oxygen Generation as a Major Cause for Parasitic Reactions During Cycling of Aprotic Lithium–Oxygen Batteries. *Nat. Energy* **2017**, *2*, 17036.
- (12) Mahne, N.; Renfrew, S. E.; McCloskey, B. D.; Freunberger, S. A. Electrochemical Oxidation of Lithium Carbonate Generates Singlet Oxygen. *Angew. Chem., Int. Ed.* **2018**, *57*, 5529–5533.
- (13) Mahne, N.; Fontaine, O.; Thotiyl, M. O.; Wilkening, M.; Freunberger, S. A. Mechanism and Performance of Lithium–Oxygen Batteries - A Perspective. *Chem. Sci.* **2017**, *8*, 6716–6729.
- (14) Schweitzer, C.; Schmidt, R. Physical Mechanisms of Generation and Deactivation of Singlet Oxygen. *Chem. Rev.* **2003**, *103*, 1685–1758.
- (15) Adam, W.; Kazakov, D. V.; Kazakov, V. P. Singlet-Oxygen Chemiluminescence in Peroxide Reactions. *Chem. Rev.* **2005**, *105*, 3371–3387.
- (16) Khan, A. U.; Kasha, M. Red Chemiluminescence of Molecular Oxygen in Aqueous Solution. *J. Chem. Phys.* **1963**, *39*, 2105–2106.
- (17) Khan, A. U.; Kasha, M. Rotational Structure in the Chemiluminescence Spectrum of Molecular Oxygen in Aqueous Systems. *Nature* **1964**, *204*, 241–243.
- (18) Khan, A. U. The Discovery of the Chemical Evolution of Singlet Oxygen. Some Current Chemical, Photochemical, and Biological Applications. *Int. J. Quantum Chem.* **1991**, *39*, 251–267.
- (19) Mayeda, E. A.; Bard, A. J. Production of Singlet Oxygen in Electrogenerated Radical Ion Electron Transfer Reactions. *J. Am. Chem. Soc.* **1973**, *95*, 6223–6226.
- (20) Mayeda, E. A.; Bard, A. J. Singlet Oxygen. The Suppression of Its Production in Dismutation of Superoxide Ion by Superoxide Dismutase. *J. Am. Chem. Soc.* **1974**, *96*, 4023–4024.
- (21) Foote, C. S. Detection of Singlet Oxygen in Complex Systems: A Critique. In *Biochemical and Clinical Aspects of Oxygen*; Caughey, W. S., Ed.; Academic Press, 1979; pp 603–626.
- (22) Khan, A. U.; Kasha, M. Chemiluminescence Arising from Simultaneous Transitions in Pairs of Singlet Oxygen Molecules. *J. Am. Chem. Soc.* **1970**, *92*, 3293–3300.
- (23) Khan, A. U. Singlet Molecular Oxygen. A New Kind of Oxygen. *J. Phys. Chem.* **1976**, *80*, 2219–2228.
- (24) Khan, A. U. Theory of Electron Transfer Generation and Quenching of Singlet Oxygen [¹S_g⁺ and ¹Δ_g] by Superoxide Anion. The Role of Water in the Dismutation of O₂^{•−}. *J. Am. Chem. Soc.* **1977**, *99*, 10–12.
- (25) Khan, A. U. Activated Oxygen: Singlet Molecular Oxygen and Superoxide Anion. *Photochem. Photobiol.* **1978**, *28*, 615–626.
- (26) Danen, W. C.; Arudi, R. L. Generation of Singlet Oxygen in the Reaction of Superoxide Anion Radical with Diacyl Peroxides. *J. Am. Chem. Soc.* **1978**, *100*, 3944–3945.
- (27) Foote, C. S.; Shook, F. C.; Abakerli, R. A. Chemistry of Superoxide Ion. 4. Singlet Oxygen Is Not a Major Product of Dismutation. *J. Am. Chem. Soc.* **1980**, *102*, 2503–2504.
- (28) Nanni, E. J.; Birge, R. R.; Hubbard, L. M.; Morrison, M. M.; Sawyer, D. T. Oxidation and Dismutation of Superoxide Ion Solutions to Molecular Oxygen. Singlet vs. Triplet State. *Inorg. Chem.* **1981**, *20*, 737–741.
- (29) Aubry, J. M.; Rigaudy, J.; Ferradini, C.; Pucheault, J. A Search for Singlet Oxygen in the Disproportionation of Superoxide Anion. *J. Am. Chem. Soc.* **1981**, *103*, 4965–4966.
- (30) Arudi, R. L.; Bielski, B. H. J.; Allen, A. O. Search for Singlet Oxygen Luminescence in the Disproportionation of HO₂/O₂. *Photochem. Photobiol.* **1984**, *39*, 703–706.
- (31) Khan, A. U. Direct Spectral Evidence of the Generation of Singlet Molecular Oxygen in the Reaction of Potassium Superoxide with Water. *J. Am. Chem. Soc.* **1981**, *103*, 6516–6517.
- (32) Kanofsky, J. R. Singlet Oxygen Production in Superoxide Ion-Halocarbon Systems. *J. Am. Chem. Soc.* **1986**, *108*, 2977–2979.
- (33) Alfano, A. J.; Christe, K. O. Singlet Delta Oxygen Production from a Gas-Solid Reaction. *Angew. Chem., Int. Ed.* **2002**, *41*, 3252–3254.
- (34) Li, Q.; Chen, F.; Zhao, W.; Xu, M.; Fang, B.; Zhang, Y.; Duo, L.; Jin, Y.; Sang, F. A Spectroscopic Study on Singlet Oxygen Production from Different Reaction Paths Using Solid Inorganic Peroxides as Starting Materials. *Bull. Korean Chem. Soc.* **2007**, *28*, 1656–1660.
- (35) Li, Q.; Chen, F.; Zhao, W.; Xu, M.; Fang, B.; Zhang, Y.; Duo, L.; Jin, Y.; Sang, F. Singlet Oxygen Production in the Reaction of Potassium Superoxide with Chlorine. *Chem. Lett.* **2007**, *36*, 496–497.
- (36) MacManus-Spencer, L. A.; Edlund, B. L.; McNeill, K. Singlet Oxygen Production in the Reaction of Superoxide with Organic Peroxides. *J. Org. Chem.* **2006**, *71*, 796–799.
- (37) Hassoun, J.; Croce, F.; Armand, M.; Scrosati, B. Investigation of the O₂ Electrochemistry in a Polymer Electrolyte Solid-State Cell. *Angew. Chem., Int. Ed.* **2011**, *50*, 2999–3002.
- (38) Zhang, S.; Nava, M. J.; Chow, G. K.; Lopez, N.; Wu, G.; Britt, D. R.; Nocera, D. G.; Cummins, C. C. On the Incompatibility of Lithium–O₂ Battery Technology with CO₂. *Chem. Sci.* **2017**, *8*, 6117–6122.
- (39) Schafzahl, L.; Mahne, N.; Schafzahl, B.; Wilkening, M.; Slugovc, C.; Borisov, S. M.; Freunberger, S. A. Singlet Oxygen during Cycling of the Aprotic Sodium–O₂ Battery. *Angew. Chem., Int. Ed.* **2017**, *56*, 15728–15732.
- (40) Mourad, E.; Petit, Y. K.; Spezia, R.; Samojlov, A.; Summa, F. F.; Prehal, C.; Leybold, C.; Mahne, N.; Slugovc, C.; Fontaine, O.; Brutti, S.; Freunberger, S. A. Singlet Oxygen from Cation Driven Superoxide Disproportionation and Consequences for Aprotic Metal–O₂ Batteries. *Energy Environ. Sci.* **2019**, *12*, 2559–2568.

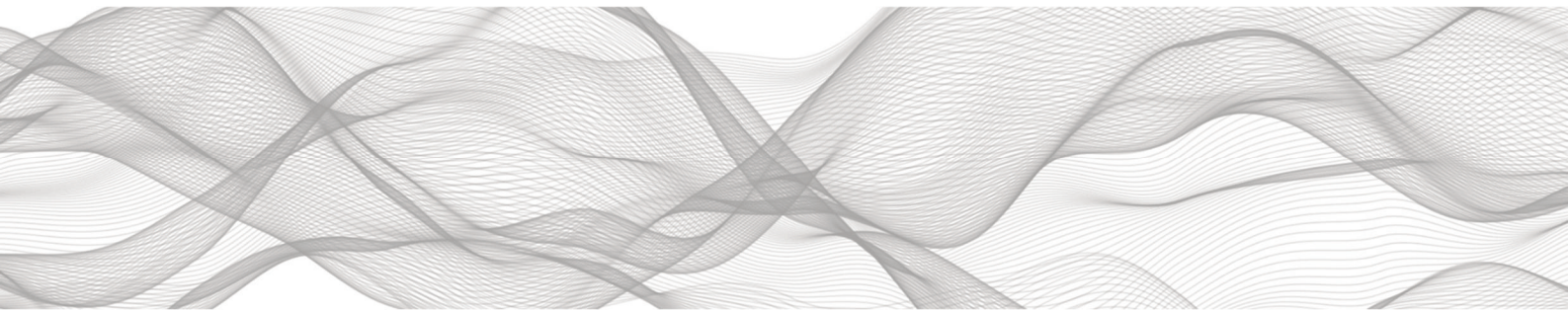
- (41) Petit, Y. K.; Mourad, E.; Prehal, C.; Leypold, C.; Windschbacher, A.; Mijailovic, D.; Slugovc, C.; Borisov, S. M.; Zojer, E.; Brutti, S.; Fontaine, O.; Freunberger, S. A. Mechanism of Mediated Alkali Peroxide Oxidation and Triplet versus Singlet Oxygen Formation. *Nat. Chem.* **2021**, *13*, 465–471.
- (42) Roberts, J. L.; Sawyer, D. T. Facile Degradation by Superoxide Ion of Carbon Tetrachloride, Chloroform, Methylene Chloride, and p, p'-DDT in Aprotic Media. *J. Am. Chem. Soc.* **1981**, *103*, 712–714.
- (43) Corey, E. J.; Mehrotra, M. M.; Khan, A. U. Water Induced Dismutation of Superoxide Anion Generates Singlet Molecular Oxygen. *Biochem. Biophys. Res. Commun.* **1987**, *145*, 842–846.
- (44) Kanofsky, J. R.; Sugimoto, H.; Sawyer, D. T. Singlet Oxygen Production from the Reaction of Superoxide Ion with Halocarbons in Acetonitrile. *J. Am. Chem. Soc.* **1988**, *110*, 3698–3699.
- (45) MacManus-Spencer, L. A.; McNeill, K. Quantification of Singlet Oxygen Production in the Reaction of Superoxide with Hydrogen Peroxide Using a Selective Chemiluminescent Probe. *J. Am. Chem. Soc.* **2005**, *127*, 8954–8955.
- (46) Koppenol, W. H.; Butler, J. Mechanism of Reactions Involving Singlet Oxygen and the Superoxide Anion. *FEBS Lett.* **1977**, *83*, 1–6.
- (47) McCloskey, B. D.; Bethune, D. S.; Shelby, R. M.; Mori, T.; Scheffler, R.; Speidel, A.; Sherwood, M.; Luntz, A. C. Limitations in Rechargeability of Li-O₂ Batteries and Possible Origins. *J. Phys. Chem. Lett.* **2012**, *3*, 3043–3047.
- (48) Petit, Y. K.; Leypold, C.; Mahne, N.; Mourad, E.; Schafzahl, L.; Slugovc, C.; Borisov, S. M.; Freunberger, S. A. DABCONium: An Efficient and High-Voltage Stable Singlet Oxygen Quencher for Metal-O₂ Cells. *Angew. Chem., Int. Ed.* **2019**, *58*, 6535–6539.
- (49) Kwak, W.-J.; Freunberger, S. A.; Kim, H.; Park, J.; Nguyen, T. T.; Jung, H.-G.; Byon, H. R.; Sun, Y.-K. Mutual Conservation of Redox Mediator and Singlet Oxygen Quencher in Lithium–Oxygen Batteries. *ACS Catal.* **2019**, *9*, 9914–9922.
- (50) Zaichenko, A.; Schröder, D.; Janek, J.; Mollenhauer, D. Pathways to Triplet or Singlet Oxygen during the Dissociation of Alkali Metal Superoxides: Insights by Multireference Calculations of Molecular Model Systems. *Chem. - Eur. J.* **2020**, *26*, 2395–2404.
- (51) Houchins, G.; Pande, V.; Viswanathan, V. Mechanism for Singlet Oxygen Production in Li-Ion and Metal-Air Batteries. *ACS Energy Lett.* **2020**, *5*, 1893–1899.
- (52) Pierini, A.; Brutti, S.; Bodo, E. Superoxide Anions Disproportionation Induced by Li⁺ and H⁺: Pathways to ¹O₂ Release in Li-O₂ Batteries. *ChemPhysChem* **2020**, *21*, 2060–2067.
- (53) Kwak, W. J.; Kim, H.; Petit, Y. K.; Leypold, C.; Nguyen, T. T.; Mahne, N.; Redfern, P.; Curtiss, L. A.; Jung, H. G.; Borisov, S. M.; Freunberger, S. A.; Sun, Y. K. Deactivation of Redox Mediators in Lithium-Oxygen Batteries by Singlet Oxygen. *Nat. Commun.* **2019**, *10*, 4–11.
- (54) Liang, Z.; Zou, Q.; Xie, J.; Lu, Y. C. Suppressing Singlet Oxygen Generation in Lithium-Oxygen Batteries with Redox Mediators. *Energy Environ. Sci.* **2020**, *13*, 2870–2877.
- (55) Samojlov, A.; Schuster, D.; Kahr, J.; Freunberger, S. A. Surface and Catalyst Driven Singlet Oxygen Formation in Li-O₂ Cells. *Electrochim. Acta* **2020**, *362*, 137175.
- (56) Córdoba, D.; Rodríguez, H. B.; Calvo, E. J. Singlet Oxygen Formation during the Oxygen Reduction Reaction in DMSO LiTFSI on Lithium Air Battery Carbon Electrodes. *ChemistrySelect* **2019**, *4*, 12304–12307.
- (57) Lozano, I.; Córdoba, D.; Rodríguez, H. B.; Landa-Medrano, I.; Ortiz-Vitoriano, N.; Rojo, T.; de Larramendi, I. R.; Calvo, E. J. Singlet Oxygen Formation in Na–O₂ Battery Cathodes Catalyzed by Ammonium Brønsted Acid. *J. Electroanal. Chem.* **2020**, *872*, 2–8.
- (58) Kasha, M.; Khan, A. U. The Physics, Chemistry, and Biology, of Singlet Molecular Oxygen. *Ann. N. Y. Acad. Sci.* **1970**, *171*, 5–23.
- (59) Bromberg, A.; Foote, C. S. Solvent Shift of Singlet Oxygen Emission Wavelength. *J. Phys. Chem.* **1989**, *93*, 3968–3969.
- (60) Memming, R. Reactions of Excited Molecules at Electrodes. In *Comprehensive Treatise of Electrochemistry Vol. 7 - Kinetics and Mechanisms of Electrode Processes*; Conway, B. E., Bockris, J. O., Yeager, E., Khan, S. U. M., White, R. E., Eds.; Springer US: Boston, MA, 1983; pp 578–587.
- (61) Rohatgi-Mukherjee, K. K. Physical Properties of the Electronically Excited Molecules. In *Fundamentals Of Photochemistry*; New Age international, 1978; pp 90–125.
- (62) Ho, R. Y. N.; Liebman, J. F.; Valentine, J. S. Overview of the Energetics and Reactivity of Oxygen. In *Active Oxygen in Chemistry*; Foote, C. S., Valentine, J. S., Greenberg, A., Liebman, J. F., Eds.; Springer Netherlands: Dordrecht, 1996; pp 1–23.
- (63) Koppenol, W. H. Reactions Involving Singlet Dioxygen and the Superoxide Anion. *Nature* **1976**, *262*, 420–421.
- (64) Merkel, P. B.; Kearns, D. R. Remarkable Solvent Effects on the Lifetime of ¹Δ_g Oxygen. *J. Am. Chem. Soc.* **1972**, *94*, 1029–1030.
- (65) Merkel, P. B.; Nilsson, R.; Kearns, D. R. Deuterium Effects on Singlet Oxygen Lifetimes in Solutions. A New Test of Singlet Oxygen Reactions. *J. Am. Chem. Soc.* **1972**, *94*, 1030–1031.
- (66) Schmidt, R.; Afshari, E. Collisional Deactivation of O₂(¹Δ_g) by Solvent Molecules. Comparative Experiments with ¹⁶O₂ and ¹⁸O₂. *Berichte der Bunsengesellschaft für Phys. Chemie* **1992**, *96*, 788–794.
- (67) *Wavelength to Colour Relationship*; Academo, 2020. <https://academo.org/demos/wavelength-to-colour-relationship/> (accessed 01-20-2020).
- (68) Foote, C. S.; Clennan, E. L. Properties and Reactions of Singlet Dioxygen. In *Active Oxygen in Chemistry*; Foote, C. S., Valentine, J. S., Greenberg, A., Liebman, J. F., Eds.; Springer Netherlands: Dordrecht, 1996; pp 105–140.
- (69) Smith, I. W. M. 2.4 Electronic States of Molecules and the Adiabatic Correlation Rules. In *Kinetics and Dynamics of Elementary Gas Reactions*; Baldwin, J. E., Buckingham, A. D., Kirby, G. W., Mullin, J. W., Stevens, R., West, T. S., Eds.; London, 1980; pp 50–58.
- (70) Wigner, E. P. Über Die Erhaltungssätze In Der Quantenmechanik. *Collect. Work. Eugene Paul Wigner* **1993**, 84–90.
- (71) Wigner, E.; Witmer, E. E. Über Die Struktur Der Zweiatomigen Molekelspektren Nach Der Quantenmechanik. *Eur. Phys. J. A* **1928**, *51*, 859–886.
- (72) McNaught, A. D.; Wilkinson, A. *IUPAC Compendium of Chemical Terminology*, 2nd ed.; Blackwell Scientific Publications, 1997.
- (73) Chase, M. W. NIST-JANAF Thermochemical Tables, Fourth Edition. *J. Phys. Chem. Ref. Data Monogr.* **1998**, *9*, 1–1951.
- (74) Allen, R. C. Role of Oxygen in Phagocyte Microbicidal Action. *Environ. Health Perspect.* **1994**, *102*, 201–208.
- (75) Harding, L. B.; Goddard, W. A. Intermediates in the Chemiluminescent Reaction of Singlet Oxygen with Ethylene. Ab Initio Studies. *J. Am. Chem. Soc.* **1977**, *99*, 4520–4523.
- (76) Anslyn, E. V.; Dougherty, D. A. CHAPTER 15: Thermal Pericyclic Reactions. In *Modern Physical Organic Chemistry*; University Science Books, 2006; pp 877–893.
- (77) Silver, D. M. Hierarchy of Symmetry Conservation Rules Governing Chemical Reaction Systems. *J. Am. Chem. Soc.* **1974**, *96*, 5959–5967.
- (78) Shi, W.; Deng, L.; Du, S.; Cui, R.; Yang, H.; Sha, G.; Zhang, C. O₂(¹Δ) Quenching Mechanism in Cl₂/Basic Hydrogen Peroxide (Basic Deuterium Peroxide) Gas/Liquid Reaction and the Determination of O₂(¹Δ)/BHP(BDP) Interface Free Energy. *J. Phys. Chem. C* **2008**, *112*, 9412–9417.
- (79) Storch, D. M.; Dymek, C. J.; Davis, L. P. MNDO Study of the Mechanism of O₂(¹Δ) Formation by Reaction of Cl₂ with Basic H₂O₂. *J. Am. Chem. Soc.* **1983**, *105*, 1765–1769.
- (80) Cahill, A. E.; Taube, H. The Use of Heavy Oxygen in the Study of Reactions of Hydrogen Peroxide. *J. Am. Chem. Soc.* **1952**, *74*, 2312–2318.
- (81) Evans, D. F.; Upton, M. W. Studies on Singlet Oxygen in Aqueous Solution. Part 1. Formation of Singlet Oxygen from Hydrogen Peroxide with Two-Electron Oxidants. *J. Chem. Soc., Dalton Trans.* **1985**, *6*, 1141–1145.
- (82) Marcus, R. A. On the Theory of Electron-Transfer Reactions. VI. Unified Treatment for Homogeneous and Electrode Reactions. *J. Chem. Phys.* **1965**, *43*, 679.

- (83) Marcus, R. A. Electron Transfer Reactions in Chemistry. Theory and Experiment. *Rev. Mod. Phys.* **1993**, *65*, 599–610.
- (84) Genorio, B.; Staszak-Jirkovský, J.; Assary, R. S.; Connell, J. G.; Strmcnik, D.; Diesendruck, C. E.; Lopes, P. P.; Stamenkovic, V. R.; Moore, J. S.; Curtiss, L. A.; Markovic, N. M. Superoxide (Electro)-Chemistry on Well-Defined Surfaces in Organic Environments. *J. Phys. Chem. C* **2016**, *120*, 15909–15914.
- (85) Azhar, A.; Manyepedza, T.; Oladeji, A. V.; Hendi, R.; Rees, N. V. The Electroreduction of Oxygen in Aprotic Solvents. *J. Electroanal. Chem.* **2020**, *872*, 113989.
- (86) Hendi, R.; Robbs, P. H.; Sampson, B.; Pearce, R.; Rees, N. V. The Electrochemical Reduction Kinetics of Oxygen in Dimethylsulfoxide. *J. Electroanal. Chem.* **2018**, *829*, 16–19.
- (87) Medvedev, E. S.; Stuchebrukhov, A. A. Breakdown of the Born-Oppenheimer-Condon-Marcus Approximation in Long Distance Electron Transfer. *Chem. Phys.* **2004**, *296*, 181–192.
- (88) Jensen, F. Electronic Structure Methods: Independent-Particle Models. In *Introduction to Computational Chemistry*; John Wiley & Sons, Ltd: Chichester, West Sussex, UK, 2007; pp 80–132.
- (89) Amatore, C. 1 Basic Concepts. In *Organic Electrochemistry*; Hammerich, O., Speiser, B., Eds.; CRC Press: Boca Raton, 2016; pp 3–96.
- (90) Savéant, J.-M. CHAPTER 1 Single Electron Transfer at an Electrode. In *Elements of Molecular and Biomolecular Electrochemistry*; Wiley-Interscience: Hoboken, NJ, 2006; pp 1–77.
- (91) Bard, A. J.; Faulkner, L. R. Kinetics of Electrode Reactions. In *Electrochemical Methods: Fundamentals and Applications*; John Wiley & Sons: New York, 2001; pp 87–136.
- (92) Appleby, A. J.; Zagal, J. H. Free Energy Relationships in Electrochemistry: A History That Started in 1935. *J. Solid State Electrochem.* **2011**, *15*, 1811–1832.
- (93) Closs, G. L.; Miller, J. R. Intramolecular Long-Distance Electron Transfer in Organic Molecules. *Science* **1988**, *240*, 440–447.
- (94) Miller, J. R.; et al. Intramolecular Long-Distance Electron Transfer in Radical Anions. The Effects of Free Energy and Solvent on the Reaction Rates. *J. Am. Chem. Soc.* **1984**, *106*, 3047–3049.
- (95) Oleinick, A.; Klymenko, O. V.; Svir, I.; Amatore, C. Theoretical Insights in ECL. In *Luminescence in Electrochemistry*; Miomandre, F., Audebert, P., Eds.; Springer International Publishing: Cham, Switzerland, 2017; pp 215–256.
- (96) Marcus, R. A. On the Theory of Chemiluminescent Electron-Transfer Reactions. *J. Chem. Phys.* **1965**, *43*, 2654–2657.
- (97) Kurchin, R.; Viswanathan, V. Marcus-Hush-Chidsey Kinetics at Electrode-Electrolyte Interfaces. *J. Chem. Phys.* **2020**, *153*, 134706.
- (98) Savéant, J.-M. *Elements of Molecular and Biomolecular Electrochemistry: An Electrochemical Approach to Electron Transfer Chemistry*; Wiley-Interscience: Hoboken, NJ, 2006.
- (99) Zeng, Y.; Smith, R. B.; Bai, P.; Bazant, M. Z. Simple Formula for Marcus-Hush-Chidsey Kinetics. *J. Electroanal. Chem.* **2014**, *735*, 77–83.
- (100) Santhanam, K. S. V.; Bard, A. Chemiluminescence of Electrogenerated 9,10-Diphenylanthracene Anion Radical. *J. Am. Chem. Soc.* **1965**, *87*, 139–140.
- (101) Hercules, D. M. Chemiluminescence Resulting from Electrochemically Generated Species. *Science* **1964**, *145*, 808–809.
- (102) Glass, R. S.; Faulkner, L. R. Electrogenerated Chemiluminescence from the Tris(2,2'-Bipyridine)Ruthenium(II) System. An Example of S-Route Behavior. *J. Phys. Chem.* **1981**, *85*, 1160–1165.
- (103) Dang, X.; Hupp, J. T. Interfacial Charge-Transfer Pathways: Evidence for Marcus-Type Inverted Electron Transfer in Metal Oxide Semiconductor/Inorganic Dye Systems. *J. Am. Chem. Soc.* **1999**, *121*, 8399–8400.
- (104) Gleria, M.; Memming, R. Novel Luminescence Generation by Electron Transfer from Semiconductor Electrodes to Ruthenium-Bipyridil Complexes. *Z. Phys. Chem.* **1976**, *101*, 171–179.
- (105) Gerischer, H. *Semiconductor Electrochemistry*; Technical Report for Lawrence Berkeley National Laboratory: Berkeley, CA, 1968.
- (106) Gerischer, H. Electron-Transfer Kinetics of Redox Reactions at the Semiconductor/Electrolyte Contact. A New Approach. *J. Phys. Chem.* **1991**, *95*, 1356–1359.
- (107) Bender, C. L.; Schröder, D.; Pinedo, R.; Adelmhelm, P.; Janek, J. One- or Two-Electron Transfer? The Ambiguous Nature of the Discharge Products in Sodium-Oxygen Batteries. *Angew. Chem., Int. Ed.* **2016**, *55*, 4640–4649.
- (108) Sawyer, D. T.; Valentine, J. S. How Super Is Superoxide? *Acc. Chem. Res.* **1981**, *14*, 393–400.
- (109) Sawyer, D. T.; Calderwood, T. S.; Yamaguchi, K.; Angelis, C. T. Synthesis and Characterization of Tetramethylammonium Superoxide. *Inorg. Chem.* **1983**, *22*, 2577–2583.
- (110) Koppenol, W. H.; Stanbury, D. M.; Bounds, P. L. Electrode Potentials of Partially Reduced Oxygen Species, from Dioxygen to Water. *Free Radical Biol. Med.* **2010**, *49*, 317–322.
- (111) Testa, A. C.; Reinmuth, W. H. Stepwise Reactions in Chronopotentiometry. *Anal. Chem.* **1961**, *33*, 1320–1324.
- (112) Wirz, J.; Klán, P. 2 A Crash Course in Photophysics and a Classification of Primary Photoreactions. In *Photochemistry of Organic Compounds: From Concepts to Practice*; John Wiley & Sons, Ltd: Chichester, West Sussex, UK, 2009; pp 25–72.
- (113) Andrieux, C. P.; Hapiot, P.; Saveant, J. M. Mechanism of Superoxide Ion Disproportionation in Aprotic Solvents. *J. Am. Chem. Soc.* **1987**, *109*, 3768–3775.
- (114) Compton, R. G.; Banks, C. E. Cyclic Voltammetry at Macroelectrodes. In *Understanding Voltammetry*; World Scientific: London, 2011; pp 113–162.
- (115) Sawyer, D. T.; Gibian, M. J. The Chemistry of Superoxide Ion. *Tetrahedron* **1979**, *35*, 1471–1481.
- (116) Sawyer, D. T.; Roberts, J. L. Electrochemistry of Oxygen and Superoxide Ion in Dimethylsulfoxide at Platinum, Gold and Mercury Electrodes. *J. Electroanal. Chem.* **1966**, *12*, 90–101.
- (117) Sawyer, D. T.; Chiericato, G.; Angelis, C. T.; Nanni, E. J.; Tsuchiya, T. Effects of Media and Electrode Materials on the Electrochemical Reduction of Dioxygen. *Anal. Chem.* **1982**, *54*, 1720–1724.
- (118) Evans, D. H. One-Electron and Two-Electron Transfers in Electrochemistry and Homogeneous Solution Reactions. *Chem. Rev.* **2008**, *108*, 2113–2144.
- (119) Peng, Z.; Freunberger, S. A. A.; Hardwick, L. J. J.; Chen, Y.; Giordani, V.; Bardé, F.; Novák, P.; Graham, D.; Tarascon, J.-M.; Bruce, P. G. G. Oxygen Reactions in a Non-Aqueous Li⁺ Electrolyte. *Angew. Chem., Int. Ed.* **2011**, *50*, 6351–6355.
- (120) Wang, Y.; Lu, Y.-R.; Dong, C.-L.; Lu, Y.-C. Critical Factors Controlling Superoxide Reactions in Lithium–Oxygen Batteries. *ACS Energy Lett.* **2020**, *5*, 1355–1363.
- (121) Yang, J.; Zhai, D.; Wang, H.-H.; Lau, K. C.; Schlueter, J. A.; Du, P.; Myers, D. J.; Sun, Y.-K.; Curtiss, L. A.; Amine, K. Evidence for Lithium Superoxide-like Species in the Discharge Product of a Li–O₂ Battery. *Phys. Chem. Chem. Phys.* **2013**, *15*, 3764.
- (122) Das, U.; Lau, K. C.; Redfern, P. C.; Curtiss, L. A. Structure and Stability of Lithium Superoxide Clusters and Relevance to Li–O₂ Batteries. *J. Phys. Chem. Lett.* **2014**, *5*, 813–819.
- (123) Mo, Y.; Ong, S. P.; Ceder, G. First-Principles Study of the Oxygen Evolution Reaction of Lithium Peroxide in the Lithium–Air Battery. *Phys. Rev. B: Condens. Matter Mater. Phys.* **2011**, *84*, 1–9.
- (124) Bockris, J. O. M.; Drazic, D.; Despic, A. R. The Electrode Kinetics of the Deposition and Dissolution of Iron. *Electrochim. Acta* **1961**, *4*, 325–361.
- (125) Radin, M. D.; Rodriguez, J. F.; Siegel, D. J. Lithium Peroxide Surfaces and Point Defects: Relevance for Li–Air Batteries. *Proc. Batter. Congr.* **2011**, 1–6.
- (126) Ong, S. P.; Mo, Y.; Ceder, G. Low Hole Polaron Migration Barrier in Lithium Peroxide. *Phys. Rev. B: Condens. Matter Mater. Phys.* **2012**, *85*, 2–5.
- (127) Radin, M. D.; Siegel, D. J. Charge Transport in Lithium Peroxide: Relevance for Rechargeable Metal–Air Batteries. *Energy Environ. Sci.* **2013**, *6*, 2370–2379.

- (128) Luntz, A. C.; Viswanathan, V.; Voss, J.; Varley, J. B.; Nørskov, J. K.; Scheffler, R.; Speidel, A. Tunneling and Polaron Charge Transport through Li_2O_2 in Li-O_2 Batteries. *J. Phys. Chem. Lett.* **2013**, *4*, 3494–3499.
- (129) Mathiesen, N. R.; Yang, S.; García-Lastra, J. M.; Vegge, T.; Siegel, D. J. Charge Transport in Alkali-Metal Superoxides: A Systematic First-Principles Study. *Chem. Mater.* **2019**, *31*, 9156–9167.
- (130) Gerischer, H.; Mindt, W. The Mechanisms of the Decomposition of Semiconductors by Electrochemical Oxidation and Reduction. *Electrochim. Acta* **1968**, *13*, 1329–1341.
- (131) Osseo-Asare, K. Semiconductor Electrochemistry and Hydro-metallurgical Dissolution Processes. *Hydrometallurgy* **1992**, *29*, 61–90.
- (132) Bergner, B. J.; Schürmann, A.; Peppler, K.; Garsuch, A.; Janek, J. TEMPO: A Mobile Catalyst for Rechargeable Li-O_2 Batteries. *J. Am. Chem. Soc.* **2014**, *136*, 15054–15064.
- (133) Chen, Y.; Freunberger, S. A.; Peng, Z.; Fontaine, O.; Bruce, P. G. Charging a Li-O_2 Battery Using a Redox Mediator. *Nat. Chem.* **2013**, *5*, 489–494.
- (134) Bergner, B. J.; Hofmann, C.; Schürmann, A.; Schröder, D.; Peppler, K.; Schreiner, P. R.; Janek, J. Understanding the Fundamentals of Redox Mediators in Li-O_2 Batteries: A Case Study on Nitroxides. *Phys. Chem. Chem. Phys.* **2015**, *17*, 31769–31779.
- (135) Lim, H.-D.; Song, H.; Kim, J.; Gwon, H.; Bae, Y.; Park, K.-Y.; Hong, J.; Kim, H.; Kim, T.; Kim, Y. H.; Lepró, X.; Ovalle-Robles, R.; Baughman, R. H.; Kang, K. Superior Rechargeability and Efficiency of Lithium-Oxygen Batteries: Hierarchical Air Electrode Architecture Combined with a Soluble Catalyst. *Angew. Chem., Int. Ed.* **2014**, *53*, 3926–3931.
- (136) Liang, Z.; Lu, Y. C. Critical Role of Redox Mediator in Suppressing Charging Instabilities of Lithium-Oxygen Batteries. *J. Am. Chem. Soc.* **2016**, *138*, 7574–7583.
- (137) Balaish, M.; Kraysberg, A.; Ein-Eli, Y. A Critical Review on Lithium-Air Battery Electrolytes. *Phys. Chem. Chem. Phys.* **2014**, *16*, 2801–2822.
- (138) Gollnick, K.; Schnatterer, A. 9,10-Dicyanoanthracene-Sensitized Photooxygenation of α,α' -Dimethylstilbenes. Mechanism and Kinetics of the Competing Singlet Oxygen and Electron Transfer Photooxygenation Reactions. *Photochem. Photobiol.* **1986**, *43*, 365–378.
- (139) Kotani, H.; Ohkubo, K.; Fukuzumi, S. Photocatalytic Oxygenation of Anthracenes and Olefins with Dioxygen via Selective Radical Coupling Using 9-Mesityl-10-Methylacridinium Ion as an Effective Electron-Transfer Photocatalyst. *J. Am. Chem. Soc.* **2004**, *126*, 15999–16006.
- (140) Niederländer, H. A. G.; Gooijer, C.; Velthorst, N. H. Chemiluminescence Detection in Liquid Chromatography Based on Photo-Oxygenation Involving Reactive Oxygen Intermediates. *Anal. Chim. Acta* **1994**, *285*, 143–159.
- (141) Posner, G. H.; González, L.; Cumming, J. N.; Klinedinst, D.; Shapiro, T. A. Synthesis and Antimalarial Activity of Heteroatom-Containing Bicyclic Endoperoxides. *Tetrahedron* **1997**, *53*, 37–50.
- (142) Barton, D. H. R.; Haynes, R. K.; Leclerc, G.; Magnus, P. D.; Menzies, I. D. New Reactions of Triplet Oxygen Which Avoid the Spin Barrier. *J. Chem. Soc., Perkin Trans. 1* **1975**, *1* (20), 2055–2065.
- (143) Amatore, C.; Brown, A. R. Paired Electrosynthesis at the Femtoliter Scale: Formation of 9,10-Anthracenedione from the Oxidation of Anthracene and Reduction of Dioxygen. *J. Am. Chem. Soc.* **1996**, *118*, 1482–1486.
- (144) Bielski, B. H. J.; Saito, E. Deuterium Isotope Effect on the Decay Kinetics of Perhydroxyl Radical. *J. Phys. Chem.* **1971**, *75*, 2263–2266.

PART III

TOO LONG; DIDN'T READ



*We can see what's always been there.
Seeing what's next is the tough part.*

—Phil Edwards

Conclusions and Outlook

This thesis had two major focal points: First, the transport of oxygen in the electrolyte and second, the oxygen kinetics at the cathode of Li/O₂ batteries. Both represent important aspects of the reaction paths that oxygen undergoes inside such batteries. Although not obvious, both interact with each other and influence the overall battery performance: larger solubility and faster diffusion of O₂ leads to higher concentration of intermediates near the electrode surface, resulting in different morphologies of the discharge product and limiting behaviors.

The publication “Diffusivity and Solubility of Oxygen in Solvents for Metal/Oxygen Batteries: A Combined Theoretical and Experimental Study” dealt with the adsorption and transport of oxygen inside the electrolyte. For the first time, a consistent set of Henry’s law constants and diffusion coefficients of oxygen in a series of glymes with different chain length (monoglyme to pentaglyme) and different perfluorinated solvents was determined. The presented methods are suitable for a wide range of solvents with different properties. For example, unlike perfluorinated solvents, glymes are able to dissolve electrolyte salts commonly used in Li/O₂ batteries. The Henry’s law constants and diffusion coefficients of the solvents used also span roughly one order of magnitude. Evaluating these parameters in solvents and electrolytes is vital towards a better quantitative description of oxygen transport. This can be used not only to determine limiting currents, but also to rationalize discharge capacities and the distribution of discharge products. A dual approach for determining these parameters was chosen: oxygen uptake experiments and molecular dynamics simulations. In all nine investigated solvents, the difference between simulated and measured diffusion coefficients is small in comparison to the magnitude of the coefficients, showing that both developed techniques are suitable for their determination. In addition, both can be adapted to determine these values in Li⁺-containing electrolytes where, for example, the use of electrochemical methods is prone to errors due to side reactions or low conductivity of the electrolyte. The use of simulations also allows the exploration of hypothetical solvents and



solvent mixtures, as well as optimizations of them, which have not been described in literature up so far.

The review article “Singlet Oxygen in Electrochemical Cells: A Critical Review of Literature and Theory” provided an extensive discussion of singlet oxygen in metal/O₂ batteries. Singlet oxygen is the assumed responsible for the observed degradation of electrolyte and electrode components in metal/O₂ batteries. While the topic of singlet oxygen from superoxides is by far not new, dating back to the 1960s, the phenomena has been discussed in metal/O₂ batteries and especially in Li/O₂ batteries as of 2016. While validation, evaluation and understanding of the formation of ¹O₂ is essential for improving metal/O₂ batteries, the discussion is hampered from the outset by missing or incorrect citations of relevant literature since the beginning. The review provides a complete literature overview of the historical development of the topic, covering not only recent findings in metal/O₂ systems but also relevant neighboring research fields such as the proton induced disproportionation of superoxide and the Na/O₂ battery. Moreover, the review discusses for the first time the Marcus(–Hush–Chidsey) theory as a model to describe and understand singlet oxygen in electrochemistry and, in particular, Li/O₂ batteries. Three main points can be summarized from the analysis:

First, there is still no definite proof of ¹O₂ formation in Li/O₂ batteries. Evidence is mainly based on the use of trapping agents or quenchers, which can be an indicator of singlet oxygen, but they are prone to side reactions, resulting in false positive results. Luminescence was only found in electrochemical experiments and were linked to Li₂CO₃ and H₂O, hinting at possible side reactions or electrogenerated chemiluminescence. A general class of reactions, which must be considered in any case, are electron-transfer oxygenations. This class of reactions do not involve singlet oxygen but can mimic many of its reactions. Peroxycarbonates as a product from the reaction of (su)peroxides with CO₂ must also be taken into account.

Second, the disproportionation of superoxide, whether induced by H⁺ or an alkali cation, seems unlikely to be a source of singlet oxygen, both in aqueous solution and in organic solvents. From a spin conservation point of view, both triplet and singlet oxygen are possible as reaction products of a disproportionation reaction, but triplet oxygen is the strongly preferred product due to the larger Gibbs energy of reaction. The chemical oxidation of superoxides and peroxides can result in the formation of ¹O₂ if appropriate oxidants are chosen.

Third, direct electrochemical generation of singlet oxygen from superoxide intermediates or peroxides can be excluded in a Marcus–Hush–Chidsey theory framework. Electron transfer reactions at metallic electrodes do not lead to excited states for dissolved reactants. Instead, a limiting behavior can be expected, resulting in oxidation at a constant rate. These arguments do not only hold for $^1\text{O}_2$ but for excited states of molecules in general.

Singlet oxygen formation is inherently a complex subject, both in terms of theoretical description and in its experimental detection. Formation of $^1\text{O}_2$ in metal/ O_2 batteries cannot be completely ruled out at this point, but future experiments have to show that side reactions leading to false positive results can be clearly excluded or quantified.

This thesis advances our understanding and description of the transport and chemistry of oxygen in aprotic Li/ O_2 batteries. The developed experimental methods and simulations allow the determination of Henry’s law constants and diffusion coefficients of oxygen in solvents and electrolytes. A comprehensive description of $^1\text{O}_2$ formation in Li/ O_2 batteries based on our current knowledge is given.

At this point, the question arises as to the prospects of research on Li/ O_2 and metal/ O_2 batteries in general. It is still questionable whether Li/ O_2 batteries will find application as energy storage systems. Due to the reactive oxygen species involved, such as superoxides, peroxides and peroxy carbonates, and other remaining challenges during cell cycling, it still seems still unrealistic that Li/ O_2 batteries can compete with future or even today’s lithium-ion batteries in terms of energy efficiency and cycling stability. Moreover, current calculations and simulations suggest that the volumetric energy density of Li/ O_2 batteries will be too low to enable their use in electric vehicles, which was initially the main target.^{29,140} Nevertheless, the high theoretical energy density of Li/ O_2 batteries and the urgent need for improved battery chemistries to pave the way to a fully electrified society will encourage further research in this field.

Relevant issues and questions for future investigations and studies, not only in the field of Li/ O_2 batteries, can be derived from the results presented in this thesis.

The progress of metal/ O_2 batteries is hampered by a lack of thermodynamic and kinetic data, for example, standard potentials of the involved intermediates, equilibrium constants, and rates of reaction. This is especially true for Li/ O_2 batteries, where transient intermediates such as superoxides are involved. A profound understanding of the

underlying reaction mechanisms and the interplay of the many reactive species in metal/O₂ batteries is necessary to enable further progress.

While a basic understanding of the reaction mechanisms leading to Li₂O₂ already exists in literature, a complete understanding of the kinetics involving superoxides and peroxides in Li/O₂ batteries and the many possible side reactions is still missing. The electrochemistry of oxygen is not only relevant in the case of metal/O₂ batteries but also in fuel cells, solar energy conversion (artificial photosynthesis), the respiratory chain of biological cells, water electrolysis and electrochemical sensors, as well as metal corrosion processes. Mechanistic investigations on the kinetics and the interplay of superoxide and peroxide species with CO₂ are of particular interest for further development of metal/O₂ and other battery concepts like metal/CO₂ batteries.

The Li/O₂ battery stores oxygen, one of its active materials, in the gas phase above the electrolyte. This already leads to special requirements on the cell design criteria compared to other battery technologies. However, this is known and addressed in literature. In contrast, an aspect often ignored in the theoretical description of Li/O₂ batteries is the deposition of electronically insulating Li₂O₂ on the electrode. Most electrochemical models and the results obtained from them assume diffusion of reactant and product into and out of a semi-infinite space. An example is the Randles–Ševčík equation in cyclic voltammetry or the Cottrell equation in chronoamperometry. Since this is not necessarily true for Li/O₂ batteries, these models cannot simply be applied, but must be appropriately modified to reflect the initial conditions. Such modified models already exist in the literature and should find their way into battery research. A similar problem arises when applying Butler–Volmer kinetics or Marcus theory to describe electrochemical reaction in general. In addition, it must be checked whether the initial conditions fall within the limits of the models (e.g., 1e⁻ transfer vs 2e⁻ transfer or inner vs outer shell electron transfer).

In recent years, research in the field of electrochemistry has picked up momentum again, mainly due to the electrification of all areas of life and industries. While the research on practical applications and materials is well covered, research on electron transfer mechanisms and the development of fundamental theories has stagnated. However, a fundamental understanding of electrochemistry can be expected to be much more valuable for the development of advanced solutions for society needs than trial-and-error studies.¹⁴⁹

Stakes are high and times are pressing in the face of climate change and the transition to renewable energies. Yet the prospects in electrochemistry are promising, and there is plenty to learn and win. This work is a step towards a deeper understanding of the reactions and transport phenomena taking place in Li/O₂ batteries, which will help to pave the way towards future energy storage systems.

Bibliography

- [1] Kurzweil, R. The Law of Accelerating Returns. In *Alan Turing: Life and Legacy of a Great Thinker*; Springer Berlin Heidelberg: Berlin, Heidelberg, 2004; Vol. 4, pp 381–416. DOI: 10.1007/978-3-662-05642-4_16.
- [2] Rafelski, L. E.; Piper, S. C.; Keeling, R. F. Climate Effects on Atmospheric Carbon Dioxide over the Last Century. *Tellus B Chem. Phys. Meteorol.* **2009**, *61*, 718–731. DOI: 10.1111/j.1600-0889.2009.00439.x.
- [3] Hegerl, G. C.; von Storch, H.; Hasselmann, K.; Santer, B. D.; Cubasch, U.; Jones, P. D. Detecting Greenhouse-Gas-Induced Climate Change with an Optimal Fingerprint Method. *J. Clim.* **1996**, *9*, 2281–2306. DOI: 10.1175/1520-0442(1996)009<2281:DGGICC>2.0.CO;2.
- [4] Gesetz für den Ausbau erneuerbarer Energien (Erneuerbare-Energien-Gesetz - EEG 2021), legislation, BGBl. P. 3138, https://www.gesetze-im-internet.de/eeg_2014/ (accessed 2021 - 04 -20).
- [5] Erneuerbare Energien, Bundesministerium für Wirtschaft und Energie <https://www.bmwi.de/Redaktion/DE/Dossier/erneuerbare-energien.html> (accessed 2021 -08 -11).
- [6] Yoshino, A.; Sanechika, K.; Nakajima, T. Secondary Battery. Patent No.: US 4,668,595 A, 1987.
- [7] Eftekhari, A. On the Theoretical Capacity/Energy of Lithium Batteries and Their Counterparts. *ACS Sustain. Chem. Eng.* **2019**, *7*, 3684–3687. DOI: 10.1021/acssuschemeng.7b04330.
- [8] Janek, J.; Zeier, W. G. A Solid Future for Battery Development. *Nat. Energy* **2016**, *1*, 16141. DOI: 10.1038/nenergy.2016.141.
- [9] Adelhelm, P. Editorial: The Energy Challenge, Batteries, and Why Simple Math Matters. *Angew. Chemie Int. Ed.* **2018**, *57*, 6710–6711. DOI: 10.1002/anie.201803221.



- [10] Janek, J.; Adelhelm, P. Zukunftstechnologien. In *Handbuch Lithium-Ionen-Batterien*; Springer Berlin Heidelberg: Berlin, Heidelberg, 2013; pp 199–217. DOI: 10.1007/978-3-642-30653-2_16.
- [11] Gores, H. J.; Barthel, J.; Zugmann, S.; Moosbauer, D.; Amereller, M.; Hartl, R.; Maurer, A. Liquid Nonaqueous Electrolytes. In *Handbook of Battery Materials*; Wiley-VCH Verlag GmbH & Co. KGaA: Weinheim, Germany, 2011; pp 525–626. DOI: 10.1002/9783527637188.ch17.
- [12] Scrosati, B.; Hassoun, J.; Sun, Y.-K. Lithium-Ion Batteries. A Look into the Future. *Energy Environ. Sci.* **2011**, *4*, 3287. DOI: 10.1039/c1ee01388b.
- [13] Abraham, K. M.; Jiang, Z. A Polymer Electrolyte-Based Rechargeable Lithium/Oxygen Battery. *J. Electrochem. Soc.* **1996**, *143*, 1–5. DOI: 10.1149/1.1836378.
- [14] Luntz, A. C.; McCloskey, B. D. Nonaqueous Li–Air Batteries: A Status Report. *Chem. Rev.* **2014**, *114*, 11721–11750. DOI: 10.1021/cr500054y.
- [15] McCloskey, B. D.; Bethune, D. S.; Shelby, R. M.; Mori, T.; Scheffler, R.; Speidel, A.; Sherwood, M.; Luntz, A. C. Limitations in Rechargeability of Li–O₂ Batteries and Possible Origins. *J. Phys. Chem. Lett.* **2012**, *3*, 3043–3047. DOI: 10.1021/jz301359t.
- [16] Viswanathan, V.; Thygesen, K. S.; Hummelshøj, J. S.; Nørskov, J. K.; Girishkumar, G.; McCloskey, B. D.; Luntz, A. C. Electrical Conductivity in Li₂O₂ and Its Role in Determining Capacity Limitations in Non-Aqueous Li–O₂ Batteries. *J. Chem. Phys.* **2011**, *135*, 214704. DOI: 10.1063/1.3663385.
- [17] Johnson, L.; Li, C.; Liu, Z.; Chen, Y.; Freunberger, S. A.; Ashok, P. C.; Praveen, B. B.; Dholakia, K.; Tarascon, J.-M.; Bruce, P. G. The Role of LiO₂ Solubility in O₂ Reduction in Aprotic Solvents and Its Consequences for Li–O₂ Batteries. *Nat. Chem.* **2014**, *6*, 1091–1099. DOI: 10.1038/nchem.2101.
- [18] Freunberger, S. A.; Chen, Y.; Peng, Z.; Griffin, J. M.; Hardwick, L. J.; Bardé, F.; Novák, P.; Bruce, P. G. Reactions in the Rechargeable Lithium–O₂ Battery with Alkyl Carbonate Electrolytes. *J. Am. Chem. Soc.* **2011**, *133*, 8040–8047. DOI: 10.1021/ja2021747.

- [19] Sharon, D.; Afri, M.; Noked, M.; Garsuch, A.; Frimer, A. A.; Aurbach, D. Oxidation of Dimethyl Sulfoxide Solutions by Electrochemical Reduction of Oxygen. *J. Phys. Chem. Lett.* **2013**, *4*, 3115–3119. DOI: 10.1021/jz4017188.
- [20] Freunberger, S. A.; Chen, Y.; Drewett, N. E.; Hardwick, L. J.; Bardé, F.; Bruce, P. G. The Lithium-Oxygen Battery with Ether-Based Electrolytes. *Angew. Chemie Int. Ed.* **2011**, *50*, 8609–8613. DOI: 10.1002/anie.201102357.
- [21] Ottakam Thotiyl, M. M.; Freunberger, S. A.; Peng, Z.; Bruce, P. G. The Carbon Electrode in Nonaqueous Li-O₂ Cells. *J. Am. Chem. Soc.* **2013**, *135*, 494–500. DOI: 10.1021/ja310258x.
- [22] Schaefer, J. L.; Lu, Y.; Moganty, S. S.; Agarwal, P.; Jayaprakash, N.; Archer, L. A. Electrolytes for High-Energy Lithium Batteries. *Appl. Nanosci.* **2012**, *2*, 91–109. DOI: 10.1007/s13204-011-0044-x.
- [23] McCloskey, B. D.; Speidel, A.; Scheffler, R.; Miller, D. C.; Viswanathan, V.; Hummelshøj, J. S.; Nørskov, J. K.; Luntz, A. C. Twin Problems of Interfacial Carbonate Formation in Nonaqueous Li-O₂ Batteries. *J. Phys. Chem. Lett.* **2012**, *3*, 997–1001. DOI: 10.1021/jz300243r.
- [24] Wandt, J.; Jakes, P.; Granwehr, J.; Gasteiger, H. A.; Eichel, R.-A. Singlet Oxygen Formation during the Charging Process of an Aprotic Lithium–Oxygen Battery. *Angew. Chemie Int. Ed.* **2016**, *55*, 6892–6895. DOI: 10.1002/ange.201602142.
- [25] Schürmann, A.; Haas, R.; Murat, M.; Kuritz, N.; Balaish, M.; Ein-Eli, Y.; Janek, J.; Natan, A.; Schröder, D. Diffusivity and Solubility of Oxygen in Solvents for Metal/Oxygen Batteries: A Combined Theoretical and Experimental Study. *J. Electrochem. Soc.* **2018**, *165*, A3095–A3099. DOI: 10.1149/2.0601813jes.
- [26] Schürmann, A.; Luerßen, B.; Mollenhauer, D.; Janek, J.; Schröder, D. Singlet Oxygen in Electrochemical Cells: A Critical Review of Literature and Theory. *Chem. Rev.* **2021**, *121*, 12445–12464. DOI: 10.1021/acs.chemrev.1c00139.
- [27] Semkow, K. W.; Sammells, A. F. A Lithium Oxygen Secondary Battery. *J. Electrochem. Soc.* **1987**, *134*, 2084–2085. DOI: 10.1149/1.2100826.

- [28] Abraham, K. M. A Brief History of Non-Aqueous Metal-Air Batteries. *ECS Trans.* **2008**, *3*, 67. DOI: 10.1149/1.2838193.
- [29] Gallagher, K. G.; Goebel, S.; Greszler, T.; Mathias, M.; Oelerich, W.; Eroglu, D.; Srinivasan, V. Quantifying the Promise of Lithium-Air Batteries for Electric Vehicles. *Energy Environ. Sci.* **2014**, *7*, 1555. DOI: 10.1039/c3ee43870h.
- [30] Girishkumar, G.; McCloskey, B.; Luntz, A. C.; Swanson, S.; Wilcke, W. Lithium-Air Battery: Promise and Challenges. *J. Phys. Chem. Lett.* **2010**, *1*, 2193–2203. DOI: 10.1021/jz1005384.
- [31] McCloskey, B. D. Attainable Gravimetric and Volumetric Energy Density of Li-S and Li Ion Battery Cells with Solid Separator-Protected Li Metal Anodes. *J. Phys. Chem. Lett.* **2015**, *6*, 4581–4588. DOI: 10.1021/acs.jpcclett.5b01814.
- [32] Kwak, W.-J.; Rosy; Sharon, D.; Xia, C.; Kim, H.; Johnson, L. R.; Bruce, P. G.; Nazar, L. F.; Sun, Y.-K.; Frimer, A. A.; Noked, M.; Freunberger, S. A.; Aurbach, D. Lithium-Oxygen Batteries and Related Systems: Potential, Status, and Future. *Chem. Rev.* **2020**, *120*, 6626–6683. DOI: 10.1021/acs.chemrev.9b00609.
- [33] Nasybulin, E.; Xu, W.; Engelhard, M. H.; Nie, Z.; Burton, S. D.; Cosimbescu, L.; Gross, M. E.; Zhang, J.-G. Effects of Electrolyte Salts on the Performance of Li-O₂ Batteries. *J. Phys. Chem. C* **2013**, *117*, 2635–2645. DOI: 10.1021/jp311114u.
- [34] Younesi, R.; Hahlin, M.; Roberts, M.; Edström, K. The SEI Layer Formed on Lithium Metal in the Presence of Oxygen: A Seldom Considered Component in the Development of the Li-O₂ Battery. *J. Power Sources* **2013**, *225*, 40–45. DOI: 10.1016/j.jpowsour.2012.10.011.
- [35] Assary, R. S.; Lu, J.; Du, P.; Luo, X.; Zhang, X.; Ren, Y.; Curtiss, L. A.; Amine, K. The Effect of Oxygen Crossover on the Anode of a Li-O₂ Battery Using an Ether-Based Solvent: Insights from Experimental and Computational Studies. *ChemSusChem* **2013**, *6*, 51–55. DOI: 10.1002/cssc.201200810.
- [36] Tasaki, K.; Goldberg, A.; Lian, J.; Walker, M.; Timmons, A.; Harris, S. J. Solubility of Lithium Salts Formed on the Lithium-Ion Battery Negative Electrode Surface in Organic Solvents. *J. Electrochem. Soc.* **2009**, *156*, A1019. DOI: 10.1149/1.3239850.

- [37] Kitaura, H.; Zhou, H. Electrochemical Performance of Solid-State Lithium-Air Batteries Using Carbon Nanotube Catalyst in the Air Electrode. *Adv. Energy Mater.* **2012**, *2*, 889–894. DOI: 10.1002/aenm.201100789.
- [38] Kitaura, H.; Zhou, H. Electrochemical Performance and Reaction Mechanism of All-Solid-State Lithium-Air Batteries Composed of Lithium, $\text{Li}_{1+x}\text{Al}_y\text{Ge}_{2-y}(\text{PO}_4)_3$ Solid Electrolyte and Carbon Nanotube Air Electrode. *Energy Environ. Sci.* **2012**, *5*, 9077–9084. DOI: 10.1039/c2ee22381c.
- [39] Wang, X.; Zhu, D.; Song, M.; Cai, S.; Zhang, L.; Chen, Y. A Li-O₂/Air Battery Using an Inorganic Solid-State Air Cathode. *ACS Appl. Mater. Interfaces* **2014**, *6*, 11204–11210. DOI: 10.1021/am501315n.
- [40] Wang, Y.; Zhou, H. To Draw An Air Electrode Of A Li-Air Battery By Pencil. *Energy Environ. Sci.* **2011**, *4*, 1704. DOI: 10.1039/c0ee00759e.
- [41] Wang, J.; Huang, G.; Chen, K.; Zhang, X. An Adjustable-Porosity Plastic Crystal Electrolyte Enables High-Performance All-Solid-State Lithium-Oxygen Batteries. *Angew. Chemie* **2020**, *132*, 9468–9473. DOI: 10.1002/ange.202002309.
- [42] Wang, S.; Wang, J.; Liu, J.; Song, H.; Liu, Y.; Wang, P.; He, P.; Xu, J.; Zhou, H. Ultra-Fine Surface Solid-State Electrolytes for Long Cycle Life All-Solid-State Lithium-Air Batteries. *J. Mater. Chem. A* **2018**, *6*, 21248–21254. DOI: 10.1039/C8TA08095J.
- [43] Manthiram, A.; Li, L. Hybrid and Aqueous Lithium-Air Batteries. *Adv. Energy Mater.* **2015**, *5*, 1401302. DOI: 10.1002/aenm.201401302.
- [44] Li, L.; Zhao, X.; Manthiram, A. A Dual-Electrolyte Rechargeable Li-Air Battery with Phosphate Buffer Catholyte. *Electrochem. commun.* **2012**, *14*, 78–81. DOI: 10.1016/j.elecom.2011.11.007.
- [45] Li, L.; Manthiram, A. Dual-Electrolyte Lithium-Air Batteries: Influence of Catalyst, Temperature, and Solid-Electrolyte Conductivity on the Efficiency and Power Density. *J. Mater. Chem. A* **2013**, *1*, 5121–5127. DOI: 10.1039/c3ta01241g.

- [46] Li, L.; Manthiram, A. Decoupled Bifunctional Air Electrodes for High-Performance Hybrid Lithium-Air Batteries. *Nano Energy* **2014**, *9*, 94–100. DOI: 10.1016/j.nanoen.2014.07.002.
- [47] Visco, S. J.; Katz, B. D.; Nimon, Y. S.; De Jonghe, L. C. Protected Active Metal Electrode and Battery Cell Structures with Non-Aqueous Interlayer Architecture. Patent No.: US 7,282,295 B2, 2007.
- [48] Visco, S. J.; Nimon, V.; Jonghe, L. C. De; Volfkovich, Y.; Bograchev, D. Cathode Architectures for Alkali Metal / Oxygen Batteries. Patent No.: US 8,932,771 B2, 2015.
- [49] Lu, J.; Li, L.; Park, J.-B.; Sun, Y.-K.; Wu, F.; Amine, K. Aprotic and Aqueous Li–O₂ Batteries. *Chem. Rev.* **2014**, *114*, 5611–5640. DOI: 10.1021/cr400573b.
- [50] Zheng, J. P.; Liang, R. Y.; Hendrickson, M.; Plichta, E. J. Theoretical Energy Density of Li–Air Batteries. *J. Electrochem. Soc.* **2008**, *155*, A432. DOI: 10.1149/1.2901961.
- [51] Black, R.; Adams, B.; Nazar, L. F. Non-Aqueous and Hybrid Li–O₂ Batteries. *Adv. Energy Mater.* **2012**, *2*, 801–815. DOI: 10.1002/aenm.201200001.
- [52] Xia, C.; Bender, C. L.; Bergner, B.; Peppler, K.; Janek, J. An Electrolyte Partially-Wetted Cathode Improving Oxygen Diffusion in Cathodes of Non-Aqueous Li–Air Batteries. *Electrochem. commun.* **2013**, *26*, 93–96. DOI: 10.1016/j.elecom.2012.10.020.
- [53] Read, J.; Mutolo, K.; Ervin, M.; Behl, W.; Wolfenstine, J.; Driedger, A.; Foster, D. Oxygen Transport Properties of Organic Electrolytes and Performance of Lithium/Oxygen Battery. *J. Electrochem. Soc.* **2003**, *150*, A1351–A1356. DOI: 10.1149/1.1606454.
- [54] Kraytsberg, A.; Ein-eli, Y. Review on Li–Air Batteries — Opportunities, Limitations and Perspective. **2011**, *196*, 886–893. DOI: 10.1016/j.jpowsour.2010.09.031.
- [55] Schröder, D.; Bender, C. L.; Osenberg, M.; Hilger, A.; Manke, I.; Janek, J. Visualizing Current-Dependent Morphology and Distribution of Discharge Products in Sodium- Oxygen Battery Cathodes. *Sci. Rep.* **2016**, *6*, 1–7. DOI: 10.1038/srep24288.

- [56] Bruce, P. G.; Freunberger, S. A.; Hardwick, L. J.; Tarascon, J.-M. Li-O₂ and Li-S Batteries with High Energy Storage. *Nat. Mater.* **2012**, *11*, 19–29. DOI: 10.1038/nmat3237.
- [57] Xu, W.; Wang, J.; Ding, F.; Chen, X.; Nasybulin, E.; Zhang, Y.; Zhang, J.-G. Lithium Metal Anodes for Rechargeable Batteries. *Energy Environ. Sci.* **2014**, *7*, 513–537. DOI: 10.1039/C3EE40795K.
- [58] Winter, M. The Solid Electrolyte Interphase – The Most Important and the Least Understood Solid Electrolyte in Rechargeable Li Batteries. *Zeitschrift für Phys. Chemie* **2009**, *223*, 1395–1406. DOI: 10.1524/zpch.2009.6086.
- [59] Aurbach, D.; Zinigrad, E.; Cohen, Y.; Teller, H. A Short Review of Failure Mechanisms of Lithium Metal and Lithiated Graphite Anodes in Liquid Electrolyte Solutions. *Solid State Ionics* **2002**, *148*, 405–416. DOI: 10.1016/S0167-2738(02)00080-2.
- [60] Ottakam Thotiyl, M. M.; Freunberger, S. A.; Peng, Z.; Chen, Y.; Liu, Z.; Bruce, P. G. A Stable Cathode for the Aprotic Li-O₂ Battery. *Nat. Mater.* **2013**, *12*, 1050–1056. DOI: 10.1038/nmat3737.
- [61] Peng, Z.; Freunberger, S. a; Chen, Y.; Bruce, P. G.; Battery, L. A Reversible and Higher-Rate Li-O₂ Battery. *Science* **2012**, *337*, 563–566. DOI: 10.1126/science.1223985.
- [62] Ogasawara, T.; Débart, A.; Holzapfel, M.; Novák, P.; Bruce, P. G. Rechargeable Li₂O₂ Electrode for Lithium Batteries. *J. Am. Chem. Soc.* **2006**, *128*, 1390–1393. DOI: 10.1021/ja056811q.
- [63] Jung, H.; Jeong, Y. S.; Park, J.; Sun, Y.; Scrosati, B.; Lee, Y. J. Ruthenium-Based Electrocatalysts Supported on Reduced Graphene Oxide for Lithium-Air Batteries. *ACS Nano* **2013**, *7*, 3532–3539. DOI: 10.1021/nn400477d.
- [64] Lu, Y.; Xu, Z.; Gasteiger, H. A.; Chen, S.; Hamad-Schifferli, K.; Shao-Horn, Y. Platinum–Gold Nanoparticles: A Highly Active Bifunctional Electrocatalyst for Rechargeable Lithium–Air Batteries. *J. Am. Chem. Soc.* **2010**, *132*, 12170–12171. DOI: 10.1021/ja1036572.
- [65] Chen, Y.; Freunberger, S. A.; Peng, Z.; Fontaine, O.; Bruce, P. G. Charging a Li-O₂ Battery Using a Redox Mediator. *Nat. Chem.* **2013**, *5*, 489–494. DOI: 10.1038/nchem.1646.

- [66] Bergner, B. J.; Schürmann, A.; Pepler, K.; Garsuch, A.; Janek, J. TEMPO: A Mobile Catalyst for Rechargeable Li-O₂ Batteries. *J. Am. Chem. Soc.* **2014**, *136*, 15054–15064. DOI: 10.1021/ja508400m.
- [67] Bergner, B. J.; Hofmann, C.; Schürmann, A.; Schröder, D.; Pepler, K.; Schreiner, P. R.; Janek, J. Understanding the Fundamentals of Redox Mediators in Li-O₂ Batteries: A Case Study on Nitroxides. *Phys. Chem. Chem. Phys.* **2015**, *17*, 31769–31779. DOI: 10.1039/C5CP04505C.
- [68] Lim, H.; Lee, B.; Zheng, Y.; Hong, J.; Kim, J.; Gwon, H.; Ko, Y.; Lee, M.; Cho, K.; Kang, K. Rational Design of Redox Mediators for Advanced Li-O₂ Batteries. *Nat. Energy* **2016**, *1*, 16066. DOI: 10.1038/nenergy.2016.66.
- [69] McCloskey, B. D.; Scheffler, R.; Speidel, A.; Bethune, D. S.; Shelby, R. M.; Luntz, A. C. On the Efficacy of Electrocatalysis in Nonaqueous Li-O₂ Batteries. *J. Am. Chem. Soc.* **2011**, *133*, 18038–18041. DOI: 10.1021/ja207229n.
- [70] Bryantsev, V. S.; Uddin, J.; Giordani, V.; Walker, W.; Addison, D.; Chase, G. V. The Identification of Stable Solvents for Nonaqueous Rechargeable Li-Air Batteries. *J. Electrochem. Soc.* **2013**, *160*, A160–A171. DOI: 10.1149/2.027302jes.
- [71] Sawyer, D. T.; Gibian, M. J. The Chemistry of Superoxide Ion. *Tetrahedron* **1979**, *35*, 1471–1481. DOI: 10.1016/0040-4020(79)80032-0.
- [72] Sawyer, D. T.; Roberts, J. L. Electrochemistry of Oxygen and Superoxide Ion in Dimethylsulfoxide at Platinum, Gold and Mercury Electrodes. *J. Electroanal. Chem.* **1966**, *12*, 90–101. DOI: 10.1016/0022-0728(66)80021-9.
- [73] Zhu, D.; Zhang, L.; Song, M.; Wang, X.; Mei, J.; Lau, L. W. M.; Chen, Y. Solvent Autoxidation, Electrolyte Decomposition, and Performance Deterioration of the Aprotic Li-O₂ Battery. *J. Solid State Electrochem.* **2013**, *17*, 2865–2870. DOI: 10.1007/s10008-013-2202-4.
- [74] Younesi, R.; Hahlin, M.; Björefors, F.; Johansson, P.; Edström, K. Li-O₂ Battery Degradation by Lithium Peroxide (Li₂O₂): A Model Study. *Chem. Mater.* **2013**, *25*, 77–84. DOI: 10.1021/cm303226g.

- [75] Veith, G. M.; Nanda, J.; Delmau, L. H.; Dudney, N. J. Influence of Lithium Salts on the Discharge Chemistry of Li–Air Cells. *J. Phys. Chem. Lett.* **2012**, *3*, 1242–1247. DOI: 10.1021/jz300430s.
- [76] Zhang, S.; Nava, M. J.; Chow, G. K.; Lopez, N.; Wu, G.; Britt, D. R.; Nocera, D. G.; Cummins, C. C. On the Incompatibility of Lithium-O₂ Battery Technology with CO₂. *Chem. Sci.* **2017**, *8*, 6117–6122. DOI: 10.1039/c7sc01230f.
- [77] Roberts, J. L.; Calderwood, T. S.; Sawyer, D. T. Nucleophilic Oxygenation of Carbon Dioxide by Superoxide Ion in Aprotic Media to Form the C₂O₆²⁻ Ion Species. *J. Am. Chem. Soc.* **1984**, *106*, 4667–4670. DOI: 10.1021/ja00329a003.
- [78] Wadhawan, J. D.; Welford, P. J.; Maisonhaute, E.; Climent, V.; Lawrence, N. S.; Compton, R. G.; McPeak, H. B.; Hahn, C. E. W. Microelectrode Studies of the Reaction of Superoxide with Carbon Dioxide in Dimethyl Sulfoxide. *J. Phys. Chem. B* **2001**, *105*, 10659–10668. DOI: 10.1021/jp012160i.
- [79] Hassoun, J.; Croce, F.; Armand, M.; Scrosati, B. Investigation of the O₂ Electrochemistry in a Polymer Electrolyte Solid-State Cell. *Angew. Chemie Int. Ed.* **2011**, *50*, 2999–3002. DOI: 10.1002/anie.201006264.
- [80] Mahne, N.; Schafzahl, B.; Leypold, C.; Leypold, M.; Grumm, S.; Leitgeb, A.; Strohmeier, G. A.; Wilkening, M.; Fontaine, O.; Kramer, D.; Slugovc, C.; Borisov, S. M.; Freunberger, S. A. Singlet Oxygen Generation as a Major Cause for Parasitic Reactions During Cycling of Aprotic Lithium–Oxygen Batteries. *Nat. Energy* **2017**, *2*, 17036. DOI: 10.1038/nenergy.2017.36.
- [81] Krauskopf, T.; Richter, F. H.; Zeier, W. G.; Janek, J. Physicochemical Concepts of the Lithium Metal Anode in Solid-State Batteries. *Chem. Rev.* **2020**, *120*, 7745–7794. DOI: 10.1021/acs.chemrev.0c00431.
- [82] Compton, R. G.; Banks, C. E. *Understanding Voltammetry*, Third Edit.; World Scientific: London, 2011. DOI: 10.1142/p783.
- [83] Hammerich, O.; Speiser, B. *Organic Electrochemistry*; CRC Press, 2016.

- [84] Costentin, C.; Evans, D. H.; Robert, M.; Savéant, J.-M.; Singh, P. S. Electrochemical Approach to Concerted Proton and Electron Transfers. Reduction of the Water–Superoxide Ion Complex. *J. Am. Chem. Soc.* **2005**, *127*, 12490–12491. DOI: 10.1021/ja053911n.
- [85] Sawyer, D. T.; Valentine, J. S. How Super Is Superoxide? *Acc. Chem. Res.* **1981**, *14*, 393–400. DOI: 10.1021/ar00072a005.
- [86] Peng, Z.; Freunberger, S. A. A.; Hardwick, L. J. J.; Chen, Y.; Giordani, V.; Bardé, F.; Novák, P.; Graham, D.; Tarascon, J.-M.; Bruce, P. G. G. Oxygen Reactions in a Non-Aqueous Li⁺ Electrolyte. *Angew. Chemie Int. Ed.* **2011**, *50*, 6351–6355. DOI: 10.1002/anie.201100879.
- [87] Laoire, C. O.; Mukerjee, S.; Abraham, K. M.; Plichta, E. J.; Hendrickson, M. A. Elucidating the Mechanism of Oxygen Reduction for Lithium–Air Battery Applications. *J. Phys. Chem. C* **2009**, *113*, 20127–20134. DOI: 10.1021/jp908090s.
- [88] Herranz, J.; Garsuch, A.; Gasteiger, H. A. Using Rotating Ring Disc Electrode Voltammetry to Quantify the Superoxide Radical Stability of Aprotic Li–Air Battery Electrolytes. *J. Phys. Chem. C* **2012**, *116*, 19084–19094. DOI: 10.1021/jp304277z.
- [89] Andrieux, C. P.; Hapiot, P.; Saveant, J. M. Mechanism of Superoxide Ion Disproportionation in Aprotic Solvents. *J. Am. Chem. Soc.* **1987**, *109*, 3768–3775. DOI: 10.1021/ja00246a040.
- [90] Savéant, J.-M. *Elements of Molecular and Biomolecular Electrochemistry: An Electrochemical Approach to Electron Transfer Chemistry*; Wiley-Interscience: Hoboken, New Jersey, 2006.
- [91] Aurbach, D.; McCloskey, B. D.; Nazar, L. F.; Bruce, P. G. Advances in Understanding Mechanisms Underpinning Lithium–Air Batteries. *Nat. Energy* **2016**, *1*, 1–11. DOI: 10.1038/nenergy.2016.128.
- [92] Laoire, C. O.; Mukerjee, S.; Abraham, K. M.; Plichta, E. J.; Hendrickson, M. A. Influence of Nonaqueous Solvents on the Electrochemistry of Oxygen in the Rechargeable Lithium–Air Battery. *J. Phys. Chem. C* **2010**, *114*, 9178–9186. DOI: 10.1021/jp102019y.

- [93] Aetukuri, N. B.; McCloskey, B. D.; Garcíá, J. M.; Krupp, L. E.; Viswanathan, V.; Luntz, A. C. Solvating Additives Drive Solution-Mediated Electrochemistry and Enhance Toroid Growth in Non-Aqueous Li-O₂ Batteries. *Nat. Chem.* **2015**, *7*, 50–56. DOI: 10.1038/nchem.2132.
- [94] Cong, G.; Wang, W.; Lai, N. C.; Liang, Z.; Lu, Y. C. A High-Rate and Long-Life Organic–Oxygen Battery. *Nat. Mater.* **2019**, *18*, 390–396. DOI: 10.1038/s41563-019-0286-7.
- [95] Bender, C. L.; Schröder, D.; Pinedo, R.; Adelhelm, P.; Janek, J. One- or Two-Electron Transfer? The Ambiguous Nature of the Discharge Products in Sodium-Oxygen Batteries. *Angew. Chemie Int. Ed.* **2016**, *55*, 4640–4649. DOI: 10.1002/anie.201510856.
- [96] Ren, X.; Wu, Y. A Low-Overpotential Potassium-Oxygen Battery Based on Potassium Superoxide. *J. Am. Chem. Soc.* **2013**, *135*, 2923–2926. DOI: 10.1021/ja312059q.
- [97] Hardwick, L. J.; de León, C. P. Rechargeable Multi-Valent Metal-Air Batteries. *Johnson Matthey Technol. Rev.* **2018**, *62*, 134–149. DOI: 10.1595/205651318X696729.
- [98] Schröder, D.; Janek, J.; Adelhelm, P. Nonlithium Aprotic Metal/Oxygen Batteries Using Na, K, Mg, or Ca as Metal Anode. In *Encyclopedia of Electrochemistry*; Wiley, 2020; pp 1–29. DOI: 10.1002/9783527610426.bard110018.
- [99] Vardar, G.; Nelson, E. G.; Smith, J. G.; Naruse, J.; Hiramatsu, H.; Bartlett, B. M.; Sleightholme, A. E. S.; Siegel, D. J.; Monroe, C. W. Identifying the Discharge Product and Reaction Pathway for a Secondary Mg/O₂ Battery. *Chem. Mater.* **2015**, *27*, 7564–7568. DOI: 10.1021/acs.chemmater.5b03608.
- [100] Shiga, T.; Hase, Y.; Kato, Y.; Inoue, M.; Takechi, K. A Rechargeable Non-Aqueous Mg–O₂ Battery. *Chem. Commun.* **2013**, *49*, 9152. DOI: 10.1039/c3cc43477j.
- [101] Reinsberg, P.; Bondue, C. J.; Baltruschat, H. Calcium–Oxygen Batteries as a Promising Alternative to Sodium–Oxygen Batteries. *J. Phys. Chem. C* **2016**, *120*, 22179–22185. DOI: 10.1021/acs.jpcc.6b06674.

- [102] Gerbig, O.; Merkle, R.; Maier, J. Electron and Ion Transport In Li_2O_2 . *Adv. Mater.* **2013**, *25*, 3129–3133. DOI: 10.1002/adma.201300264.
- [103] Radin, M. D.; Siegel, D. J. Charge Transport in Lithium Peroxide: Relevance for Rechargeable Metal-Air Batteries. *Energy Environ. Sci.* **2013**, *6*, 2370–2379. DOI: 10.1039/c3ee41632a.
- [104] Radin, M. D.; Rodriguez, J. F.; Siegel, D. J. Lithium Peroxide Surfaces and Point Defects: Relevance for Li-Air Batteries. *Proc. Batter. Congr.* **2011**, 1–6.
- [105] Luntz, A. C.; Viswanathan, V.; Voss, J.; Varley, J. B.; Nørskov, J. K.; Scheffler, R.; Speidel, A. Tunneling and Polaron Charge Transport through Li_2O_2 in Li- O_2 Batteries. *J. Phys. Chem. Lett.* **2013**, *4*, 3494–3499. DOI: 10.1021/jz401926f.
- [106] McCloskey, B. D.; Valery, A.; Luntz, A. C.; Gowda, S. R.; Wallraff, G. M.; Garcia, J. M.; Mori, T.; Krupp, L. E. Combining Accurate O_2 and Li_2O_2 Assays to Separate Discharge and Charge Stability Limitations in Nonaqueous Li- O_2 Batteries. *J. Phys. Chem. Lett.* **2013**, *4*, 2989–2993. DOI: 10.1021/jz401659f.
- [107] McCloskey, B. D.; Bethune, D. S.; Shelby, R. M.; Girishkumar, G.; Luntz, A. C. Solvents' Critical Role in Nonaqueous Lithium-Oxygen Battery Electrochemistry. *J. Phys. Chem. Lett.* **2011**, *2*, 1161–1166. DOI: 10.1021/jz200352v.
- [108] Battino, R.; Clever, H. L. The Solubility of Gases in Liquids. *Chem. Rev.* **1966**, *66*, 395–463. DOI: 10.1021/cr60242a003.
- [109] Pierotti, R. A. A Scaled Particle Theory of Aqueous and Nonaqueous Solutions. *Chem. Rev.* **1976**, *76*, 717–726. DOI: 10.1021/cr60304a002.
- [110] Reiss, H.; Frisch, H. L.; Lebowitz, J. L. Statistical Mechanics of Rigid Spheres. *J. Chem. Phys.* **1959**, *31*, 369–380. DOI: 10.1063/1.1730361.
- [111] Reiss, H.; Frisch, H. L.; Helfand, E.; Lebowitz, J. L. Aspects of the Statistical Thermodynamics of Real Fluids. *J. Chem. Phys.* **1960**, *32*, 119–124. DOI: 10.1063/1.1700883.
- [112] Uhlig, H. H. The Solubilities of Gases and Surface Tension. *J. Phys. Chem.* **1937**, *41*, 1215–1226. DOI: 10.1021/j150387a007.

- [113] Calvert, J. G. Glossary of Atmospheric Chemistry Terms (Recommendations 1990). *Pure Appl. Chem.* **1990**, *62*, 2167–2219. DOI: 10.1351/pac199062112167.
- [114] Battino, R. The Ostwald Coefficient of Gas Solubility. *Fluid Phase Equilib.* **1984**, *15*, 231–240. DOI: 10.1016/0378-3812(84)87009-0.
- [115] Wohlfarth, C. *Surface Tension of Pure Liquids and Binary Liquid Mixtures - Supplement to Volume IV/24*; Lechner, M. D., Ed.; Springer Berlin Heidelberg: Berlin, Heidelberg, 2016. DOI: 10.1007/978-3-662-48336-7.
- [116] Haas, R.; Murat, M.; Weiss, M.; Janek, J.; Natan, A.; Schröder, D. Understanding the Transport of Atmospheric Gases in Liquid Electrolytes for Lithium–Air Batteries. *J. Electrochem. Soc.* **2021**, *168*, 070504. DOI: 10.1149/1945-7111/ac0d66.
- [117] Lawrence Clever, H.; Battino, R.; Miyamoto, H.; Yampolski, Y.; Young, C. L. IUPAC-NIST Solubility Data Series. 103. Oxygen and Ozone in Water, Aqueous Solutions, and Organic Liquids (Supplement to Solubility Data Series Volume 7). *J. Phys. Chem. Ref. Data* **2014**, *43*. DOI: 10.1063/1.4883876.
- [118] Sato, T.; Hamada, Y.; Sumikawa, M.; Araki, S.; Yamamoto, H. Solubility of Oxygen in Organic Solvents and Calculation of the Hansen Solubility Parameters of Oxygen. *Ind. Eng. Chem. Res.* **2014**, *53*, 19331–19337. DOI: 10.1021/ie502386t.
- [119] Freire, M. G.; Carvalho, P. J.; Queimada, A. J.; Marrucho, I. M.; Coutinho, J. A. P. Surface Tension of Liquid Fluorocompounds. *J. Chem. Eng. Data* **2006**, *51*, 1820–1824. DOI: 10.1021/je060199g.
- [120] Debye, P. Das Elektrische Ionenfeld Und Das Aussalzen. *Zeitschrift für Phys. Chemie* **1927**, *130U*, 56–64. DOI: 10.1515/zpch-1927-13008.
- [121] Bockris, J. O.; Egan, H. The Salting-Out Effect and Dielectric Constant. *Trans. Faraday Soc.* **1948**, *44*, 151. DOI: 10.1039/tf9484400151.
- [122] Bockris, J. O.; Bowler-Reed, J.; Kitchener, J. A. The Salting-In Effect. *Trans. Faraday Soc.* **1951**, *47*, 184. DOI: 10.1039/tf9514700184.

- [123] McDevit, W. F.; Long, F. A. The Activity Coefficient of Benzene in Aqueous Salt Solutions. *J. Am. Chem. Soc.* **1952**, *74*, 1773–1777. DOI: 10.1021/ja01127a048.
- [124] Varzi, A.; Thanner, K.; Scipioni, R.; Di Lecce, D.; Hassoun, J.; Dörfler, S.; Altheus, H.; Kaskel, S.; Prehal, C.; Freunberger, S. A. Current Status and Future Perspectives of Lithium Metal Batteries. *J. Power Sources* **2020**, *480*. DOI: 10.1016/j.jpowsour.2020.228803.
- [125] Prehal, C.; Samojlov, A.; Nachtnebel, M.; Lovicar, L.; Kriechbaum, M.; Amenitsch, H.; Freunberger, S. A. In Situ Small-Angle X-Ray Scattering Reveals Solution Phase Discharge of Li–O₂ Batteries with Weakly Solvating Electrolytes. *Proc. Natl. Acad. Sci.* **2021**, *118*, e2021893118. DOI: 10.1073/pnas.2021893118.
- [126] Ren, X.; Zhang, S. S.; Tran, D. T.; Read, J. Oxygen Reduction Reaction Catalyst on Lithium/Air Battery Discharge Performance. *J. Mater. Chem.* **2011**, *21*, 10118. DOI: 10.1039/c0jm04170j.
- [127] Bard, A. J.; Faulkner, L. R. *Electrochemical Methods: Fundamentals and Applications*; John Wiley & Sons: New York, 2001.
- [128] Marcus, R. A. Electron Transfer Reactions in Chemistry. Theory and Experiment. *Rev. Mod. Phys.* **1993**, *65*, 599–610. DOI: 10.1103/RevModPhys.65.599.
- [129] Marcus, R. A. On the Theory of Electron-Transfer Reactions. VI. Unified Treatment for Homogeneous and Electrode Reactions. *J. Chem. Phys.* **1965**, *43*, 679. DOI: 10.1063/1.1696792.
- [130] Appleby, A. J.; Zagal, J. H. Free Energy Relationships in Electrochemistry: A History That Started in 1935. *J. Solid State Electrochem.* **2011**, *15*, 1811–1832. DOI: 10.1007/s10008-011-1394-8.
- [131] Closs, G. L.; Miller, J. R. Intramolecular Long-Distance Electron Transfer in Organic Molecules. *Science* **1988**, *240*, 440–447. DOI: 10.1126/science.240.4851.440.

- [132] Miller, J. R. Intramolecular Long-Distance Electron Transfer in Radical Anions. The Effects of Free Energy and Solvent on the Reaction Rates. *J. Am. Chem. Soc.* **1984**, *106*, 3047–3049. DOI: 10.1021/ja00322a058.
- [133] Miomandre, F.; Audebert, P. Luminescence in Electrochemistry; Miomandre, F., Audebert, P., Eds.; Springer International Publishing: Cham, Switzerland, 2017. DOI: 10.1007/978-3-319-49137-0.
- [134] Gerischer, H. *Semiconductor Electrochemistry*; Technical Report for Lawrence Berkeley National Laboratory, Berkeley, California, 1968.
- [135] Gerischer, H. Electron-Transfer Kinetics of Redox Reactions at the Semiconductor/Electrolyte Contact. A New Approach. *J. Phys. Chem.* **1991**, *95*, 1356–1359. DOI: 10.1021/j100156a060.
- [136] Schmickler, W.; Santos, E. *Interfacial Electrochemistry*; 2010. DOI: 10.1007/978-3-642-04937-8.
- [137] Gerischer, H.; Mindt, W. The Mechanisms of the Decomposition of Semiconductors by Electrochemical Oxidation and Reduction. *Electrochim. Acta* **1968**, *13*, 1329–1341. DOI: 10.1016/0013-4686(68)80060-X.
- [138] Osseo-Asare, K. Semiconductor Electrochemistry and Hydrometallurgical Dissolution Processes. *Hydrometallurgy* **1992**, *29*, 61–90. DOI: 10.1016/0304-386X(92)90006-L.
- [139] Kurchin, R.; Viswanathan, V. Marcus-Hush-Chidsey Kinetics at Electrode-Electrolyte Interfaces. *J. Chem. Phys.* **2020**, *153*. DOI: 10.1063/5.0023611.
- [140] Christensen, J.; Albertus, P.; Sanchez-Carrera, R. S.; Lohmann, T.; Kozinsky, B.; Liedtke, R.; Ahmed, J.; Kojic, A. A Critical Review of Li/Air Batteries. *J. Electrochem. Soc.* **2011**, *159*, R1–R30. DOI: 10.1149/2.086202jes.
- [141] Houchins, G.; Pande, V.; Viswanathan, V. Mechanism for Singlet Oxygen Production in Li-Ion and Metal-Air Batteries. *ACS Energy Lett.* **2020**, 1893–1899. DOI: 10.1021/acsenerylett.0c00595.

- [142] Pierini, A.; Brutti, S.; Bodo, E. Superoxide Anions Disproportionation Induced by Li^+ and H^+ : Pathways to $^1\text{O}_2$ Release in Li- O_2 Batteries. *ChemPhysChem* **2020**, *21*, 2060–2067. DOI: 10.1002/cphc.202000318.
- [143] Petit, Y. K.; Mourad, E.; Prehal, C.; Leybold, C.; Windischbacher, A.; Mijailovic, D.; Slugovc, C.; Borisov, S. M.; Zojer, E.; Brutti, S.; Fontaine, O.; Freunberger, S. A. Mechanism of Mediated Alkali Peroxide Oxidation and Triplet versus Singlet Oxygen Formation. *Nat. Chem.* **2021**, *13*, 465–471. DOI: 10.1038/s41557-021-00643-z.
- [144] Gileadi, E. The Enigma of Metal Deposition. *J. Electroanal. Chem.* **2011**, *660*, 247–253. DOI: 10.1016/j.jelechem.2011.01.025.
- [145] Pinto, L. M. C.; Spohr, E.; Quaino, P.; Santos, E.; Schmickler, W. Why Silver Deposition Is so Fast: Solving the Enigma of Metal Deposition. *Angew. Chemie Int. Ed.* **2013**, *52*, 7883–7885. DOI: 10.1002/anie.201301998.
- [146] Viswanathan, V.; Nørskov, J. K.; Speidel, A.; Scheffler, R.; Gowda, S.; Luntz, A. C. Li- O_2 Kinetic Overpotentials: Tafel Plots from Experiment and First-Principles Theory. *J. Phys. Chem. Lett.* **2013**, *4*, 556–560. DOI: 10.1021/jz400019y.
- [147] Sankarasubramanian, S.; Seo, J.; Mizuno, F.; Singh, N.; Prakash, J. Elucidating the Oxygen Reduction Reaction Kinetics and the Origins of the Anomalous Tafel Behavior at the Lithium–Oxygen Cell Cathode. *J. Phys. Chem. C* **2017**, *121*, 4789–4798. DOI: 10.1021/acs.jpcc.6b09747.
- [148] Fraggedakis, D.; McEldrew, M.; Smith, R. B.; Krishnan, Y.; Zhang, Y.; Bai, P.; Chueh, W. C.; Shao-Horn, Y.; Bazant, M. Z. Theory of Coupled Ion-Electron Transfer Kinetics. *Electrochim. Acta* **2021**, *367*, 137432. DOI: 10.1016/j.electacta.2020.137432.
- [149] Calvo, E. J. Where to Go in Electrochemistry? A Personal View. *J. Solid State Electrochem.* **2020**, *24*, 2053–2054. DOI: 10.1007/s10008-020-04760-6.
- [150] De Levie, R. What's in a Name? *J. Chem. Educ.* **2000**, *77*, 610–612. DOI: 10.1021/ed077p610.

- [151] Inzelt, G. Milestones of the Development of Kinetics of Electrode Reactions. *J. Solid State Electrochem.* **2011**, *15*, 1373–1389. DOI: 10.1007/s10008-011-1301-3.

PART IV

APPENDICES



Appendix to the Introduction

A.1 SUM OF MECHANISMS IN A GIVEN SCHEME OF SQUARES

Electrochemical reactions often involve protonation or association reactions in the solution besides the actual electron transfer at the electrode. And many systems consist of more than one electron transfer or protonation reaction (e.g., the reduction of oxygen to hydrogen peroxide in aprotic electrolytes). In such a case, a scheme of squares is invaluable in mechanistically deciphering complex sequences of electron and proton transfers. Naturally, the question about the number of possible reaction mechanisms between the starting reactants and a certain product in a scheme of squares arises. Figure A.1 shows a generalized scheme of squares, which only contains electron and proton transfers, and all species are possible. In addition, all arrows represent forward reactions.

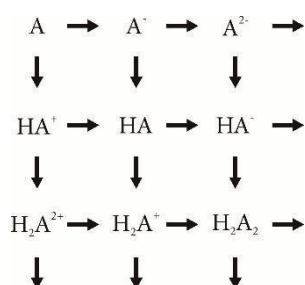
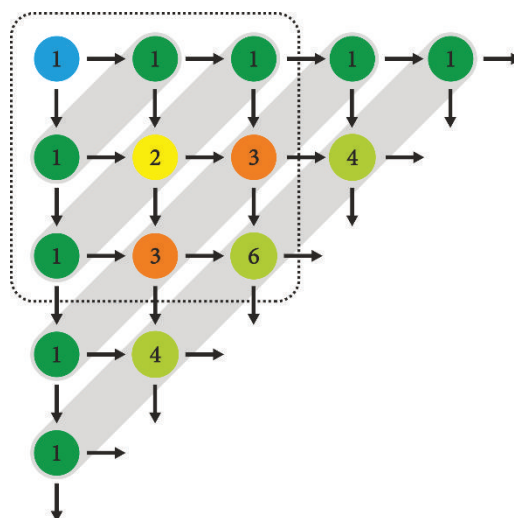


Figure A.1. Generalized scheme of squares for the transfer of electrons and protons to a starting molecule A.

To calculate the maximum sum of reaction mechanisms between reactants and a given product in the scheme, one starts from the top left corner of the scheme (where the reactants are located). Obviously, there is only one way to land at this point of the scheme, which is starting from here. Therefore, the corner is assigned a 1 (blue in Figure A.2). It is also obvious that there is only one possible reaction mechanism connecting A and A^- , as well as A and HA^+ . A^- and HA^+ are therefore also assigned a 1. Vice versa, there is always only one possible reaction mechanism connecting A with a specie in the top row or the left column of the square, which are marked green in Figure A.2 (it is not possible to move up or left in the scheme). Now, what about an intermediate somewhere in the middle? For example, to get to the yellow circle, the system must proceed via one of the two circles directly left or above it. That means, however many ways there are to travel to one of these circles, the sum of these will be the number of mechanisms resulting in the yellow circle. In this case, there are two possible reaction

Figure A.2. Number of possible reaction paths to a given point in the scheme, starting from the reactants in the left top corner (blue circle). The number of possible paths correspond to the Pascal numbers. The original scheme of squares is framed.



mechanisms, $A \rightarrow A^- \rightarrow HA$ or $A \rightarrow HA^+ \rightarrow HA$, and the yellow circle is assigned with a 2. This formalism is extended to the whole scheme of squares in Figure A.2. Interestingly, the numbers of reaction paths start the same way, build the same way as the Pascal numbers, and thus must always equal the Pascal numbers. Essentially, the scheme is cut out of Pascal's triangle and tilted 45° to the left, and the well-known rows from Pascal's triangle are shown in grey in Figure A.2.

The formalism can also be easily adopted to more complicated scheme of squares. In these cases, the resulting numbers are not part of Pascal's triangle.

A.2 NUMERICAL VALUES AND FIT PARAMETERS OF FIGURE 3.1

Table A.1. Surface tension and Henry's law constants for solvents commonly used in Li/O₂ batteries.

compound	$\sigma / \text{mN m}^{-1}$	$H_{\text{O}_2}^{\text{CP}} / \text{mol L}^{-1} \text{bar}^{-1}$	L	$\ln L$
monoglyme ^{25,115}	23.9	$1.0 \cdot 10^{-2}$	0.2479	-1.395
diglyme ^{25,116}	29.4	$7.1 \cdot 10^{-3}$	0.1760	-1.737
triglyme ^{25,116}	31.8	$5.8 \cdot 10^{-3}$	0.1438	-1.940
tetraglyme ^{25,116}	33.5	$5.2 \cdot 10^{-3}$	0.1289	-2.049
DMSO ^{25,116}	42.9	$2.7 \cdot 10^{-3}$	0.0669	-2.704
DOL ^{115,117}	32.6	$6.6 \cdot 10^{-3}$	0.1632	-1.813
ACN ^{115,117}	28.4	$8.1 \cdot 10^{-3}$	0.2008	-1.606
DMA ^{115,118}	35.4	$5.18 \cdot 10^{-3}$	0.1285	-2.052
DMF ^{115,117}	35.2	$4.5 \cdot 10^{-3}$	0.1115	-2.193
perfluorooctane ^{116,119}	14.5	$2.13 \cdot 10^{-2}$	0.5280	-0.639
perfluorononane ^{116,119}	15.4	$2.08 \cdot 10^{-2}$	0.5156	-0.662
perfluorodecaline ^{116,119}	19.4	$1.85 \cdot 10^{-2}$	0.4586	-0.780

Table A.2. Fit parameter of the regression curve shown in Figure 3.1.

parameter	value
intercept	0.4959 ± 0.0921
slope / m mN ⁻¹	-0.0745 ± 0.0031

Supporting Information for Publication I

B.1 DETERMINATION OF GAS VOLUMES

To measure the internal volume of the devices for solubility and diffusion measurements, the apparatus was evacuated and a Hamilton syringe was connected to the apparatus, instead of the vacuum pump. Defined volumes of air were added with the help of the Hamilton-syringe (0–2 mL). The ball valve to the syringe was opened up and closed quickly, letting the pressure inside the syringe and the cell equilibrate. The amount of gas at the start and the end of one step is constant, which is shown in Equation (B.1) (with the initial pressure inside the cell p_i , the atmospheric pressure p_{at} , the final pressure after equilibrating p_f , the cell volume V_{cell} , the volume of the adapter between ball valve and Hamilton syringe $V_{adapter}$ and the added volume of the syringe V_s). Equation (B.1) is transformed into Equation (B.2), which allows the direct determination of the needed volumes (see Figure B.1) with an appropriate diagram.

$$p_i V_{cell} + p_{at} V_{adapter} + p_{at} V_s = p_f V_{cell} + p_f V_{adapter} \quad (B.1)$$

$$\frac{p_{at} V_s}{p_{at} - p_f} = \frac{p_f - p_i}{p_{at} - p_f} V_{cell} - V_{adapter} \quad (B.2)$$

The intercept in Figure B.1b should be constant over all measurements and can be used as an internal reference.

B.2 OXYGEN UPTAKE EXPERIMENTS FOR HENRY'S LAW CONSTANTS

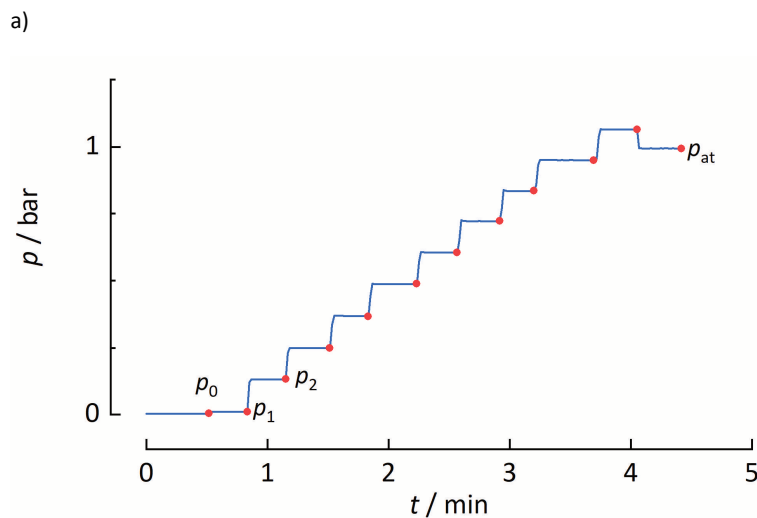
For the determination of $H_{O_2}^{cp}$ of the used solvents, an in-house designed cell was used (see Figure B.2a). A glass flask with magnetic stir bar was connected to a ball valve via a KF flange. The ball valve was connected to a stainless-steel cross fitting (6 mm, Swagelok). To this cross fitting an oxygen supply and a vacuum pump were connected as well, each separated by a manual ball valve or needle valve (all 6 mm, Swagelok). Finally, a pressure sensor was connected directly to the cross fitting.

For the determination of $H_{O_2}^{cp}$, about 6 mL of solvent was filled into the glass flask inside an argon filled glove box (MBraun, <5 ppm H₂O and O₂) and attached to the apparatus. The apparatus was then transferred into an oven with 25 °C, to minimize the influence of

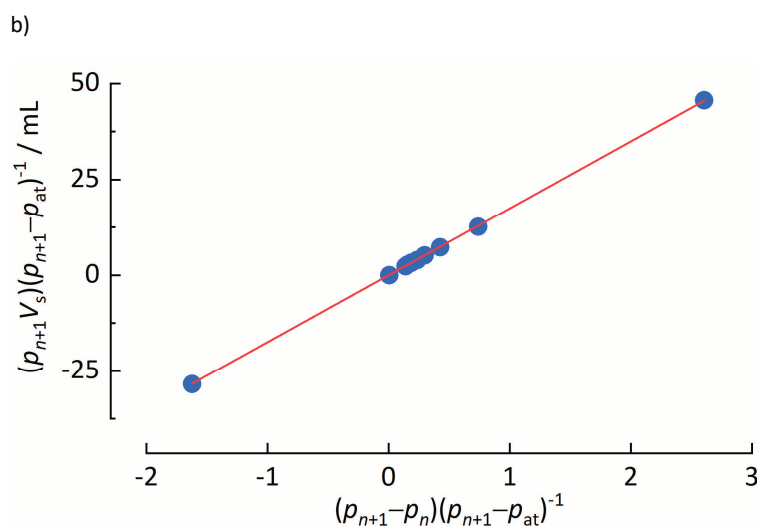
B

Figure B.1. Example of the determination of the total volume of a used apparatus.

a) Total pressure recorded to determine the total volume of the Henry's law constant apparatus. The apparatus was evacuated to a pressure p_0 . Defined volumes of air were added with the help of a Hamilton syringe. In the first step from p_0 to p_1 , only the dead volume of the syringe was added ($V_s = 0$ mL), every further step corresponds to $V_s = 2$ mL volume of air. In the end, the apparatus was opened to measure the atmospheric pressure p_{at} .



b) Graph used to calculate the total volume of the Henry's law constant apparatus (see Equation (B.1) and (B.2)). The slope of the linear equation was found to be 17.52 ± 0.03 mL, which is the apparatus volume V_{cell} . The intercept, which is the negative volume of the adapter from the apparatus to the Hamilton syringe, was found to be -0.14 ± 0.04 mL. The same method was used to determine the volume of the diffusion cell.



temperature changes. The whole apparatus was evacuated several times until the resulting vapour pressure in the apparatus was constant and near to literature values. This ensures that the solvent is completely degassed, and the atmosphere above the solvent only consists of the solvent used. The valve to the glass flask was closed and the upper part was flooded with oxygen (see Figure B.2b). The valve was opened again carefully leading to a sharp pressure drop. The stirrer was turned on after 30 s waiting time until the pressure was again constant. The valve was closed again and the steps were repeated until a final pressure around 1 bar was achieved. The flask was weighted after the experiment

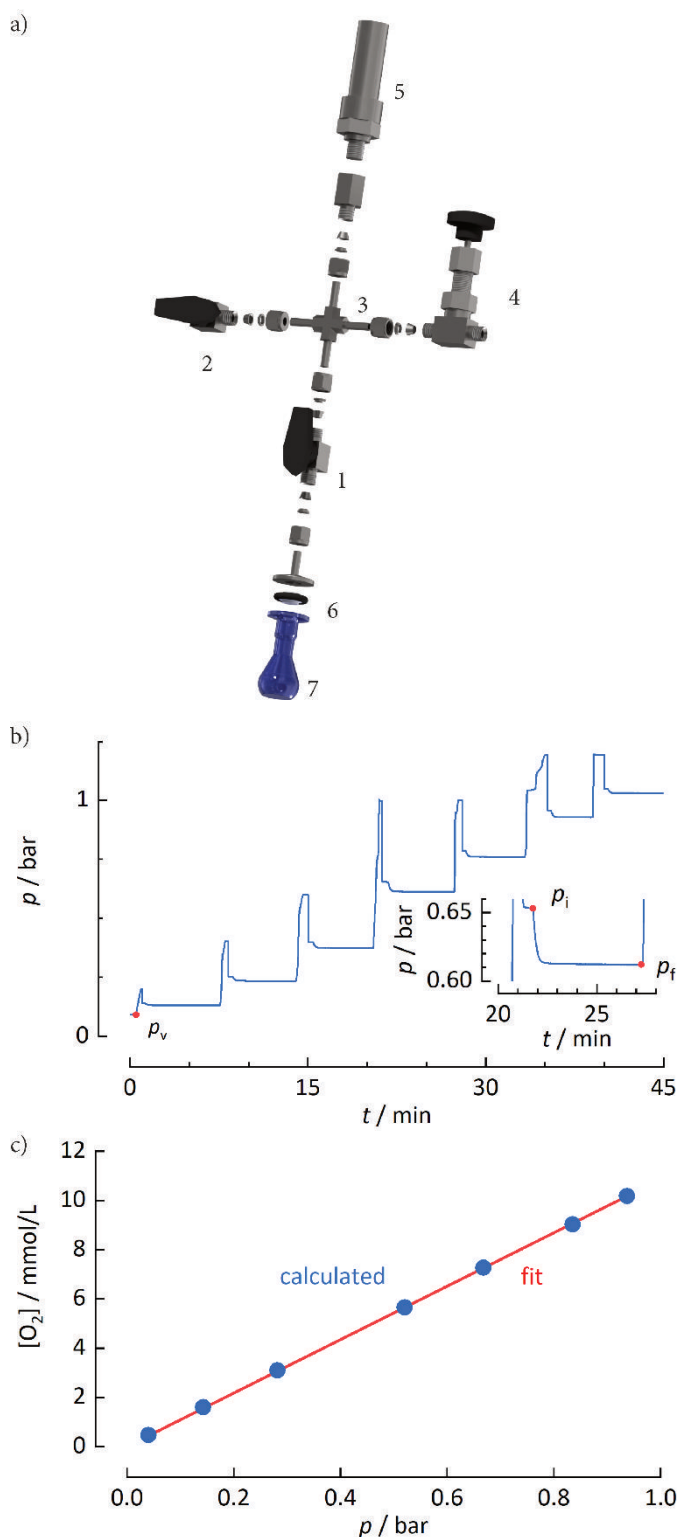


Figure B.2. Determination of the Henry's law constants.

a) Used Henry's law constant apparatus with: 1, 2 = ball valve, 3 = cross fitting, 4 = needle valve, 5 = pressure sensor, 6 = KF flange, 7 = sample flask, not shown: magnetic stir bar and clamp for KF flange.

b) Example of the recorded total pressure of all steps to determine the Henry's law constant of monoglyme. The entire apparatus was evacuated repeatedly until the recorded pressure was constant. For each step, the valve to the glass flask was closed and the upper part of the apparatus was flooded with oxygen, which corresponds to the recorded pressure rise. The valve was opened again leading to a sharp pressure drop. The stirrer was turned on at time of p_i until the pressure was again constant. The valve was closed again and the steps were repeated until a final pressure around 1 bar was achieved.

c) Graphical depiction of oxygen concentrations that were calculated from experimental data to determine the Henry's law constant of O_2 in monoglyme (calculation based on Equation (B.3) and (B.4)). The Henry's law constant $H_{O_2}^{cp}$ is represented by the slope of the linear equation, which was found to be $10.85 \pm 0.02 \text{ mmol L}^{-1} \text{ bar}^{-1}$, while the intercept was set to zero, given that it has no physical meaning.

and p_i and p_f of every step and p_v was determined. The initial pressure p_i corresponds to the pressure at the point in time, when the stirrer was turned on. The final pressure p_f corresponds to the pressure before oxygen was again let in. The pressure of oxygen p_{O_2} at one step corresponds to the pressure p_f corrected for the vapour pressure p_v of the solvent (Equation (B.3)). Finally, Equation (B.4) could be applied to determine the concentration of oxygen in the solution. Due to the fact, that the experiments were performed in steps, the solvent already contains oxygen from previous steps. To account for this amount of oxygen, it is necessary to add the calculated oxygen concentrations of all previous steps.

$$p_{O_2,n} = p_{f,n} - p_v \quad (B.3)$$

$$[O_2]_n = \frac{\rho_s}{RTm_s} \sum_1^n (p_{i,n} - p_{f,n}) \quad (B.4)$$

B.3 OXYGEN UPTAKE EXPERIMENTS FOR DIFFUSION COEFFICIENTS

For the determination of the diffusion coefficients of oxygen in the used solvents, an in-house designed cell was used (see Figure B.3). The central part of the apparatus consists of a stainless steel chamber with three 6 mm connections and a CF sealed lid. A pressure sensor was connected directly to the chamber. An oxygen reservoir and a vacuum pump were connected as well to the chamber, each separated by a manual ball valve (all 6 mm Swagelok). The reservoir was connected to an oxygen supply line, also separated by a ball valve (Swagelok). To measure the internal volume of the cell, the procedure described above was used. For the determination of D_{O_2} , 1 mL of solvent was filled into the thin film cell with an Eppendorf micropipette inside an argon filled glove box (MBraun, <5 ppm H₂O and O₂). The apparatus was then transferred into an oven with 25 °C, to minimize the influence of temperature changes. The whole apparatus was several times carefully evacuated until the resulting vapour pressure in the apparatus was constant and near to literature values. The valve between the oxygen reservoir and the chamber was closed, and the reservoir was filled with oxygen. The valve between thin film cell and reservoir was opened and closed carefully but quickly, leading to a sharp pressure rise in the tank. The resulting pressure drop was recorded and the procedure describe

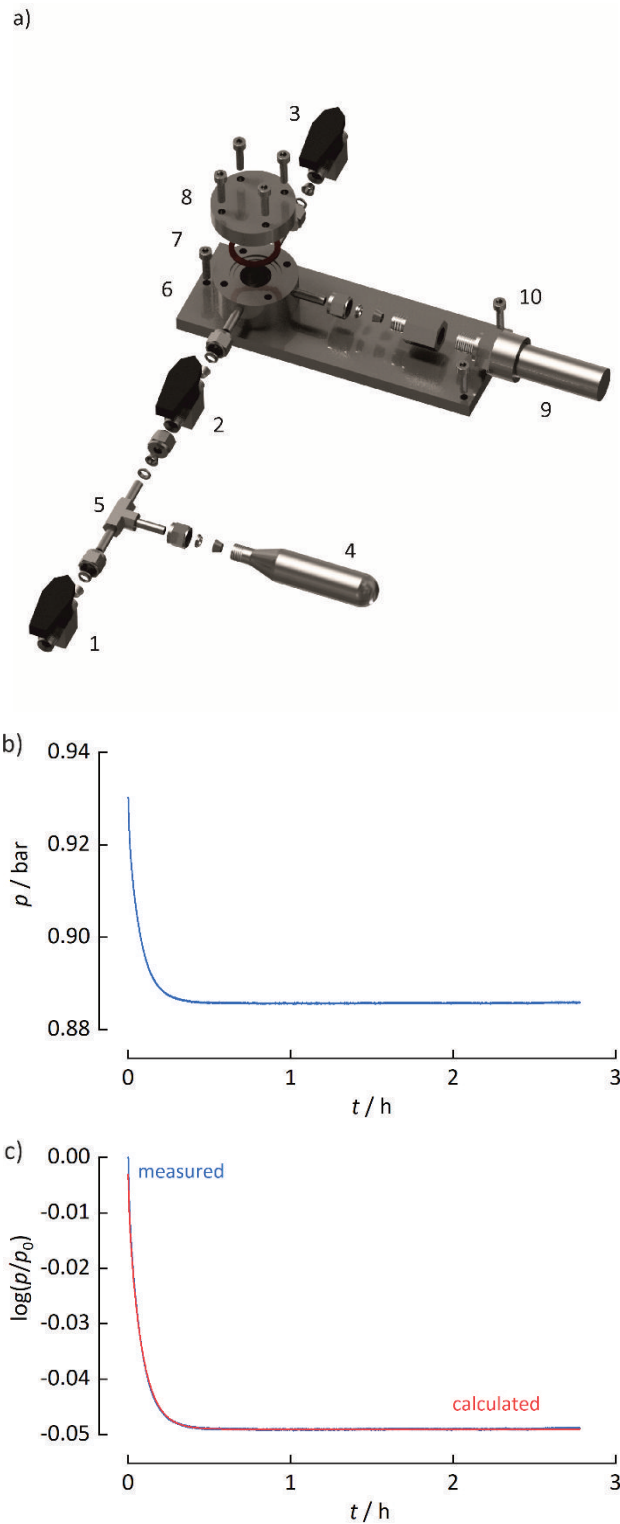


Figure B.3. Determination of the diffusion coefficients.
 a) Used thin film diffusion cell with: 1, 2, 3 = ball valve, 4 = oxygen reservoir, 5 = T-fitting, 6 = thin film cell, 7 = copper seal, 8 = lid, 9 = pressure sensor, 10 = levelling screw,
 b) Pressure decay recorded after flooding perfluorohexane with oxygen in the diffusion apparatus. The values are corrected for vapour pressure and temperature changes.
 c) Depiction of the recorded data according to the 1D diffusion model employed by Hou *et al.*, all data are plotted as $\ln(p/p_0)$ versus time t , were p_0 is the initial pressure value and $p = p(t)$ (see Equation (B.5) and (B.6)). The value determined for the constant a was used to calculate the real diffusion length L via Equation (B.7)–(B.10).

by Hartmann *et al.* and Hou *et al.* was applied to calculate the diffusion coefficients (see Equation (B.5) and (B.6)).^{1,2} The data was always corrected for vapour pressure and temperature changes. If necessary, also the leaking rate of the cell was corrected as described by Hartmann *et al.* The used fit routine gives the parameters a and b . To compensate for losses during the evacuation step, parameter a was used to calculate the real depth of the solvent L instead of the Henry's law constant $H_{O_2}^{xp}$. The therefore needed Henry's law constant was determined in a different experiment. Equation (B.7) to (B.9) give the used solvent volume, which could be, with the known area of the thin film diffusion cell, transformed into parameter L (Equation(B.10)).

$$\ln \frac{p(t)}{p_0} = \frac{8RTV_s \rho_s}{\pi^2 V_{\text{gas}} M_s H_{O_2}^{xp}} \sum_{n=0}^{\infty} \frac{1}{(2n+1)^2} \left\{ \exp\left(\frac{-(2n+1)^2 \pi^2 D_{O_2} t}{4L^2}\right) - 1 \right\} \quad (\text{B.5})$$

$$\ln \frac{p(t)}{p_0} = a \sum_{n=0}^{\infty} \frac{1}{(2n+1)^2} \{ \exp(-(2n+1)^2 bt) - 1 \} \quad (\text{B.6})$$

$$k' = \frac{8RT\rho_s}{\pi^2 M_s H_{O_2}^{xp} a} = \frac{V_{\text{gas}}}{V_s} \quad (\text{B.7})$$

$$V_{\text{cell}} = V_{\text{gas}} + V_s = \text{const.} \quad (\text{B.8})$$

$$V_s = \frac{V_{\text{cell}}}{k' + 1} \quad (\text{B.9})$$

$$L = \frac{V_s}{A} = \frac{V_s}{\pi r^2} = \frac{V_s}{3.048 \text{ cm}^2} \quad (\text{B.10})$$

B.4 DENSITIES OF n-GLYMES AND PFCS

We first compared the calculated densities of all solvents at room temperature and atmospheric conditions to known experimental values. As is shown in Table B.1, very good agreement of experimental and model-based data is achieved with differences appearing at most in the second decimal place.³⁻⁵

Table B.1. Calculated and experimental densities of the different glymes and perfluorinated molecules. Data are given in units of g cm^{-3} , all calculations were performed at $T = 298 \text{ K}$.

compound	our calculations	experimental (literature)	
monoglyme	0.849	$\sim 0.86^3$	0.86–0.87 ⁴
diglyme	0.931	$\sim 0.94^3$	0.94–0.95 ⁴
triglyme	0.973	$\sim 0.98^3$	0.98–0.99 ⁴
tetraglyme	1.003	$\sim 1.01^3$	1.00–1.01 ⁴
pentaglyme	1.019	1.025 ³	
C_6F_{14}	1.65	1.69 ⁵	
C_8F_{18}	1.74	1.77 ⁵	
C_9F_{20}	1.78	1.80 ⁵	
t- $\text{C}_{10}\text{F}_{18}$	1.92	1.92 ²	

B.5 SELF-DIFFUSION COEFFICIENTS

The self-diffusion coefficients for the PFCs and glymes were calculated from the slope of the mean square displacement (MSD) of the molecules, which is shown in Figure B.4.

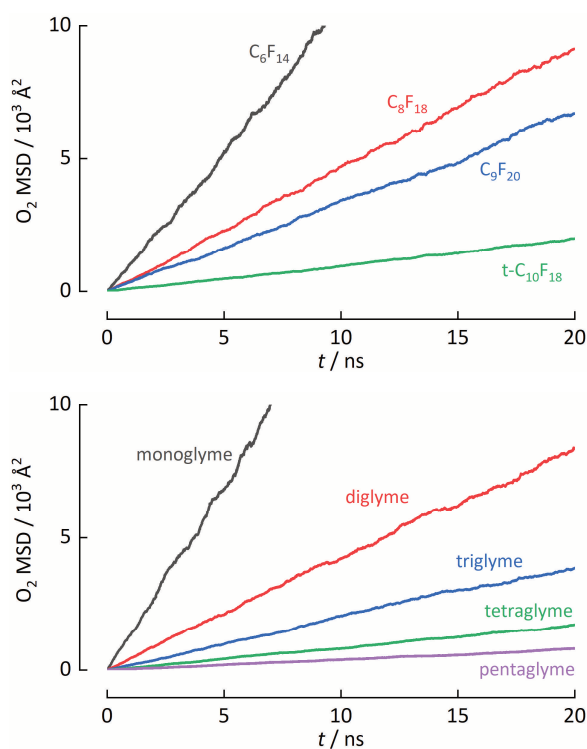
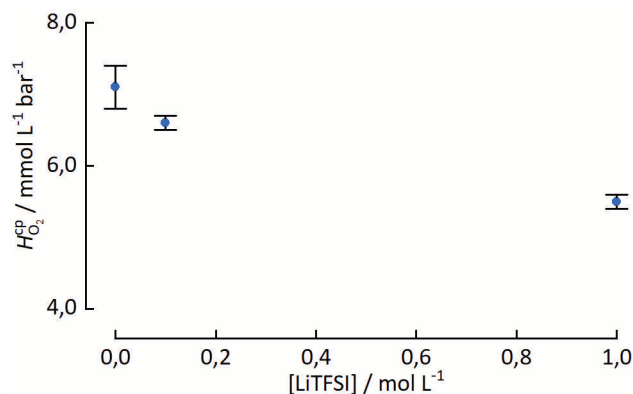


Figure B.4. Data for the determination of the self-diffusion coefficients from MD simulations.
a) MSD for the used PFC.
b) MSD for the used glymes.
The self-diffusion coefficient is extracted from the slope using the equation $\langle r - \langle r \rangle \rangle^2 = 6Dt$.

B.6 IMPACT OF CONDUCTING SALT ON HENRY'S LAW CONSTANT

We also measured the impact of LiTFSI on the solubility of oxygen in diglyme. As expected, the Henry's law constant for oxygen drops significantly for higher concentrations of LiTFSI.⁶

Figure B.5. Dependency of $H_{O_2}^{CP}$ from [LiTFSI] in diglyme. The solubility of oxygen in diglyme drops with rising concentrations of LiTFSI. This behaviour can be understood as a salting out effect.



B.7 REFERENCES

- [1] Ying, H.; Baltus, R. E. Experimental Measurement of the Solubility and Diffusivity of CO₂ in Room-Temperature Ionic Liquids Using a Transient Thin-Liquid-Film Method. *Ind. Eng. Chem. Res.* **2007**, *46*, 8166–8175. DOI: 10.1021/ie070501u.
- [2] Hartmann, P.; Grübl, D.; Sommer, H.; Janek, J.; Bessler, W. G.; Adelhelm, P. Pressure Dynamics in Metal-Oxygen (Metal-Air) Batteries: A Case Study on Sodium Superoxide Cells. *J. Phys. Chem. C* **2014**, *118*, 1461–1471. DOI: 10.1021/jp4099478.
- [3] Conesa, A.; Shen, S.; Coronas, A. Liquid Densities, Kinematic Viscosities, and Heat Capacities of Some Ethylene Glycol Dimethyl Ethers at Temperatures from 283.15 to 423.15 K. *Int. J. Thermophys.* **1998**, *19*, 1343–1358. DOI: 10.1023/A:1021927417610.
- [4] Tang, S.; Zhao, H. Glymes as Versatile Solvents for Chemical Reactions and Processes: From the Laboratory to Industry. *RSC Adv.* **2014**, *4*, 11251. DOI: 10.1039/c3ra47191h.
- [5] Freire, M. G.; Ferreira, A. G. M.; Fonseca, I. M. A.; Marrucho, I. M.; Coutinho, J. A. P. Viscosities of Liquid Fluorocompounds. *J. Chem. Eng. Data* **2008**, *53*, 538–542. DOI: 10.1021/je700632z.

- [6] Gittleson, F. S.; Jones, R. E.; Ward, D. K.; Foster, M. E. Oxygen Solubility and Transport in Li–Air Battery Electrolytes: Establishing Criteria and Strategies for Electrolyte Design. *Energy Environ. Sci.* **2017**, *10*, 1167–1179. DOI: 10.1039/C6EE02915A.

Symbols

$[X]$	mol L^{-1}	concentration of X
$[X]^*$	mol L^{-1}	starting concentration of X
A		pre-exponential factor
A_s	m^2	electrode surface area
D_i	$\text{cm}^2 \text{s}^{-1}$	diffusion coefficient of i
C_g^L	mol L^{-1}	concentration of gas in the liquid phase
C_g^{atm}	mol L^{-1}	concentration of gas in the atmosphere
E	V	electrode potential
E°	V	standard electrode potential
E_a	J	activation energy
E_i	J	interaction energy
E^{eq}	V	equilibrium potential
F	C mol^{-1}	Faraday constant
$f(\varepsilon)$		Fermi distribution
H^{sp}	$\text{mol L}^{-1} \text{bar}^{-1}$	Henry's law constant
H^{np}	bar^{-1}	Henry's law constant
i	A	current
i_a	A	anodic current
i_c	A	cathodic current
i_{lim}	A	limiting current
j	A m^{-2}	current density
j_0	A m^{-2}	exchange current density
j_i	$\text{mol cm}^{-2} \text{s}^{-1}$	flux of i
K		equilibrium constant
k_0	cm s^{-1}	standard rate constant
k_a	cm s^{-1}	anodic rate constant
k_B	J K^{-1}	Boltzmann constant
k_c	cm s^{-1}	cathodic rate constant
L		solubility
M_i	g mol^{-1}	molar mass of i
m_s	g	mass of used solvent
n		stoichiometric number of electrons involved in an electrode reaction
O		oxidized reactant
p_i	Pa	pressure of i or pressure at point i
r	m	radius

C

R	$\text{J mol}^{-1} \text{K}^{-1}$	universal gas constant
R		reduced reactant
T	K	temperature
ν	Hz	frequency factor
V_i	m^3	volume of i
$W(\varepsilon)$	eV^{-1}	probability density function
w_{th}	W h kg^{-1}	theoretical specific energy
$W_{\text{V,th}}$	W h L^{-1}	theoretical energy density
α		transfer coefficient
$\gamma_i(\varepsilon)$	$\text{cm}^3 \text{eV}$	proportionality factor of i
δ	m	thickness of electrolyte layer
ΔG^\ddagger	J mol^{-1}	Gibbs energy of activation
$\Delta_r G$	J mol^{-1}	Gibbs energy of reaction
ε	eV	energy of state
ε_{F}	eV	Fermi level
ε°	eV	electron energy corresponding to the standard potential of a redox couple
η	V	applied overpotential
η_{dyn}	Pa s	dynamic viscosity
λ	eV	reorganization energy for electron transfer
λ_i	eV	inner (vibrational) component of the reorganization energy for electron transfer
λ_o	eV	outer (solvational) component of the reorganization energy for electron transfer
$\rho(\varepsilon)$	$\text{cm}^{-2} \text{eV}^{-1}$	density of states
ρ_s	g cm^{-3}	density of used solvent
σ	N m^{-1}	surface tension

Acronyms

1-Me-AZADO	1-methyl-2-azaadamantane-N-oxyl
4-methoxy-TEMPO	(4-methoxy-2,2,6,6-tetramethylpiperidin-1-yl)oxyl
A ⁻	conjugated base of acid HA
ACN	acetonitrile
AZADO	2-azaadamantane-N-oxyl
CPET	coupled proton electron transfer
CV	cyclic voltammetry
diglyme	1-methoxy-2-(2-methoxyethoxy)ethane, diethylene glycol dimethyl ether
DMA	<i>N,N</i> -dimethylacetamide
DMF	<i>N,N</i> -dimethylformamide
DMPZ	dimethylphenazine
DMSO	dimethyl sulfoxide
DN	Gutmann donor number
DOL	1,3-dioxolane
EEG	Renewable Energy Sources Act (Erneuerbare-Energien-Gesetz)
EIS	electrochemical impedance spectroscopy
<i>et al.</i>	et alii
HA	acid
LAGP	$\text{Li}_{1.5}\text{Al}_{0.5}\text{Ge}_{1.5}(\text{PO}_4)_3$
LATP	$\text{Li}_{1.3}\text{Al}_{0.3}\text{Ti}_{1.7}(\text{PO}_4)_3$
LiBOB	lithium bis(oxalato)borate
LiClO ₄	lithium perchlorate
LiNO ₃	lithium nitrate
LiPF ₆	lithium hexafluorophosphate
LISICON	lithium super ionic conductor, $\text{Li}_{1+x+y}(\text{Ti,Ge})_{2-x}\text{Si}_y\text{P}_{3-y}\text{O}_{12}$
LiOTf	lithium trifluoromethanesulfonate
LiTFSI	lithium bis(trifluoromethanesulfonyl)imide
LLZO	$\text{Li}_7\text{La}_3\text{Zr}_2\text{O}_{12}$
MHC	Marcus-Hush-Chidsey theory
monoglyme	1,2-dimethoxyethane
NCM	$\text{LiNi}_x\text{Co}_y\text{Mn}_{1-x-y}\text{O}$
OER	oxygen evolution reaction
ORR	oxygen reduction reaction
TEMPO	(2,2,6,6-tetramethylpiperidin-1-yl)oxyl

D

tetraglyme	tetraethylene glycol dimethyl ether
TMPD	<i>N,N,N',N'</i> -tetramethyl- <i>p</i> -phenylenediamine
triglyme	triethylene glycol dimethyl ether
TTF	tetrathiafulvalene
XPS	X-ray photoelectron spectroscopy
XRD	X-ray diffraction

Contributions

E.1 PUBLICATIONS

- [1] Schürmann, A.; Luerßen, B.; Mollenhauer, D.; Janek, J.; Schröder, D. Singlet Oxygen in Electrochemical Cells: A Critical Review of Literature and Theory. *Chem. Rev.* **2021**, *121*, 20, 12445–12464. DOI: 10.1021/acs.chemrev.1c00139.
- [2] Janek, J., Pompe, C., Sann, J., Schröder, D., Schürmann, A., Schlussbericht für das BMBF-Forschungsvorhaben BenchBatt. Teilvorhaben: Berechnung und Validierung der Leistungsfähigkeit von Post-Lithium-Ionen-Batterien. *Technische Informationsbibliothek (TIB)*, **2020**. DOI: 10.2314/KXP:1698719604.
- [3] Schürmann, A.; Haas, R.; Murat, M.; Kuritz, N.; Balaish, M.; Ein-Eli, Y.; Janek, J.; Natan, A.; Schröder, D. Diffusivity and Solubility of Oxygen in Solvents for Metal/Oxygen Batteries: A Combined Theoretical and Experimental Study. *J. Electrochem. Soc.* **2018**, *165*, A3095–A3099. DOI: 10.1149/2.0601813jes.
- [4] Bergner, B. J.; Hofmann, C.; Schürmann, A.; Schröder, D.; Pepler, K.; Schreiner, P. R.; Janek, J. Understanding the Fundamentals of Redox Mediators in Li-O₂ Batteries: A Case Study on Nitroxides. *Phys. Chem. Chem. Phys.* **2015**, *17*, 31769–31779. DOI: 10.1039/C5CP04505C.
- [5] Bergner, B. J.; Schürmann, A.; Pepler, K.; Garsuch, A.; Janek, J. TEMPO: A Mobile Catalyst for Rechargeable Li-O₂ Batteries. *J. Am. Chem. Soc.* **2014**, *136*, 15054–15064. DOI: 10.1021/ja508400m.

E.2 ORAL PRESENTATIONS

- [6] Schürmann, A., Haas, R., Janek, J., Schröder, D., *The Crucial Role of Dissolved Oxygen in the Liquid Electrolyte of Metal/Oxygen Batteries* at German-Israeli-Battery-School 4, Berlin, Germany, **2019**

E

- [7] Maitra, U., Schürmann, A., Langsdorf, D., Schröder, D., Janek, J., *Digging Deeper to Achieve Practical Li-O₂ Batteries* at 69th Annual Meeting of the International Society of Electrochemistry, Bologna, Italy, **2019**
- [8] Maitra, U., Langsdorf, D., Schürmann, A., Schröder, D., Janek, J., *Shedding Light On Metal/Oxygen Batteries: Oxygen Redox Chemistry As Crucial Factor* at Materialforschungstag Mittelhessen, Marburg, Germany, **2018**
- [9] Schröder, D., Schürmann, A., Pompe, C., Janek, J., *Benchmarking Next-Generation Metal Oxygen Batteries* at Batterieforum Deutschland, Berlin, Germany, **2017**

E.3 POSTER PRESENTATIONS

- [10] Schröder, D., Schürmann, A., Pompe, C., Janek, J., *Benchmarking Next-Generation Metal Oxygen Batteries* at Batterieforum Deutschland, Berlin, Germany, **2017**
- [11] Schröder, D., Schürmann, A., Janek, J., *Discharge Products in Alkali-Metal-Oxygen Batteries: Better Insight with Operando Techniques* at IBA Meeting, Nara, Japan, **2017**
- [12] Stock, D., Schürmann, A., Dongmo, S., Schröder, D., Janek, J., *Discharge Products in Metal-Oxygen Batteries: Better Insight with Operando Techniques* at Materialforschungstag, Gießen, Germany, **2017**

And as always, thanks for watching.

—Michael Stevens, VSauce

COLOPHON

This document was typeset using the Microsoft Word document processing system. The style was inspired heavily by the thesis of Manuel Weiß. The bibliography was created using Mendeley. Robert Slimbach's Minion Pro is used as the text typeface.

CorelDRAW 2019, OriginPro 9.7 and ChemDraw 20.1.1 was used for preparing graphics. Autodesk Inventor 2020 was used for creating 3D models. Graphics used on page 1, 37, 67 and 93 were generated from “way wavy way” by ge1doot¹, used under Creative Commons Attribution-NonCommercial-ShareAlike 4.0 International². Turtletoy is created by Reinder Nijhoff (@ReinderNijhoff)^{3,4}.

¹ <https://turtletoy.net/turtle/65cb465053>

² <https://creativecommons.org/licenses/by-nc-sa/4.0/>

³ <https://reindernijhoff.net/>

⁴ <https://twitter.com/ReinderNijhoff>

Reaction Mechanisms at Cathodes in Lithium/Oxygen Batteries.

23.12.2021, Adrian Schürmann